U. S. Department of Commerce

National Oceanic and Atmospheric Administration (NOAA)

National Environmental Satellite, Data, and Information Service (NESDIS)

Geostationary Extended Observations (GeoXO) Hyperspectral InfraRed Sounder Value Assessment Report

NOAA Technical Report

Contributors: Jeffrey Adkins, Frank Alsheimer, Phillip Ardanuy, Sid Boukabara, Sean Casey, Monica Coakley, Joseph Conran, Lidia Cucurull, Jaime Daniels, Sarah D. Ditchek, Frank Gallagher, Kevin Garrett, Jordan Gerth, Mitch Goldberg, Steve Goodman, Ed Grigsby, Michael Griffin, Vanessa Griffin, Michael Hardesty, Flavio Iturbide, Satya Kalluri, Robert Knuteson, Alexander Krimchansky, Christopher Lauer, Dan Lindsey, Will McCarty, Joel McCorkel, Joanne Ostroy, David Pogorzala, Hank Revercomb, Richard Rivera, Matt Seybold, Timothy Schmit, Bill Smith, Pamela Sullivan, Elsayed Talaat, Kevin Tewey, Monica Todirita, Denis Tremblay, Dimitrious Vassiliadis, Patricia Weir, James Yoe

0. Abstract

The societal economic benefits of an operational GEO hyperspectral IR sounder were examined through recent research. Forecast benefits, resultant societal benefits, and derived societal economic benefits were explored in the areas of severe weather nowcasting and short-range forecasting, Numerical Weather Prediction (NWP) skill enhancements, hurricane and tropical storms, and other applications areas, including aviation. Recent research included literature on Observing System Experiments (OSEs) and Observing System Simulation Experiments (OSSEs), as well as existing analyses. More focused OSEs/OSSEs for severe storms and for a potential international GEO ring of sounders were developed for this study to examine NWP skill improvements. NWS users were also consulted on benefits, data usage, and forecast dissemination to decision makers. Estimating vertical atmospheric temperature, moisture, and horizontal wind profiles from radiance observations is only one of the many applications with potential benefit from high- spectral resolution infrared measurements. The list includes, but is not limited to: atmospheric composition, atmospheric circulation, planetary boundary layer structure and temporal evolution, cloud information, surface parameters, and volcanic plumes. Providing low latency, rapid refresh, and high-fidelity hyperspectral IR data to the weather enterprise would be key to severe weather prediction in providing positive forecast value for nearly every weather forecast process. The NWS weather enterprise has stated that IR hyperspectral data will be used at nearly every step of the weather forecast process by providing real-time deep tropospheric data at a much higher frequency than legacy methods.

1. Introduction

NOAA's future generation of geostationary satellites, flying in the early 2030s-2050 time range, will provide both legacy and new observations. As part of the Geostationary Extended Observations (GeoXO) pre-formulation work in 2020, a team of scientists was tasked with putting together a value assessment for one of those observational instruments: an infrared (IR) hyperspectral sounder. The primary purpose of the value assessment was to provide decision makers with sufficient information to proceed with detailed formulation studies of an IR hyperspectral sounding instrument for the GeoXO baseline constellation architecture implementation.

IR hyperspectral instruments measure, in hundreds to thousands of narrow spectral samples, the infrared radiation emitted from the Earth and determine the relative magnitude of that IR radiation. The output radiance data in these narrow spectral samples, or channels, are processed to derive, or "retrieve," geophysical properties such as vertical profiles of atmospheric temperature (T), water vapor (q), the horizontal wind components (u and v) and trace gases at multiple vertical levels of the atmosphere. Measured radiances can be assimilated into Numerical Weather Prediction (NWP) models, leading to improved model forecast skill. This has been shown using IR hyperspectral radiances from instruments aboard Low-Earth-Orbiting (LEO) satellites; geostationary measurements provide more frequent opportunities for assimilation, including more looks between clouds. The radiance measurements and retrieved vertical geophysical profiles of T, q, u, and v are the heart of the application base of IR hyperspectral measurements and are used in the weather enterprise forecast process. A key performance characteristic of an IR sounder in a geostationary orbit is the ability to stare over a given area of the Earth and make observations at high cadence. These data can be transmitted in real time to observe an evolving weather event or other area of interest.

The assessment team comprised wide-ranging stakeholder subject matter experts (SME) to systematically address the objective with team membership that included operational users from NOAA's National Weather Service (NWS), science/research community representation, engineering and development SMEs, and representatives from the NOAA Office of the Chief Economist. The team focused on providing objective data for decision makers. To this end, the team organized the assessment into five major tasks:

1) Comprehensively review the literature record of geostationary IR hyperspectral sounders for value to the weather enterprise;
2) Identify shortfalls/gaps in the analytic record to help define a targeted extension of the analytic record through mature modeling using Observing System Experiment (OSE) and Observing System Simulation Experiment (OSSE) techniques;
3) Review current and planned space-based systems that include geostationary IR hyperspectral sounding;
4) Review potential impact areas within the National Weather Service;
5) Provide economic information to determine potential societal and economic benefit of geostationary IR hyperspectral sounder observations.

This report is organized as follows. Section 2 will provide some background, Section 3 highlights several focus areas, Section 4 covers OSSE (Observing System Simulation Experiments), Section 5 and 6 cover nowcasting and economic benefits, respectively. The Summary and Conclusions are in Section 7.

2. Background

2.1 Motivation for Exploration of Hyperspectral Sounder Value

A geostationary orbital hyperspectral sounding observational capability, like any other purchase, should provide benefits (or value) that would exceed the cost of the purchase. Prior to a potential procurement, this value needs to be identified both by Observing System Simulation Experiments (OSSEs), as currently required by law for new large observing system procurements, and by exploring likely capabilities based on other hyperspectral sounders. The OSSE assessment is regulatory and is prescribed in H.R.353 - Weather Research and Forecasting Innovation Act of 2017 that states: "...OSSEs must be conducted before: (1) acquisition of major government-owned or government-leased operational observing systems with a lifecycle cost of more than $500 million…" Because every OSSE is limited by constraints and assumptions, including: a limited number of cases; limited ability to physically simulate the atmosphere and Earth system; limited ability to fully utilize the expected spectral, spatial, and temporal resolutions of the planned sensor; performance with current computational limitations rather than those 10-30 years in the future, and inability to anticipate the future data assimilation and exploitation applications, it is important to consider the OSSE results as informational rather than definitive.

Although NOAA has flown multispectral (coarser-spectral-resolution) sounders up through GOES-15, the U.S. has not yet flown a hyperspectral infrared sounder in geostationary orbit. However, technologically mature hyperspectral sounders and the benefits of the improved vertical resolution provided by hyperspectral IR sounders have been demonstrated in Low Earth Orbit (LEO) by multiple research and operational systems, e.g.: Atmospheric Infrared Sounder (AIRS) flown by NASA for 18 years (2002-present); Cross-track Infrared Sounder (CrIS) flown by NOAA (2017-present) and NASA (2011-present); and Infrared Atmospheric Sounding Interferometer (IASI) residing on the European Space Agency's (ESA) MetOp

(2006-present). Associated with these sounders there exists unequivocal documentation of significant NWP model skill improvement and benefits of the orbital overpasses to operational weather forecasters, emergency managers, and many others.

Other organizations have developed and are flying IR sounders of the type interesting to NOAA. GEO persistence adds the benefit of rapid cadence of the information (and low latency), in real time and at higher spatial resolution, with equivalently high vertical resolution. China successfully launched the Fengyun series 4 (FY-4) Geosynchronous Interferometric Infrared Sounder (GIIRS) in December 2016. The European Organisation for the Exploitation of Meteorological Satellites (EUMETSAT) is developing Meteosat Third Generation (MTG) GEO advanced hyperspectral Infrared Sounders (IRS) to fly operationally as a part of MTG-S in 2023 and beyond. The GIIRS and IRS provide detailed vertical layer-by-layer information on wind, temperature, and humidity that will potentially improve both the initialization of regional and global NWP models and weather forecasters' capability to nowcast..

EGOS-IP [WMO, 2013] set as an action: "*All meteorological geostationary satellites should be equipped with hyperspectral IR sensors for frequent temperature and humidity soundings, as well as tracer wind profiling with adequately high resolution (horizontal, vertical, time) [by] 2015-2025 for making the instruments operational.*" With MTG IRS, FY-4A and 4B GIIRS, possible Japanese Meteorological Agency (JMA) sounders planned on follow-on flights after Himawari-8 and -9, and the Korean Meteorological Agency (KMA) launch in 2028 with a geo-hyperspectral IR sounder, consistent with the WIGOS 2025 and 2040 visions, at least 3 of the 5 satellites originally envisioned by the WMO 2025 WIGOS vision are being realized within the next few years, which sets the stage for the new U.S. capability that could bring the WIGOS 2040 GEO ring vision to full reality.

2.2 What is a hyperspectral sounder?

A hyperspectral spectrometer is an optical instrument that measures light from a large number of narrow spectral samples, often contiguous. A hyperspectral sounder is an instrument that locates these narrow spectral samples along multiple spectral absorption feature edges (caused by atmospheric gases, varying with altitude, along the optical path) to enable measurements from different altitudes. The measured radiances can be used directly by Numerical Weather Prediction Models (NWP) or employed by retrievals that invert the radiative transfer equation to determine the water vapor absorption and blackbody temperature of different layers of the atmosphere.

For reference, NOAA has flown in the Geostationary Earth Orbit (GEO) IR multispectral sounders with a low number of spectral samples along the atmospheric absorption band edge, as on GOES I-M (8-12) and NOP (13-15). Finer spectral sampling was needed to resolve finer vertical features. This was accomplished by NASA on the currently operating Atmospheric Infrared Sounder (AIRS) and NOAA on the currently operational Cross-track Infrared Sounder (CrIS) flying on Suomi National Preparatory Program (NPP) and on Joint Polar Satellite System-1 (JPSS-1). A GEO platform provides a more persistent sampling and

longer light capture (dwell) for a hyperspectral sounder that enables higher horizontal and vertical resolution measurements of changing weather conditions.

A high-spectral-resolution IR sounder for NOAA's GOES-R series was planned for GOES-R/S/T and /U. The concept was originally studied for geostationary orbit for the GOES High-Resolution Interferometer Sounder (GHIS) (slated for a GOES-NOP spacecraft), then as the Advanced Baseline Sounder (ABS) which was later called the Hyperspectral Environmental Suite (HES). This hyperspectral sounder on a satellite grew out of earlier hyperspectral sounders on aircraft (e.g., Smith et al. 1990). High-vertical-resolved water vapor profiles are accurately retrieved in order to derive atmospheric wind profiles; this was first demonstrated and documented with real data by the aircraft hyper-spectral-infrared-resolution National Polar- Orbiting Operational Environmental Satellite System (NPOESS) Airborne Sounder Testbed-Interferometer (NAST-I) measurements (Zhou et al. 2002). In 2006, predominantly because of budgetary pressure, the HES was removed from the GOES-R/S series.

Definitions of the portions of the infrared spectrum vary across academic communities, industry, and ISO standard. For reference, this report will use the following ranges. Here, the shortwave IR (SWIR) spans wavelengths between 2.3 and 4 µm, the midwave IR (MWIR) spans between 4 and 8 µm and longwave IR (LWIR) spans 8-15 µm.

Operational hyperspectral IR sounders have also been demonstrated in Low Earth Orbit (LEO) by multiple research and operational systems. However, a single LEO sounder has a revisit time of 12 hours for a spot over the equator. Another primal benefit of the GEO sounder is the revisit time of only 30 minutes (24X better than a single LEO, 12x better than the existing US and European LEOs). The intrinsic nature of the geostationary orbit permits longer dwell (exposure) time of the detector over the same Earth scene and continuous data downlink. Today's advanced enabling technologies include state- of-the-art large Mercury-Cadmium-Telluride (HgCdTe) Focal Plane Arrays (FPAs), high-speed Read-Out-Integrated-Circuits (ROICs), and high speed data downlinks. As a result, a GEO hyperspectral sounder can achieve a footprint on the Earth surface of 4 km (3.5X better than LEO). For instance, the CrIS 14 km footprint yields 9% of the observed area as clear sky FOV that are assimilated for numerical weather forecast. A NOAA internal study found that this yield would nearly double to 17% for a footprint of 4 km. High-spectral IR information from instruments in LEO have shown they are among the most important in global NWP (Menzel et al. 2018). More recently, positive impact in regional NWP has been demonstrated (Lin et al. 2017).

Multispectral sensors, such as the ABI (Advanced Baseline Imager) on the GOES-R series, average over important spectral information that could otherwise be detected

with appropriate hyperspectral spectrometers (Schmit et al. 2009, Schmit et al. 2017; Schmit et al. 2018) (see Figure 2-1). Hyperspectral spectrometers in the infrared measure thermal emissions of the Earth's atmosphere and can sample narrow absorption features of water, carbon dioxide, and trace gases in the atmosphere that can be used to determine temperature, moisture, and vector winds as a function of height in the atmosphere. The additional spectral information from on/off-spectral line observations provide information on atmospheric inversions as well as boundary layer water vapor distribution (Sieglaff et al. 2009). Other benefits of a GEO hyperspectral sounder found in existing literature are summarized in the section "Summary of Study Activities" below.

While it is true that not all observed satellite data are directly assimilated in NWP, even so, satellite data represent by far the most data (by volume) that are assimilated. In addition, some of the satellite data will be used to better select the appropriate locations to be assimilated; for example, the areas with the least clouds. In order to be assimilated, the data have to arrive in time. The GEO orbit offers the advantage of lower data latency, which is particularly important when NWP regional models used operationally today by the NWS for smaller areas are running every 30 minutes. Additionally, the data spatial resolution must be consistent with the model. While the satellite data might be "too fine" for current global NWP, the models continue to improve their spatial resolutions and will approach or achieve global 1 km resolution within a decade with the deployment of exascale computing[1]. Finally, the resources needed to assimilate more data have historically been less than adequate for both research and operations.

It should also be noted that "sounding" (or estimating vertical atmospheric temperature, and moisture profiles) is only one of the many applications from high-spectral resolution infrared measurements. The list includes, but is not limited to: atmospheric composition, atmospheric motion, planetary boundary layer, inversion detection, cloud information, surface parameters, and volcanic plumes.

[1] https://www.exascaleproject.org/exascale-computing-project/

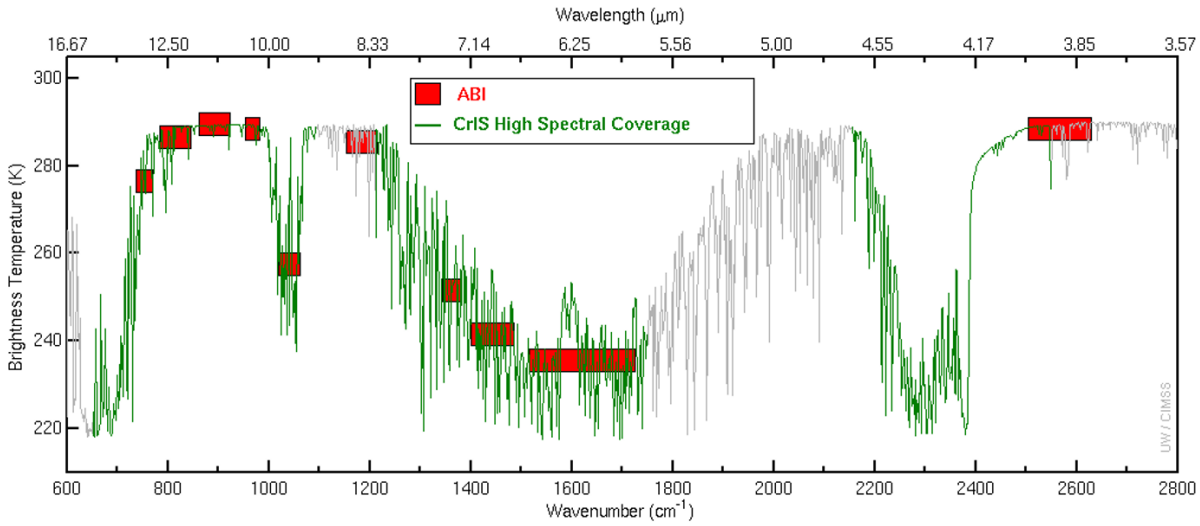

Figure 2-1. The spectral coverage of the current Advanced Baseline Imager (ABI) and a high- spectral-resolution spectrum. The ABI infrared bands (red) are at very low spectral resolutions (33– 216 cm^{-1}) (0.6 μm at 13.3 μm and 0.83 at 6.185 μm), whereas a high spectral resolution instrument would have spectral resolutions finer than 1 cm^{-1} (0.02 μm at 13.3 μm). The full high-spectral-resolution coverage is similar to IASI, whereas the highlighted spectral regions (green) are similar to the CrIS. Note that oscillations in the high resolution spectra are not noise, but represent absorption lines that contain vertical information that has been averaged over in the ABI measurements. (Credit: University of Wisconsin-Madison CIMSS)

3. Study Focus Areas

Key focus areas that were examined as part of this value assessment were severe weather nowcasting and short-range forecasting (Section 3.1), NWP Skill Enhancement Section 3.2), Hurricane Tropical Storms (Section 3.3), and aviation applications (Section 3.4). Many of these, and other, applications were discussed in Schmit et al. (2009), a paper on the potential benefits of high-spectral IR observations from the geostationary orbit. Since that publication, the potential uses have only become clearer, while leveraging the experience using data from LEO instruments.

3.1 Severe Weather Nowcasting and short-range forecasting

Schmit et al. (2009) gave a few examples of high-spectral IR information directly being used in the now/near casting arena. Now, there are many examples where derived stability indices from CrIS and ATMS retrievals from NOAA Unique Combined Atmospheric

Processing System (NUCAPS) Environmental Data Record (EDR) Products from the polar-orbiters are used for situational awareness (Iturbide-Sanchez et al. 2018). Some might think that if some high-spectral IR measurements are being assimilated, that there is no need for situational awareness. But this is not the case, for several reasons. First, due to operational constraints, not all the spectral information is assimilated. Also, due to the data latency and operational cut-off times, not all the information even makes it to the assimilation step. Thus, hyperspectral IR radiances, retrievals, and derived stability indices can be used to compare the current state of the atmosphere to improve situational awareness. In fact, high spectral resolution data can be used at many of the forecasting steps.

As an example of how sounder-derived retrievals may be used by forecasters, consider a situation in the central plains of the U.S. where an approaching trough sets up southerly low-level winds transporting higher water vapor content from the Gulf of Mexico into the region. Since weather balloons are launched only twice daily (12 UTC and 00 UTC, roughly 7 am and 7 pm local time there), there's a 12-hour data gap during the midday and afternoon hours when convective initiation often occurs. Numerical models sometimes struggle with correctly handling both water vapor return and the strength of the boundary layer inversion, so forecasters like to use extra information to assess thermodynamic fields such as CAPE and CIN that are sensitive to low-level water vapor and the temperature profile. Retrievals from an IR sounder in geostationary orbit provide just that: estimates during the early afternoon of the temperature and water vapor profiles help forecasters hone in on the timing and location of convection and predict its strength and evolution. GEO soundings provide advantages over LEO soundings due to much lower latency, a better chance of avoiding clouds in a given location given more frequent looks, and the ability to "loop" the data in order to assess the time rate of change of fields such as low- level water vapor.

3.2 NWP Skill Enhancement

High- spectral IR observations in NWP from AIRS data were studied in the mid-2000s (e.g., Chahine et al. 2006); now there are many studies and operational examples showing the impact of IASI and CrIS in both global and regional NWP (Menzel et al. 2018). Before AIRS was launched, some modelers thought the impact would be severely limited due to it "... not being able to see through clouds". Yet now, high spectral IR observations, along with microwave measurements, have been shown to be some of the most important observations for global NWP. Assimilating AIRS data in the regional HRRR has shown benefits, even with the limited temporal and spatial coverages (H. Lin, 2017). Data from geostationary orbit have a low latency that allows more data to be assimilated (Wang et al. 2020). Currently there is a gap in the coverage from LEO hyperspectral IR sounder measurements in the low latitude regions (Bormann 2019) that the GEO perspective will fill.

High spectral resolution of the LW band is key for atmospheric profiles, NWP assimilation, and atmospheric composition. For example, the current spectral usage for CrIS and AIRS relies heavily on the LW part of the spectrum as can be seen in Figure 3-1. To date, polar-orbiting hyperspectral sounders all included the LW portion of the spectrum. But, the NCEP NWP system does not achieve the full vertical resolution advantage provided by the LW band since they do not use the spectral channels at their full spectral resolution, which may yield reduced skill for LWIR compared to SWIR. See Figure 3-2 for CrIS and AIRS spectral sub-sampling for global NWP. The sensors were designed to provide high enough spectral resolution to observe the radiance emission from in-between individual CO2 absorption lines, where there is a strong pressure-altitude dependence in the pressure broadened wings of the CO2 absorption lines. With contiguous channel spectra of these high vertical resolution radiance emissions, extraction of small scale vertical profile features through the profile retrieval can occur, although this may not be possible in operational NWP today. Global NWP exclusion of cloud effected radiances, and radiances sensitive to land surface emission may further reduce the influence on forecast skill of tropospheric profile information observed with high-spectral resolution radiance spectra.

All of our current satellite sounding sensors (i.e., ITS/CrIS, AIRS, IASI, IRS, HIRAS, and GIIRS) have included the LW spectrum thus any plans for omitting these measurements will need detailed studies in global NWP, Nowcasting, and atmospheric composition.

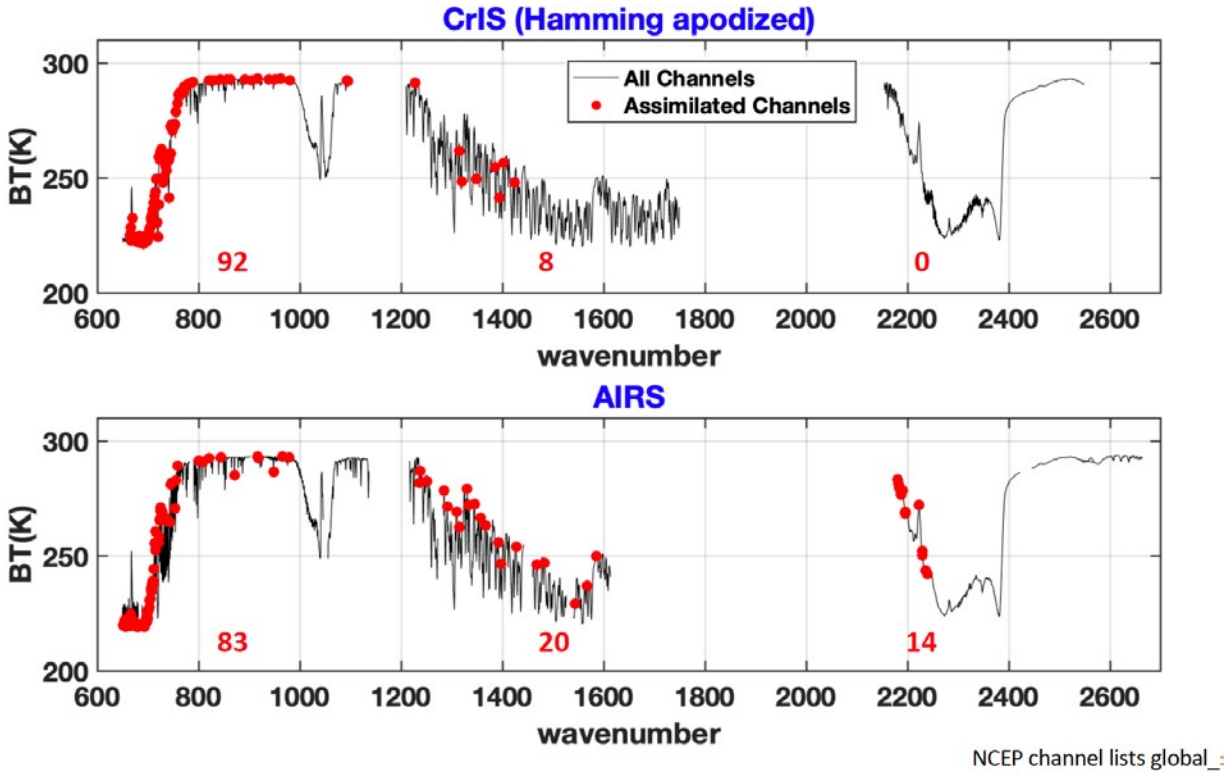

Figure 3-1: Example clear sky spectra for hamming apodized CrIS (top panel) and AIRS (lower panel) are shown via the small black circles, The NCEP selected channels (for NWP applications) within the LW sounding region are shown as the large red circles. For CrIS it is roughly every other channel, and Hamming apodized. Hence the full vertical resolution information is not being used at this time. Credit: UW/SSEC.

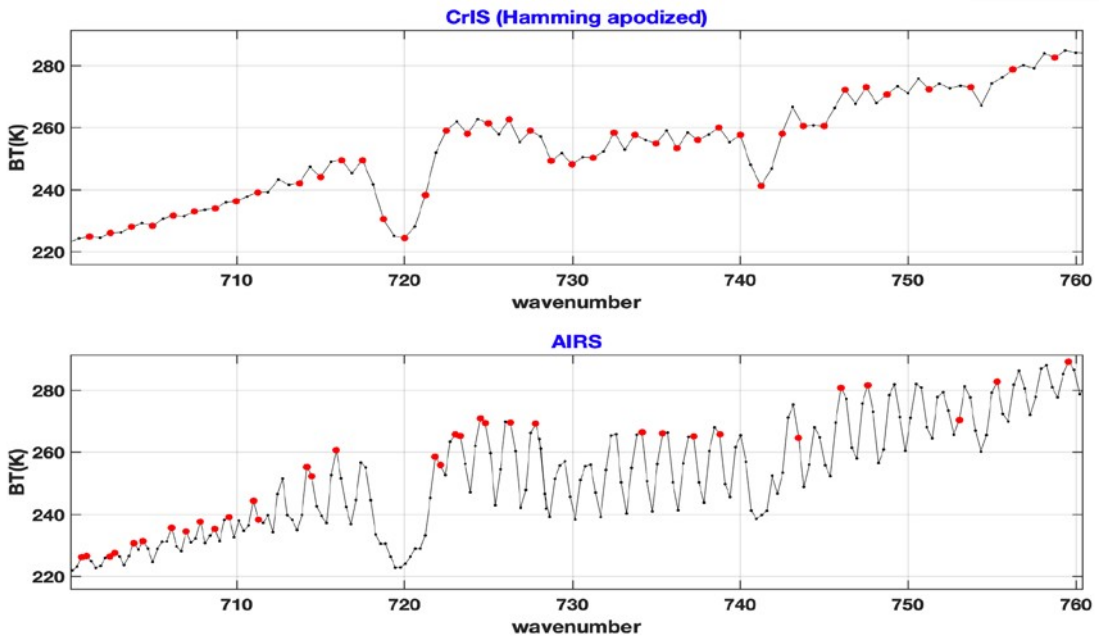

Figure 3-2: Same as above, but zoomed in on the LW section only.

Section 4 below provides detailed results of a number of recent Observing System Simulation Experiments (OSSEs) meant to estimate the impact of a GEO HSS on NWP skill.

3.3 Hurricanes and Tropical Storms

Schmit et al. (2009) introduced a few limited examples where high spectral IR observations were improving Tropical Cyclone (TC) forecasts, but expectations for better depiction of TC motion vectors had been set (Velden et al. 2005). Now there are many examples (Li et al, 2016; Liu et al, 2010; Zheng et al 2015; Lee et al 2017) of how the near-storm environment is better monitored. This includes, but not limited to better moisture and winds (Li et al, 2016; Wang et al. 2015; Wang et al 2017). In addition, the direct assimilation of radiances from high spectral resolution IR measurements has improved many NWP parameters used in TC applications.

3.4 Aviation Applications

There are many aviation application examples including monitoring SO_2 volcanic plumes and warning pilots of potential aircraft issues using temperature retrievals at very high altitudes. Knowing about an SO_2 plume is important in its own right, but can also be a proxy for possible volcanic ash. Another serious issue for some aviation regions is very cold temperatures that can affect the jet fuel. Retrieval temperature profiles from polar-orbiters have been useful for aircraft routing (Weisz et al. 2015; Weaver et al., 2019). Improved forecasts of convective weather, due to improved monitoring of atmospheric stability, will also help aviation applications. In general, the assimilation of radiances from high spectral resolution IR measurements have improved many NWP parameters related to aviation interests.

3.5 Other applications

There are many additional benefits, including Imager/Sounder synergies (the Imager can help the Sounder-only derived products, the sounder can help the imager-only derived products), winter weather, oceanic weather prediction (atmospheric vector motion), fire weather applications (moisture, PBL, wind tendencies), climate applications (especially the diurnal signatures), and atmospheric composition such as CO, SO_2, O_3, CO_2, and CH_4 (Barnet et al, 2004, Van Damme et al, 2018, Franco et al., 2018). Of course to retrieve many of these gases, the full spectral range must be measured. Figure 3-3 shows the spectral signature of a number of these gases. These plots represent the spectra with and without the said gases. Note that the low-spectral resolution ABI either does not monitor these gases or does not have as much skill when it does. In particular, note the SO2 signature associated with volcanic eruptions centered at 7.4 um (1350 cm-1) and 8.6 um (1163 cm- 1).

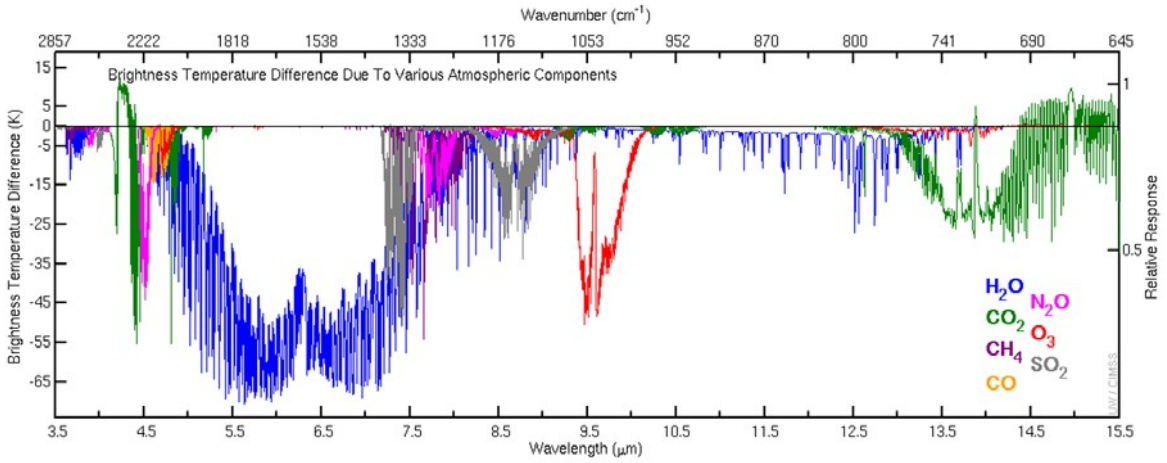

Figure 3-3. Brightness Temperature Difference Caused By Removing Atmospheric Components using the US Standard Atmosphere (1976) and the Forward Model: RTTOV v11.3 (Except 1000 DU of SO2 was calculated with PFAAST). (Credit: University of Wisconsin- Madison CIMSS)

Of course what can be retrieved depends on the spectral coverage, with a fuller spectral coverage allowing for more applications. Figure 3-4 (from Menzel et al, 2018) shows the spectral coverage for many of the high-spectral resolution IR sensors.

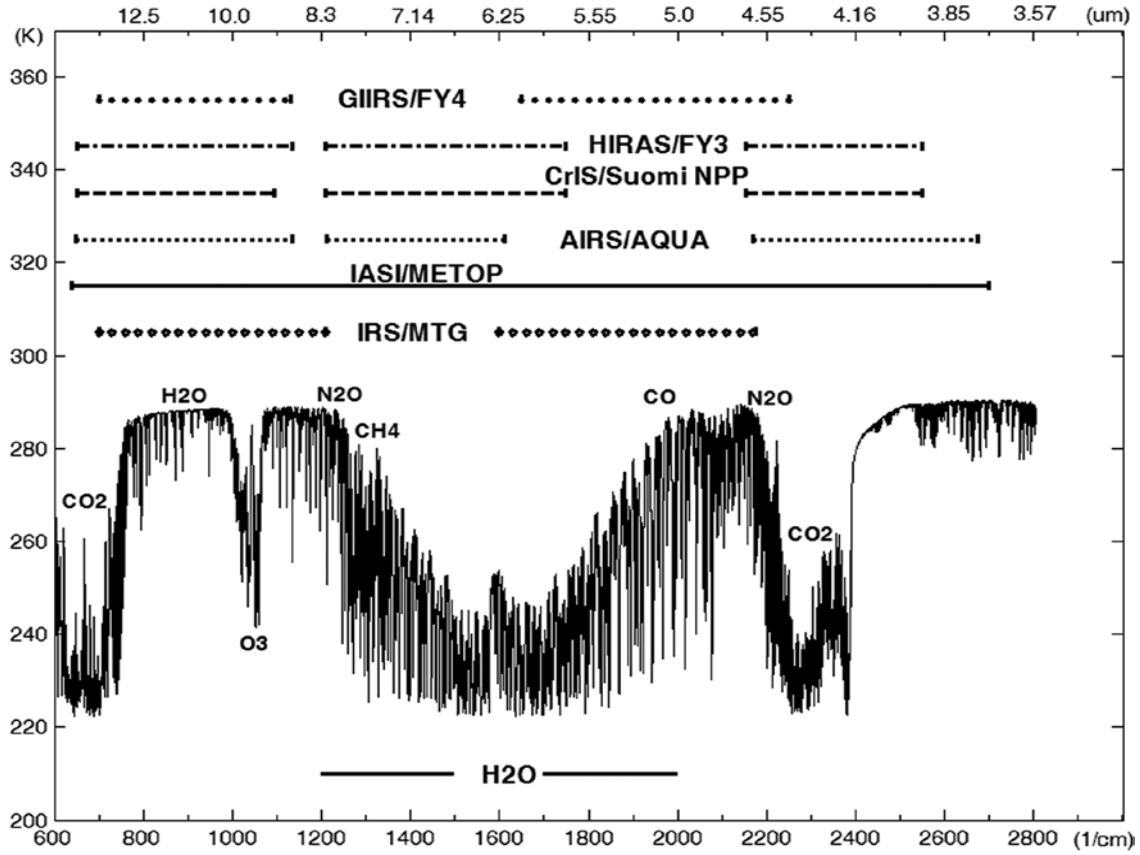

Figure 3-4. Spectral coverage of several satellite-based hyperspectral IR sounders (from Menzel et al 2018).

High spectral IR observations can also be used to monitor dust both during the day and night (DeSouza-Machado et al., 2010). Dust can be a surface transportation issue, as well as air quality.

4. OSSE Observing System Simulation Experiments

Over the past several decades, there have been Observing System Experiments (OSEs), Observing System Simulation Experiments (OSSEs), and hybrid-OSSE studies dedicated to objectively quantify the impact of GEO hyperspectral IR sounders in weather prediction. OSSEs provide a unique framework to evaluate the impact of current and proposed or future observing systems. While OSEs can be used to assess the value of existing observations, OSSEs attempt a quantitative evaluation of proposed observing technologies. Different from the real-world scenario, the "truth" is known in the OSSE system, providing a technique to quantitatively evaluate the impact of observations in terms of analysis and weather forecast skill. Briefly, an OSSE consists of a free-running numerical weather prediction forecast, typically from an operational model that provides a complete record of the assumed true state of the atmosphere. This model integration, usually referred to as the *nature run* should reproduce the main characteristics of the real atmosphere. Synthetic observations, from both conventional and space-based sources, and from the current and proposed instruments, are simulated from the nature run as perfect observations or with realistic error characteristics added. The synthetic observations are assimilated into a weather forecast model different from the model used to generate the nature run. Impact of current and proposed observations are validated against the nature run. It should be noted that the value and relevance of each OSSE will depend critically on the assumptions and simplifications (e.g., spatial, spectral, and temporal sampling and resolutions) the authors make when building their simulation. This is important as available computing power can drive simplifications that have the potential to impact the veracity of the results.

In this study, previous OSSEs and hybrid OSSEs were examined in existing literature and summarized in Figure 4-1 below. Global OSSEs and regional OSSEs are also noted there. The confidence in an OSSE is enhanced when it is possible to compare it with an OSE (e.g. OSSE results using a synthetic version of the current observing system are compared with the OSE using real data from the current observing system).

	Authors	Year	Org	Sensor	OSSE (NR & Forecast Res and refresh)	OSSE Summary	Results / Improvement
REGIONAL	Li	2018	CIMSS	GEO IASI, 4km, 1 hr	2, 9 km 3-6 hr	Quick regional rOSSE for a single case study using Weather Research and Forecasting-Nonhydrostatic Mesoscale Model (WRF-NMM) (NR) and Advanced Research version of the WRF model (WRF-ARW) (forecast)	Up to 7% improvement for T and U,V Winds
	Jones and Koch	2017	NSSL	GEO AIRS 4 km	4, 12 km 15m, 1hr	Quick rOSSE for a single case study of regional Local Severe Storm (LSS) forecasts using Global Forecast System (GFS) (NR) and WRF-ARW (forecast)	28% and 18% improvement in temperature and humidity; improved probably of storm detection (40 to 80%)
	Wang and Huang, et. Al	2013	NCAR	MTG-IRS 4 km	4, 12 km 1-6 hr	OSSE for 3 convective case studies using the NCAR Mesoscale Model Version 5 (MM5) (NR) and WRF (forecast)	20% improvement in temperature and humidity; 2.5% in winds
	Huang, Wang, et. al	2008	NCAR	MTG-IRS 4 km	4, 12 km 1-6 hr	OSSE for 3 convective case studies using the NCAR MM5 (NR) and WRF (forecast)	25% and 33% improvement in temperature and humidity; 4- 15% in winds
	Aune, Menzel	1999	CIMSS	GEO HS Sounder	60, 40 km 1 hr	Regional OSSE with NCEP Eta (NR) and GFS (data assimilation) and WRF (forecast)	40% and 44% improvement in temperature and humidity over radiometer alone
GLOBAL	Casey, Atlas, Hoffman	2018	CIMAS & NOAA/ AOML	GEO-HSS 7 km	20 Km 12 hrs	Global OSSE using constellation of GEO HS sounders with Goddard Earth Observing System Model, Version 5 (GEOS-5) (NR) and NCEP GFS (forecast)	Slight significant impact to global models (1%).
	McCarty	2016	GSFC/ GMAO	LEO 4 plane const. of MTG-IRS - like sounders	7, 28 km	GMAO Meteorological OSSE framework: GEOS-5 (NR), GEOS atmospheric data assimilation system (ADAS), 4D-EnVar (forecast)	Positive impacts out to day 2.5. Temperature error improved at low levels and near poles.
	Casey, et al.	2014	NOAA/ NESDIS	GEO AIRS	20 km	Global OSSE using ECMWF T511 (NR) and GDAS/GFS (forecast)	Slight statistically significant improvements, with best results for longer term impacts

Regional analyses shows greatest potential benefit

Global analyses shows lower potential benefit

Figure 4-1. Summary of IR sounder OSSEs and hybrid OSSEs from existing literature.

OSSE results can also be used to examine forecast impacts from different observational inputs, different sensor inputs, or even from sensor input variants. Using the Met Office global modeling system, Joo et al., 2013 (Figure 4-2) demonstrated the large impact of high-spectral-resolution IR sounders; note that most of this impact is from the LW spectral bands. Figure 4-6 shows the “observation impact and mean impact per observation of each sounder in [their] study. The impacts per sounding of the hyperspectral IR sounders, MetOp-A/IASI and Aqua/AIRS, are larger than those of the microwave sounders.” A recent OSSE suggests benefits of hyperspectral IR information in monitoring the temperature and moisture above clouds (Feng et al., 2021).

In the case of Global OSSEs, a ring of geostationary sounders was not previously explored. Additional OSEs and OSSEs were executed under this study to assess the level of impact of the infrared radiance observations from this hyperspectral sounder (HSS) in geostationary orbit. Three research groups are developing independent OSSE/OSEs to help make these assessments: the Global Modeling and Assimilation Office (GMAO) at NASA’s Goddard Space Flight Center, the Center for Satellite Application and Research (STAR) at NOAA/NESDIS and the Atlantic Oceanographic and Meteorological Laboratory at OAR/AOML, and Cooperative Institute for Meteorological Satellite Studies (CIMSS) at University of Wisconsin-Madison. The following subsections describe the experiments each of these three groups executed. The results and impact to NWP assessed from these experiments are summarized in Sections 4.1 through 4.3.

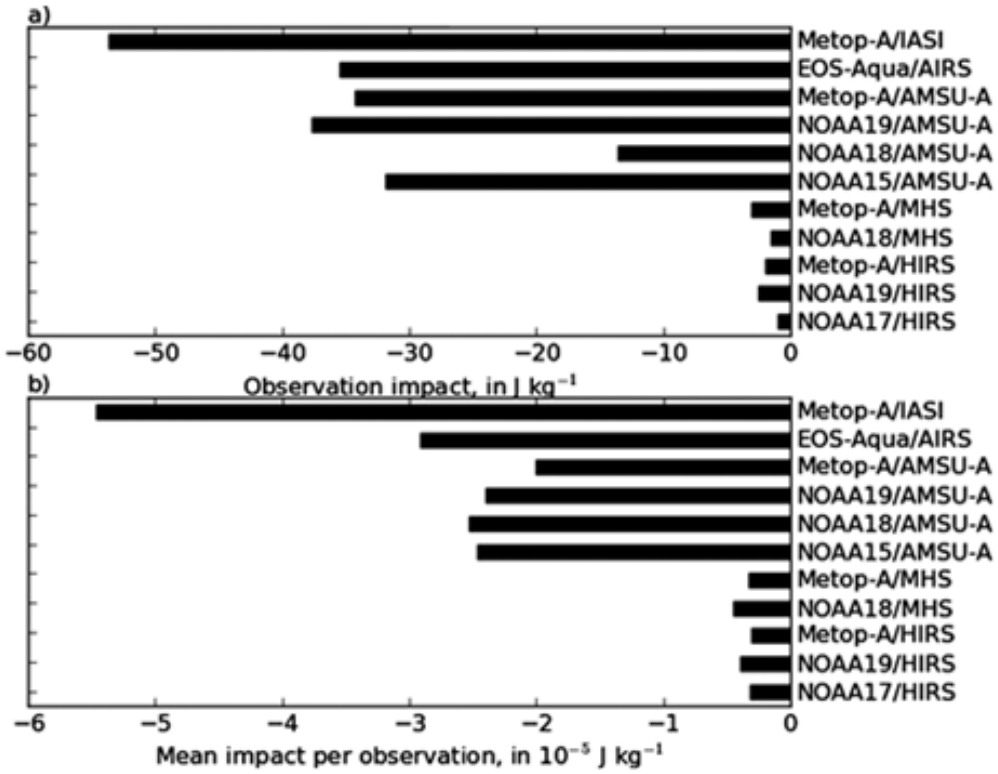

Figure 4-2 (a) Observation impact and (b) mean impact per observation of the instruments using MWS and IRS techniques in the Met Office global modelling system. (From Joo et al., 2013)

The STAR/NESDIS and AOML/OAR groups are running in coordination three OSSEs to assess the impact of an infrared hyperspectral sounder with spectral range identical to the Metop IASI instrument but with 4-km nadir sampling from the GOES-East position. The first OSSE investigates the impact of the hyperspectral sounder on global medium-range NWP using full-disk observations at 30-minute repeat time. Analysis metrics include global and regional 500 hPa height anomaly correlation, root-mean-squared (rms) wind errors, continental United States precipitation scores, and an overall forecast score (OFS) metric. The second OSSE investigates preliminary impact on the Hurricane Weather Research and Forecast System (HWRF) using full-disk GEO-HSS observations valid at model initialization time, and explores the value of both GEO-HSS observations in the initial and lateral boundary conditions as well as directly assimilated in HWRF. This assessment provides impact metrics including improvement of predicted hurricane tracks and intensity forecasts. A third OSSE investigates geostationary-based hyperspectral infrared measurements effectiveness of informing Warn-on-Forecast model projections considering 5-minute observations covering 1,000 x 1,000 km region. The Warn-on-Forecast System (WoFS) is a NOAA/National Severe Storm Laboratory (NSSL) research program to increase tornado, severe thunderstorm, and flash flood warning lead times. It states that “increasing the lead time and accuracy for hazardous weather and water warnings and forecasts, in order to

reduce loss of life, injury, and damage to the economy" is one of the strategic goals of NOAA. Metrics of this study include forecasted radar reflectivity, forecast time and location of convection and convective evolution, continental United States precipitation scores, and verification against Storm Prediction Center storm reports; however, results from this third OSSE are not available at the time of this report. Results of the two available assessments are presented in Sections 4.1.1 and 4.1.2.

4.1.1 OSSE results for Global Numerical Weather Prediction (NESDIS)

The NOAA/NESDIS Center for Satellite Applications and Research (STAR) has completed an OSSE to assess the impact of the GEO-HSS on global medium-range weather prediction utilizing the Community Global OSSE Package (CGOP). At the core of the CGOP is the GEOS-5 Nature Run (G5NR), used for both input to simulate the global observing system, and as the reference truth for forecast verification. An overview of the CGOP can be found in Boukabara et al. (2016a). For relevance in this study, the CGOP has been used to simulate conventional observations (e.g. radiosonde, aircraft data), global positioning system radio occultation (GPSRO) observations, and radiances from passive microwave and IR sensors from polar and geostationary orbit using the global observing system configuration from 2014.

This study considers only a single GEO-HSS from the GOES-E, 75° W longitude point. Unlike the many previous OSSEs, which rely on producing synthetic observations based on current GEO and LEO space platforms and orbital geometry, this study simulates a GEO-HSS instrument based on the current state of Fourier Transform Spectrometer (FTS) technology (Revercomb, Knutson, Coakley, personal communication). Specifically, the GEO-HSS simulated orbital geometry has a fixed grid projection, with a 128x128 pixel focal plane array. The design allows for a dwell time of ~4.6s for each patch, resulting in a 30-minute full-disk scan, and a 5-minute mesosector view of approximately 1000 x 1000 km. Figure 4-3 illustrates the scan geometry of the GEO-HSS with 4 km spatial resolution at the sub-satellite point, and generally less than 7 km at satellite zenith angles less than 60°. Using an orbit simulator tool, files containing the orbit and sensor geometry are created for each 30-minute full disk image including latitude, longitude, time, satellite zenith and azimuth angles, and solar zenith and azimuth angles, for the August and September 2006 time period from the G5NR.

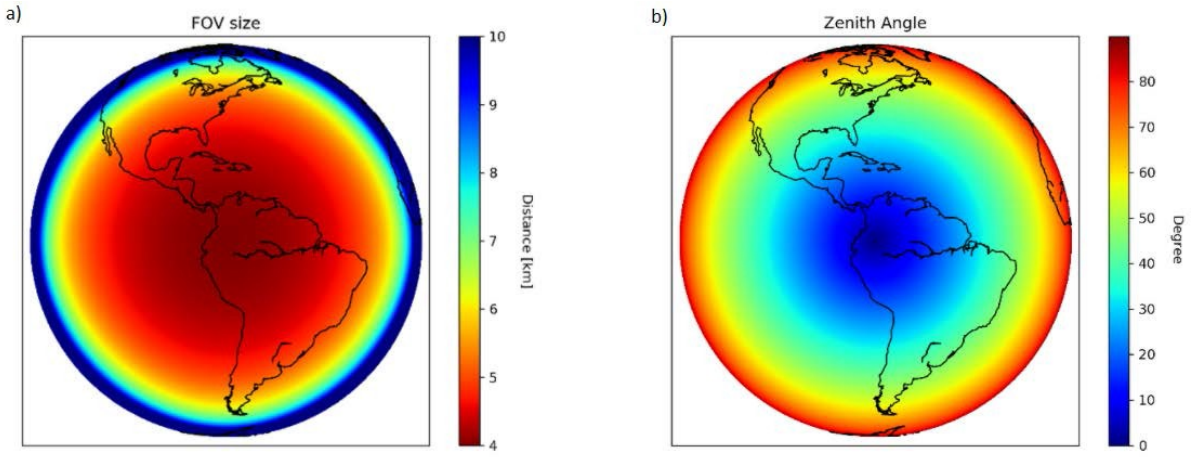

Figure 4-3. a) Field-of-view size and b) satellite zenith angle of the GEO-HSS simulated at the GOES-E 75° W longitude.

Each full disk image contains approximately 6.4M fields-of-view (FOVs). Because of the large volume of data to be produced for the GEO-HSS OSSE, only the orbit simulator output for three consecutive full disk images at and around each synoptic time the data assimilation (00Z, 06Z, 12Z, 18Z, and +/- 30 minutes) are used in the CGOP radiance simulator. Given the data assimilation technique employed, discussed below, full disk observations beyond the +/- 30 minutes would not be assimilated. To represent the GEO-HSS instrument spectral coverage in simulation, the Metop IASI instrument is chosen. Specifically, channels from the IASI-616 channel subset are simulated at each GEO-HSS FOV using the Community Radiative Transfer Model (CRTM, Chen et al. 2008, Han et al. 2006). To be consistent with the simulation of all observation types from the CGOP 2014 observing system, all radiance simulations are clear-sky, perfect observations, i.e. no hydrometeors, instrument errors, radiative transfer modeling, or representativeness errors are added to the radiance simulation. The radiances from all observation types, including IASI, were well validated in Boukabara et al. 2018. An example of the GEO-HSS full disk observations on August 1, 2006 00Z for the

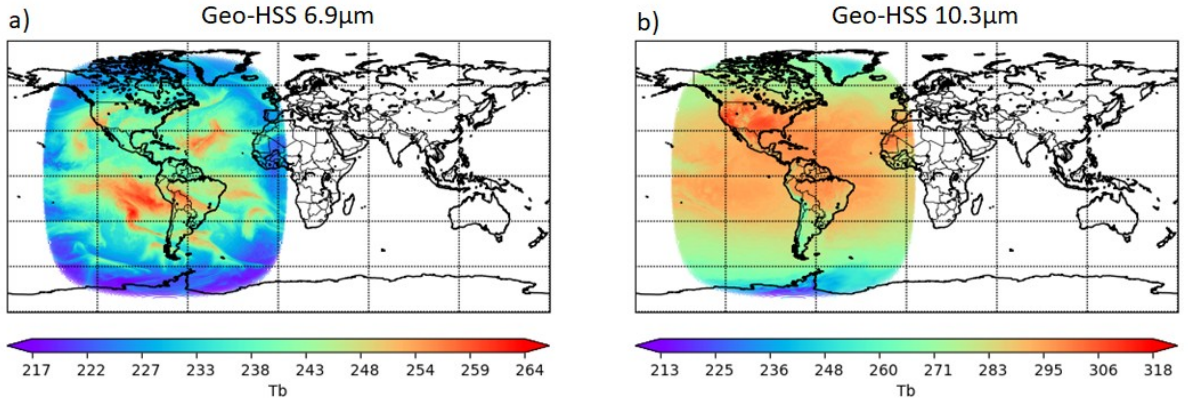

Figure 4-4. Simulated GEO-HSS clear-sky radiances for a) 6.9 µm and b) 10.3 µm, for August 1, 2006 00Z.

The original CGOP package was linked to NOAA/NCEP's Global Data Assimilation

System/Global Forecast System (GDAS/GFS) which employed the Hybrid 3DVAR scheme and GFS spectral model. For this OSSE, the CGOP was updated with a more recent version of the GDAS/GFS using the 4DEnVar (Wang and Lei, 2014) and Finite-Volume Cubed-Sphere dynamical core (Putman et al. 2007), hereafter referred to as the FV3GFS. The version of the FV3GFS used in this OSSE study became operational at NCEP in June 2019.

To assimilate the GEO-HSS observations, the Gridpoint Statistical Interpolation (GSI) component of the GDAS, which performs the variational analysis, was modified for the new observation type, but following the quality control (QC), bias correction, and observation errors for IASI, as well as the selection for channels assimilated from the 616 simulated channels.

Figure 4-5 illustrates a single spectrum of the GEO-HSS (blue), with notable features in the longwave IR (LWIR) temperature sounding region near 13 μm and atmospheric window, the 9.6 μm O_3 band, the 6.9 μm water vapor region, and the shortwave IR (SWIR) region. The black dots identify the channels from the 616 channel set that are assimilated in the GSI, which include 125 LWIR temperature sounding channels, 15 water vapor sounding channels, and 35 channels in O_3 and window regions. For comparison, the MTG IRS spectral region is shaded in gray. The original intent of this OSSE study was to simulate and assimilate an IRS-like instrument; but given CRTM limitations in simulating IRS and the need for validation, along with procedures in place to simulate and assimilate an IASI-like instrument including water vapor sounding channels, an IASI-like instrument was chosen.

Data assimilation and forecast cycling experiments are performed using the CGOP combined with the FV3GFS for August and September 2006. The FV3GFS deterministic analysis and forecast is run at C384 resolution (~25 km) while the 80-member ensemble component is run at C192 (~50 km). As mentioned previously, all operationally assimilated observations from the 2014 global observing system are assimilated in the control run (CTL), while the GEO-HSS experiment (GEO-HSS) includes the GEO-HSS observations on top of CTL. Neither experiment includes simulated GOES-13 observations.

Figure 4-6 shows the impact of performing QC and bias correction procedures during the GEO-HSS assimilation for a midwave IR water vapor channel at 1421.26 cm^{-1}. As with IASI data, only clear-sky radiances are assimilated. Figure 4-6a shows the typical observation minus background (O-B) field with large departures between the simulated observation and the simulated background field, and the improved fit in the observation minus analysis field in 4-6b. Figure 4-6c demonstrates the impact of QC, where realistic cloud screening is performed on the GEO-HSS radiances.

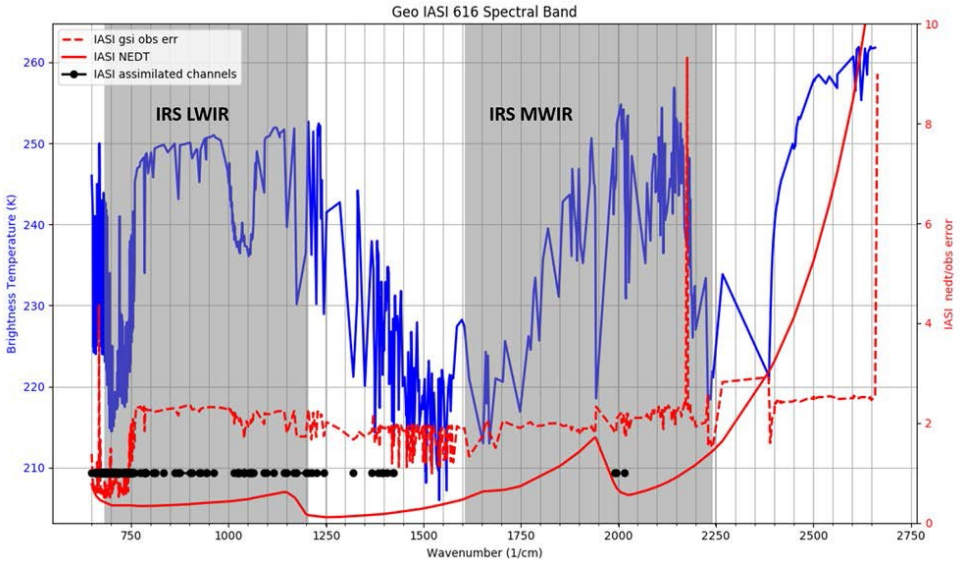

Figure 4-5. Example simulated spectrum of the GEO-HSS 616 channel set (blue), assimilated channels (black dots), along with IASI noise and typical observation errors (red solid/dashed lines), and MTG IRS spectral coverage (gray shaded areas).

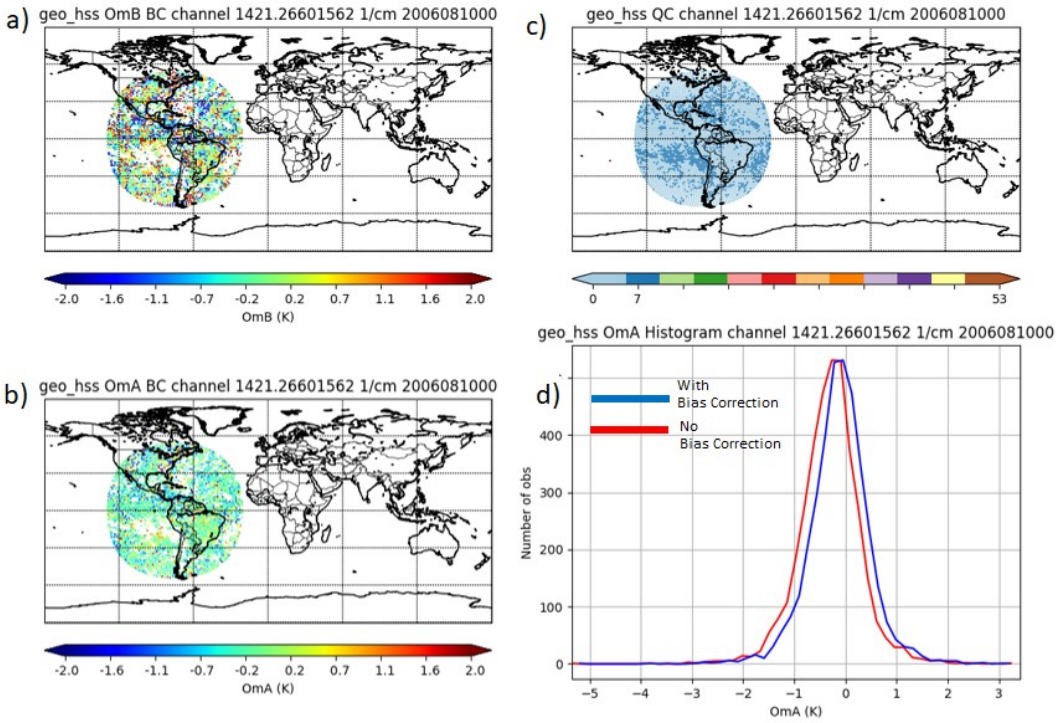

Figure 4-6. Output from 2006-08-10 00Z data assimilation cycle showing GEO-HSS a) O-B and b) O-A after quality control and bias correction, c) quality control flags, and d) O-A histograms before and after bias correction at 1421.26 cm^{-1}.

Figure 4-6d shows the histograms of O-A before and after bias correction, using the same variational bias correction as with IASI. The FV3GFS assimilates approximately 5,000 LWIR observations per cycle and 2,000 midwave/window observations, which are both a strong function of where the channels peak in the atmosphere due to cloud screening. Additionally the data are thinned to 140 km.

Several forecast metrics were assessed as part of the NCEP verification and statistics package (VSDB). An overview snapshot of the forecast impact is shown in Figure 4-8. The performance scorecard shows anomaly correlation (AC) and root-mean-square error (RMSE) for a variety of forecasted parameters, for different regions, forecast days, and atmospheric

levels. Shaded cells represent neutral impact, while green shaded regions, small triangles, and large triangles show positive impact at the 95%, 99%, and 99.9% confidence levels when assimilating GEO-HSS. Red shading and symbols are analogous to the green except it represents degradation when assimilating GEO-HSS. Overall, there is large positive impact in all regions for stratospheric heights and temperature RMSE, and positive impact on some tropospheric temperature RMSE, but degradation in layers around the tropopause for height RMSE at Day 1 and Day 3.

To highlight a few specific examples of forecast impact, Figure 4-9 shows the geopotential height AC at 500 hPa for the northern hemisphere and southern hemisphere. Although there is an improvement in the AC at all forecast times, the improvement is not statistically significant (as shown in the scorecard).

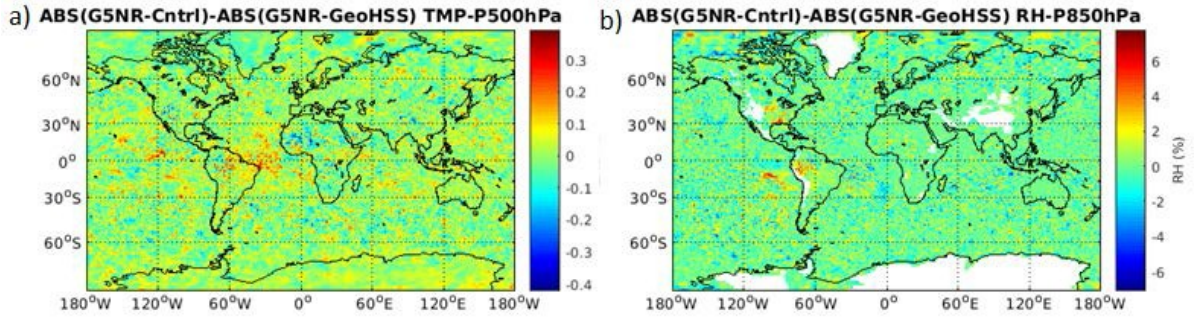

Figure 4-7. Mean difference of the absolute difference from G5NR-CTL and G5NR-GEOHSS for a) 500 hPa temperature, and b) 850 hPa relative humidity. Positive values indicate improvement.

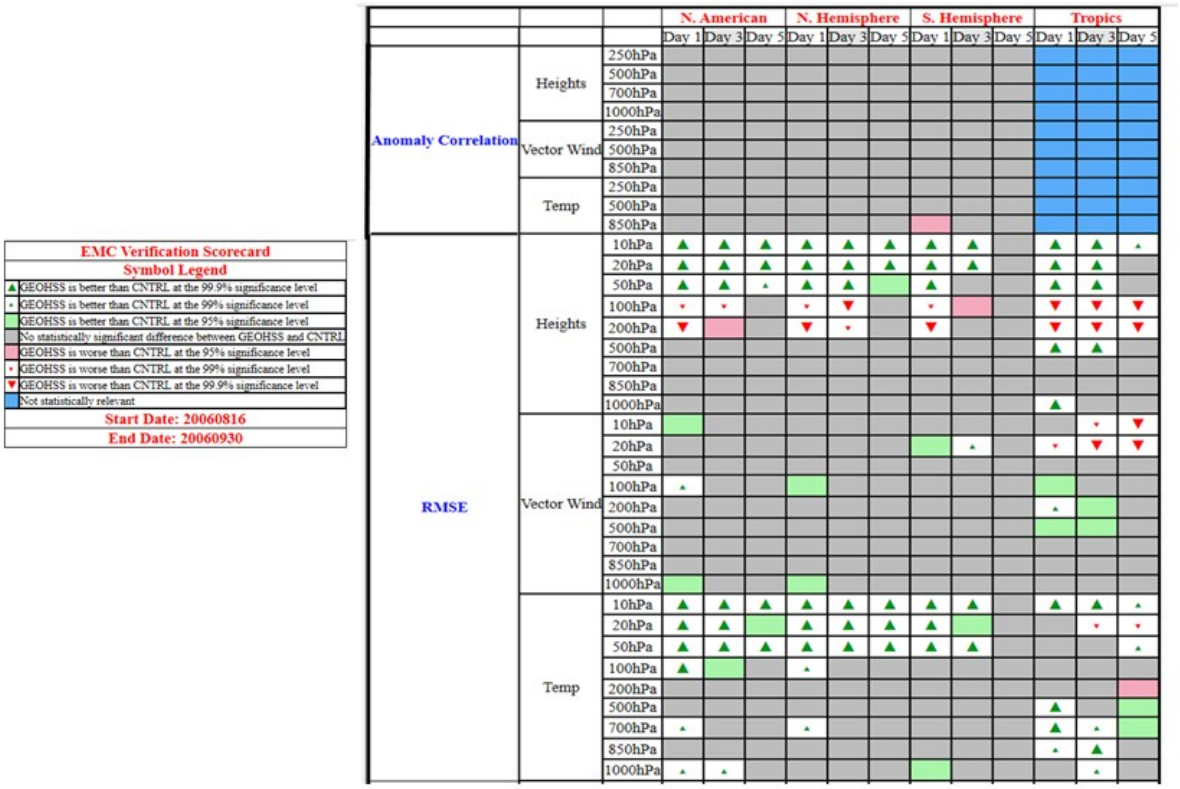

Figure 4-8. Verification scorecard demonstrating impact from the assimilation of GEOHSS observations. See legend or text for a description of symbols and shading.

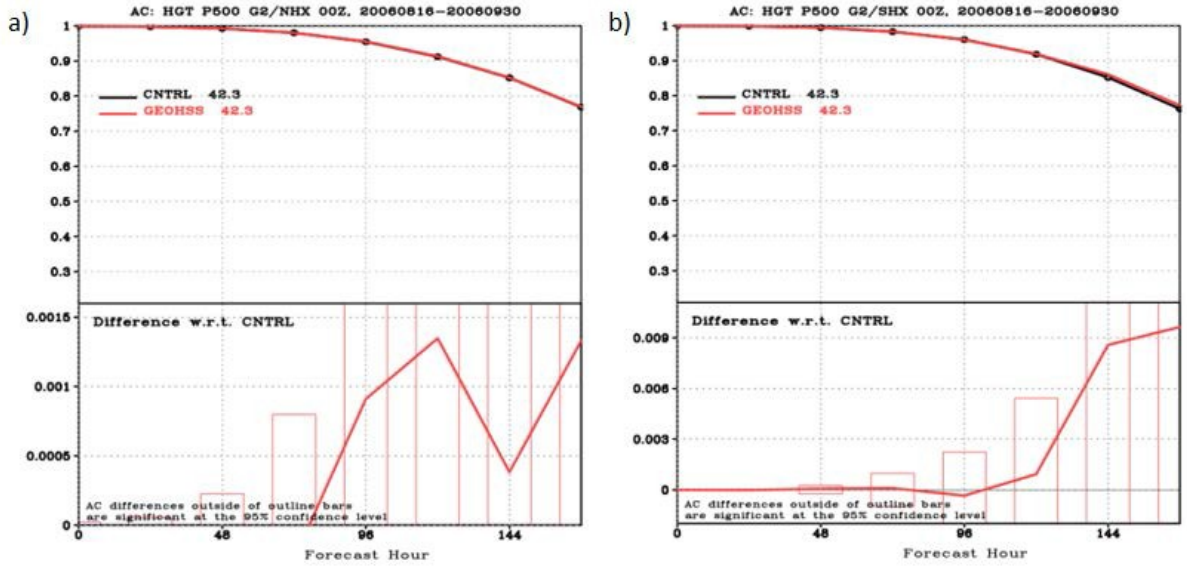

Figure 4-9. 500 hPa height anomaly correlation as a function of forecast hour for the CTL (black) and GEOHSS (red) experiments for a) Northern Hemisphere and b) Southern Hemisphere. Bottom panels show the difference of AC scores with respect to the CTL. Red bars indicate the 95% confidence interval.

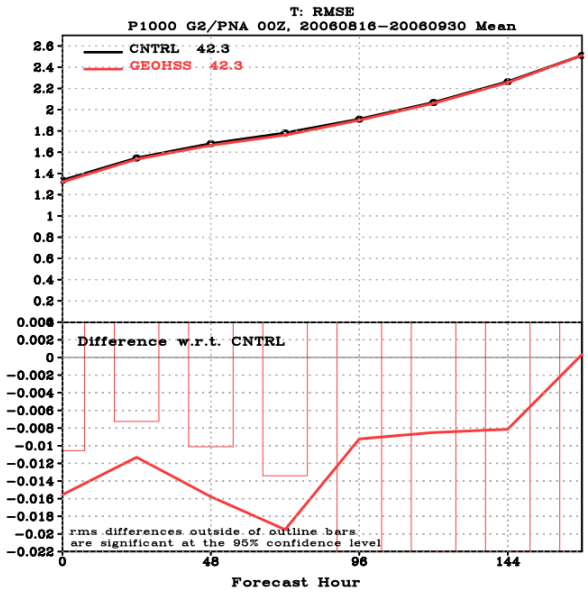

Figure 4-10. Same as in Figure 4-13, but for 1000 hPa temperature RMSE for the Pacific/North America region.

Figure 4-10 shows the 1000 hPa temperature RMSE over the Pacific/North America domain (PNA). Here, the temperature RMSE is reduced significantly at Days 1-3 when GEO-HSS is assimilated.

It is expected that with any data addition or data denial experiment, the impact can be positive for some metrics and negative for others. Therefore, based on all metrics for RMSE and AC shown in the scorecard, plus relative humidity, an Overall Forecast Score (OFS) was derived (Boukabara et al. 2016b). The OFS metric normalizes the RMSE and AC scores from both experiments for all parameters (for all lead times, levels, and regions) to compute an overall score between 0 and 1. Zhou et al (2019) also demonstrated that the relative OFSs between forecast experiments were consistent between the CGOP OSSE framework and Observing System Experiments (OSEs) using real observations. The OFS for the CTL and GEOHSS experiments are shown in Figure 4-11. The OFS for the CTL is ~0.555 while the GEOHSS OFS is ~0.56. Although the magnitude of the improvement in OFS when assimilating GEO-HSS observations is small, it is statistically significant at the 95% confidence interval.

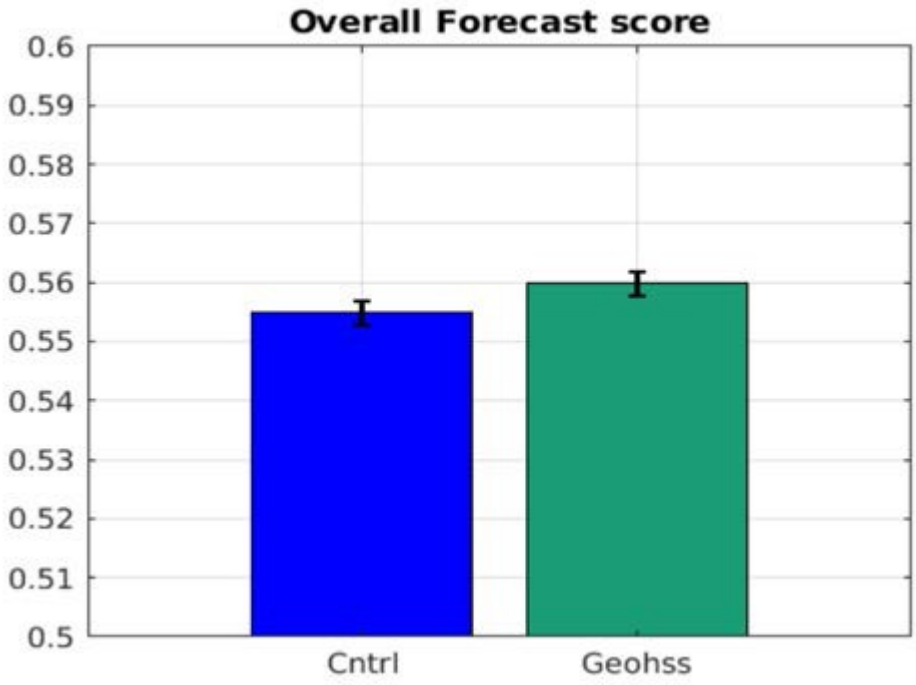

Figure 4-11. The Overall Forecast Score (OFS) shown for the CTL (blue) and GEOHSS (green) experiments.

4.1.2 OSSE results of Hurricane prediction metrics (AOML)

AOML conducted additional OSSEs in an attempt to quantify the potential impact of GEO-HSS observations on numerical weather prediction, with emphasis on hurricane analyses and forecasts. Both global experiments with FV3GFS and regional experiments with the operational hurricane HWRF were conducted.

The same orbital configuration described in section 4.1.1 was used to simulate hyperspectral infrared observations based on the IASI spectrum (IASI 616 subset), utilizing large area focal plane arrays over a full disk covering the eastern US through all of South America. In this case, the COSS (Consolidated Observing Systems Simulator) was used to simulate perfect observations from the GEOS-5 7-km Nature Run (G5NR). For the global OSSE, Geo-HSS observations were simulated at every 5th point (~20 km horizontal resolution at nadir). The temporal sampling was 6 hours, centered at the analysis time. This resolution was increased to a 1-hr interval for the HWRF runs. Global runs used 20 ensemble members, and this number increased to 40 members to generate the initial and boundary conditions for the HWRF runs. Global runs extended through August-September, based on the August-September 2014 observing system architecture. August was used for spin-up, and verification was conducted for September. A representation of the sampling distribution of assimilated GEO-HSS profiles for both the global and regional OSSEs is shown in Figure 4.12 and a representation of the percentage of profiles assimilated by channel and wavenumber is shown in Figure 4-13. During the time period under evaluation, a tropical cyclone (AL03) was identified in the G5NR (Figure 4-14). Using the global runs as initial and boundary

conditions, two OSSEs were conducted with HWRF, each including two experiments, to assess the impact of GEO-HSS observations on hurricane prediction. The HWRF OSSEs focused on the evaluation of the assimilation of GEO-HSS observations through: (1) the impact of data assimilation in the global run as a result of improved initial and boundary conditions in HWRF and (2) the direct assimilation of GEO-HSS into the hurricane system in addition to its assimilation in the global model. Results are presented below.

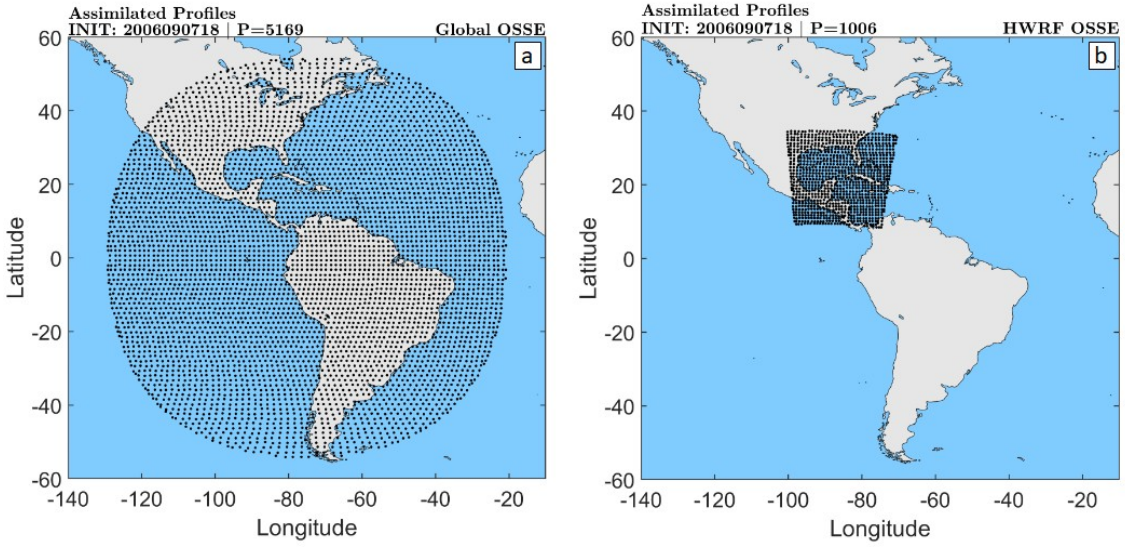

Fig. 4-12. Spatial distribution of assimilated GEO-HSS profiles (P) in the (a) global and (b) regional (HWRF) OSSEs for representative cycle 2006090718.

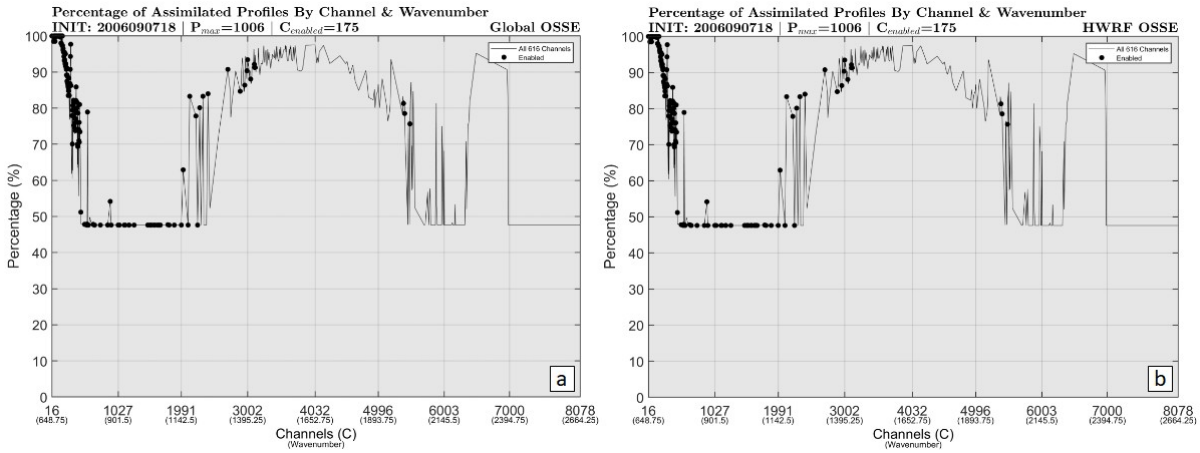

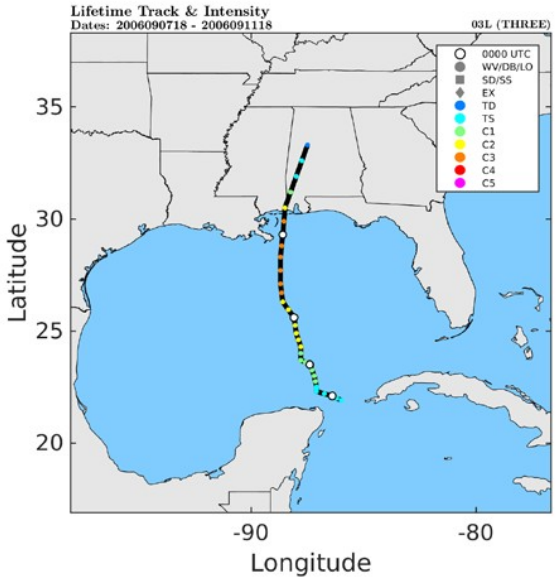

Fig. 4-14. The 3-h track of AL03 from the G5NR. White circles indicate each 0000 UTC time. Dark gray circles represent times when the storm was designated as a wave (WV), a disturbance (DB), or a low (LO). Dark gray squares represent times when the storm was designated as a subtropical depression (SD) or subtropical storm (SS). Dark gray diamonds represent times when the storm was designated as an extratropical storm (EX). The colored circles represent intensity according to the Saffir–Simpson hurricane wind scale categories: tropical depression (TD; dark blue), tropical storm (TS; cyan), category 1 hurricane (C1; green), category 2 hurricane (C2; yellow), category 3 hurricane (C3; orange), category 4 hurricane (C4; red), and category 5 hurricane (C5; magenta).

Results from the Global OSSE

Fig. 4-15 summarizes the impact of GeoHSS observations on global 500 hPa temperature root-mean-square (RMS) error. Fig. 4.15(a) highlights the difference between Control and Control+GeoHSS every 6 hours through a 240-hour forecast cycle. Red bars denote a 95% confidence interval. Note that globally, a statistically significant improvement (reduction in RMS error) is noted at forecast hours 0-42, as well as hours 204-240. This shows the value of a single GeoHSS instrument globally, even with a limited view of the globe. Fig. 4.15(b) shows a time-series of analysis-time RMS errors for Control and Control+GeoHSS through the 30-day experiment period. Note that while there are some days where analysis RMS is greater for Control+GeoHSS, for most days this RMS is lower than Control. The mean RMS values for the month are included in the legend, and show on average a 2.6% reduction in RMS error. Fig. 4.15(c) highlights the RMS error reduction in different regions of the globe. The largest reduction in RMS error is noted in the Tropics, while the lowest is in the Southern Hemisphere Extratropics. This RMS error reduction is statistically significant in all regions, as denoted by bold green type.

Fig. 4-16 is plotted in the same style as Fig. 4-15(a), for 500 hPa Geopotential Height RMS error for the (a) Northern Hemisphere Extratropics, (b) Continental US, and (c) Southern Hemisphere Extratropics. In these extratropical regions, 500 hPa Geopotential Heights are a good way to track synoptic-scale meteorological features. Little statistically significant impacts are noted, with the exception of long-term forecasts (hours 204-228) over the Southern Hemisphere Extratropics. Despite the impacts noted with respect to temperature in Fig. 4-15, Fig. 4-16 suggests that impacts on extratropical meteorology may be minimal.

(a)

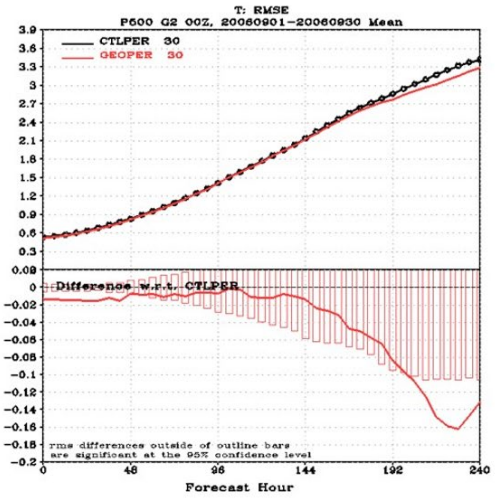

(b)

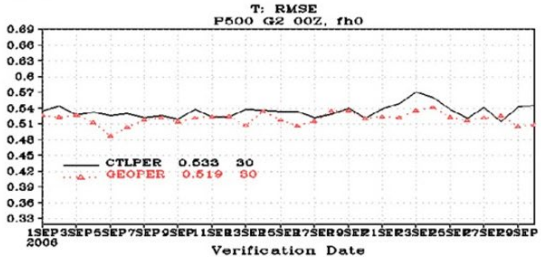

(c)

Region	Analysis Impact
Northern Hemisphere Extratropics	-2.1%
Continental US	-2.8%
Tropics	-3.5%
Southern Hemisphere Extratropics	-1.6%

Fig. 4-17 shows GeoHSS impacts on 200 hPa Tropical Vector Winds, a good predictor of mesoscale convective system movement. While little impact is noted at analysis time, the 48-72 hour forecast period shows a significant reduction in RMS error. This suggests a potential impact on downstream tropical convective systems in short- to medium-term forecasts.

Fig. 4-15. (a) Upper panel: Global 500 hPa Temperature root-mean-square (RMS) Error for Control (black) and Control+GeoHSS (red) with respect to G5NR from analysis time to 240-hour forecast. Lower panel: Difference between Control and Control+GeoHSS. Red bars denote 95% confidence interval. (b) Time series of analysis-time (forecast hour 00) RMS error through experiment period. (c) Regional differences in RMS error difference at analysis time.

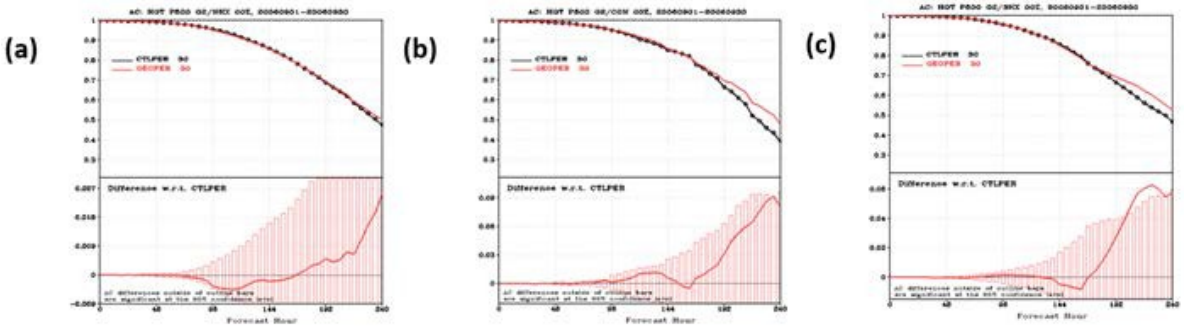

Fig. 4-16. As in Fig. 4-15(a), for 500 hPa Geopotential Height in (a) Northern Hemisphere Extratropics, (b) Continental US, and (c) Southern Hemisphere Extratropics.

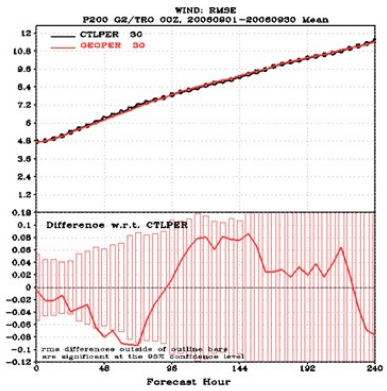

Fig. 4-17. As in Fig. 4-15(a), for 200 hPa Vector Wind over the Tropics.

Results from the Hurricane OSSEs

The regional component of this study evaluated the impact of GEO-HSS on simulated tropical cyclone AL03, a landfalling tropical cyclone from the NASA/GMAO G5NR (Fig. 4-14). Impacts were evaluated by conducting two OSSEs using the H220 version of HWRF, the latest implementation of HWRF valid as of July 2020. Both OSSEs used the same model, domain, resolution, and physics as the operational version of HWRF.

The first OSSE, hereafter called the Free Run, demonstrates the impact of having GEO-HSS in the initial and boundary conditions (IBCs) of HWRF by turning off relocation, ocean coupling, and data assimilation (DA). This means that for each cycle, HWRF solely generates forecasts from the IBCs, otherwise known as "cold starts". The IBCs for HWRF are the output from the global OSSEs. The second OSSE, hereafter called the DA Run, demonstrates the impact of assimilating GEO-HSS directly into HWRF. Ocean coupling was also turned off in this OSSE, due to the lack of ocean data from 2006. Additionally, due to the lower, 7-km resolution of the G5NR, satellite and conventional observations were only assimilated in the 4.5-km domain (D02) instead of in both D02 and the innermost, 1.5-km domain (D03) as typically done (for domain sizes, see Fig. 4-18). The IBCs for this OSSE are also the output from the global OSSEs. (See Table 4-1).

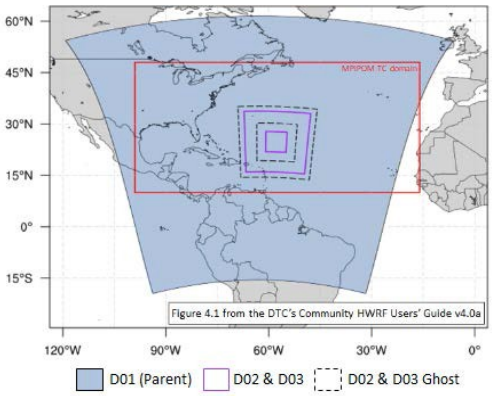

Fig. 4-18. Coverage of the HWRF 13.5-km parent domain (d01, blue shading), the vortex-following 4.5-km (D02) and 1.5-km (D03) domains (magenta boxes), the corresponding D02 and D03 ghost domains (black dashed lines), and the Atlantic MPIPOM-TC domain (red box).

Table 4-1. A description of the experiments run in each OSSE.

OSSE	Experiment	Description
OSSE #1: Free Run	GHSSFR	GEO-HSS is assimilated in the IBCs. There is no DA, relocation, or ocean coupling.
	noGHSSFR	GEO-HSS is not assimilated in the IBCs. There is no DA, relocation, or ocean coupling.
OSSE #2: DA Run	GHSSDA	GEO-HSS is assimilated in the IBCs. Satellite and conventional observations (including GEO-HSS) are assimilated in D02, only. There is no ocean coupling.
	noGHSSDA	GEO-HSS is not assimilated in the IBCs. Satellite and conventional observations (excluding GEO-HSS) are assimilated in D02, only. There is no ocean coupling.

Free Run OSSE

In both GHSSFR and noGHSSFR, overall track error between 0–42 h lead time is similar, slightly increasing from around 20 km to 40 km. After 42 h, however, track error diverges, with GHSSFR having track errors up to 50 km larger than noGHSSFR (Fig. 4-19a). These track errors were found to be associated with the first 3 cycles of the Free Run (Fig. 4-19b).

Track error can be decomposed into along-track error (Fig. 4-19c,d), which indicates whether the storm is moving faster or slower than the best track (BT), and across-track error (Fig. 4-19e,f), which indicates whether the storm is to the left of or to the right of the BT. While both the GHSSFR and the noGHSSFR were faster than and to the right of the BT, their along-track and across-track components impacted the forecasts differently. The inclusion of GEO-HSS in the IBCs minimally improves along-track forecasts between 12–48 h (Fig. 4-19c, d). On the other hand, the inclusion of GEO-HSS in the IBCs degraded the across-track forecast, with GHSSFR having larger across-track errors at lead times of greater than 36 hours (Fig. 4-19e). As with the overall track error, these across-track errors were associated with the first 3 cycles of the experiments (Fig. 4-19f).

To more easily visualize track error, Fig. 4-20 depicts track forecasts for all cycles of AL03, with the first cycle being the lightest color and the last cycle being the darkest color. Consistent with Fig. 4-19f, the first three cycles of GHSSFR (Fig. 4-20a) had track forecasts that were further east of both noGHSSFR (Fig. 4-20b) and the BT. To understand why these track differences occurred, the synoptic flow and AL03 structure in the first three cycles of GHSSFR and noGHSSFR were compared. For brevity, here, only the results from the first cycle will be shown, but results are qualitatively similar across all three cycles.

AL03 was initialized further east in GHSSFR compared to noGHSSFR (Fig. 4-21a). For the duration of each forecast, the tracks seemingly ran parallel to each other, with noGHSSFR progressing eastward slightly quicker than GHSSFR. This can be seen in the across-track error in Fig. 4-21b, where the separation between GHSSFR and noGHSSFR is nearly constant, reducing slightly with forecast lead time (Fig. 4-21b). This implies that the synoptic steering flow was similar in both the GHSSFR and noGHSSFR experiments. To visualize the synoptic flow, wind speed and geopotential height at 200 hPa are depicted in Fig. 4-22. The trough that is present over the CONUS is found in similar locations in both GHSSFR and noGHSSFR. Thus, the steering direction on AL03 would be similar, explaining the near-parallel track forecasts, and the closer proximity of noGHSSFR to the trough would explain the slightly more eastward-moving track forecast compared to GHSSFR as seen in Fig. 4-

22a. The track errors seen in Fig. 4-19, therefore, were mainly a function of initialization location of AL03 in the IBCs.

Track error and improvement were calculated again without these first three cycles for three reasons (Fig. 4-23): 1) the initialization of AL03 in the first three cycles of GHSSFR was found to be the underlying cause of the track errors at later lead times, 2) in the Free Run, storm relocation is turned off so there is no adjustment of the initialization location, and 3) the global OSSE might not be able to adequately resolve the location of AL03 when it is first forming. By removing the first three cycles from the error statistics, GHSSFR was found to improve track forecasts at nearly all lead times, with track error differences ranging from 0–35 km with an average difference of 11 km (Fig. 4-23c, d). GHSSFR was most impactful at greater than 48 h lead times, where track error was reduced by around 25 km on average.

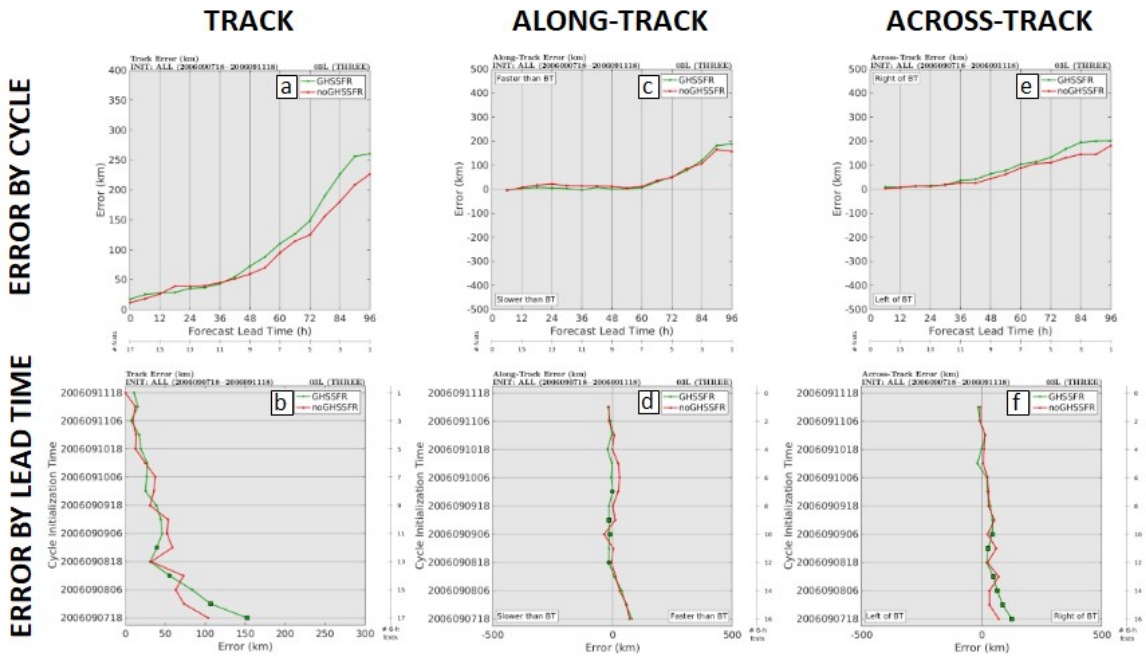

Figure 4-19: (a,b) Track errors, (c,d) along-track errors, and (e,f) across-track errors by (a,c,e) lead time and (b,d,f) cycle for GHSSFR (green line) and noGHSSFR (red line). If present, squares (circles) indicate 95% (90%) significance as determined by a paired t-test w/ serial correlation.

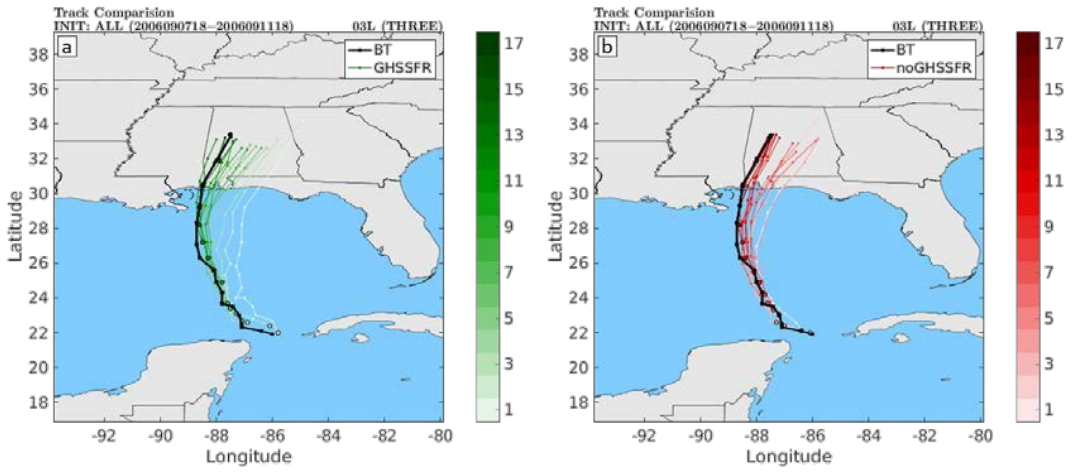

Figure 4-20. A comparison of track forecasts for (a) GHSSFR and (b) noGHSSFR to the best track (BT; black line) of AL03. The first cycle (2006090718) is shown in the lightest color while the last cycle (2006091118) is shown in the darkest color. Colored circles outlined in black indicate the location of AL03 at initialization time. Dots along each track occur every 6 h.

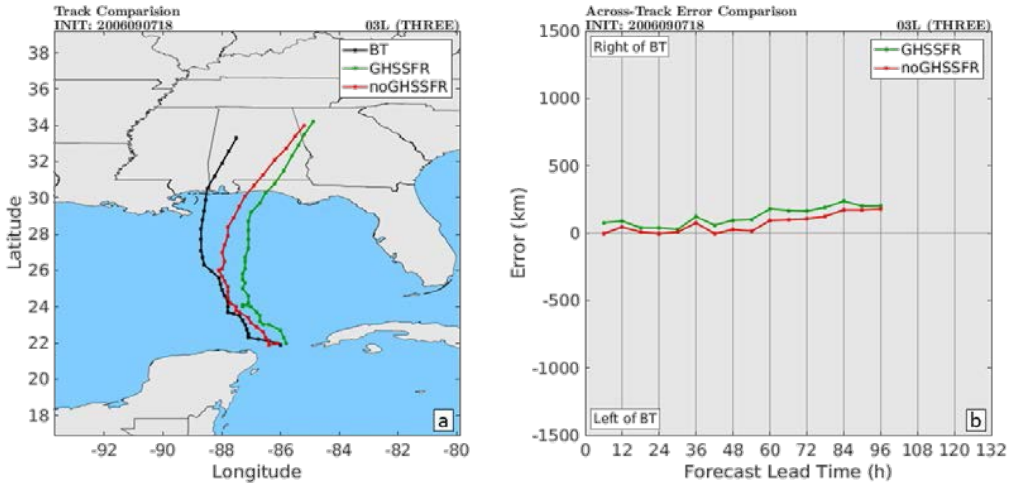

Figure 4-21. A comparison of AL03 (a) track forecasts and (b) across-track error forecasts for GHSSFR (green line) and noGHSSFR (red line) for cycle 2006090718. In (a), the best track (BT) is given by the black line. In (b), if present, squares (circles) indicate 95% (90%) significance as determined by a paired t-test w/ serial correlation.

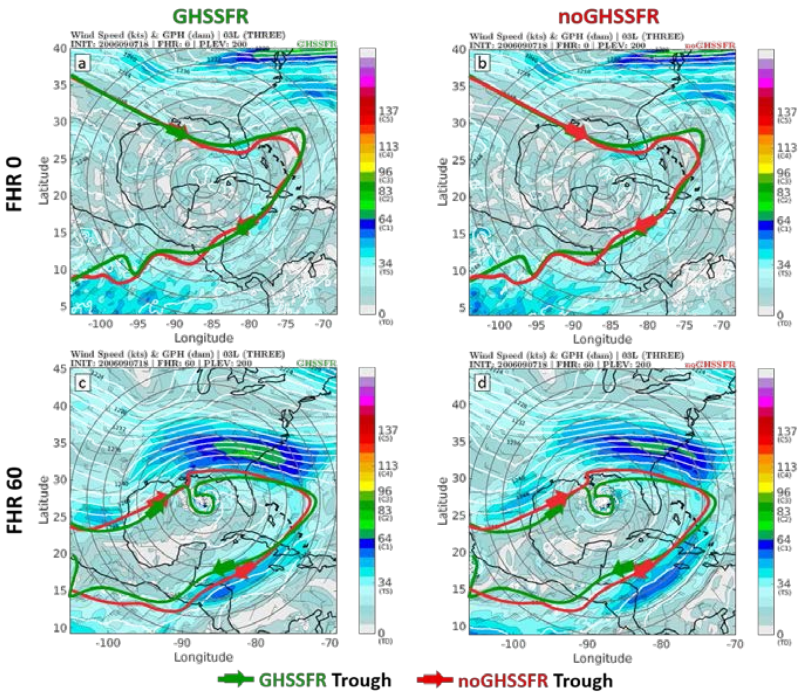

Figure 4-22. The upper-level (200-hPa) wind speed (kts; shaded and barbs) and geopotential height (GPH; dam; white contours) for (a, c) GHSSFR and (b, d) noGHSSFR at (a, b) forecast hour (FHR) 0 and (c, d) FHR 60. The green (red) line highlights the 1248 dam contour for the GHSSFR (noGHSSFR). The colorbar label represent intensity according to the Saffir–Simpson hurricane wind scale categories: tropical depression (TD; light blues), tropical storm (TS; cyans), category 1 hurricane (C1; greens), category 2 hurricane (C2; yellows), category 3 hurricane (C3; oranges), category 4 hurricane (C4; reds), and category 5 hurricane (C5; magentas).

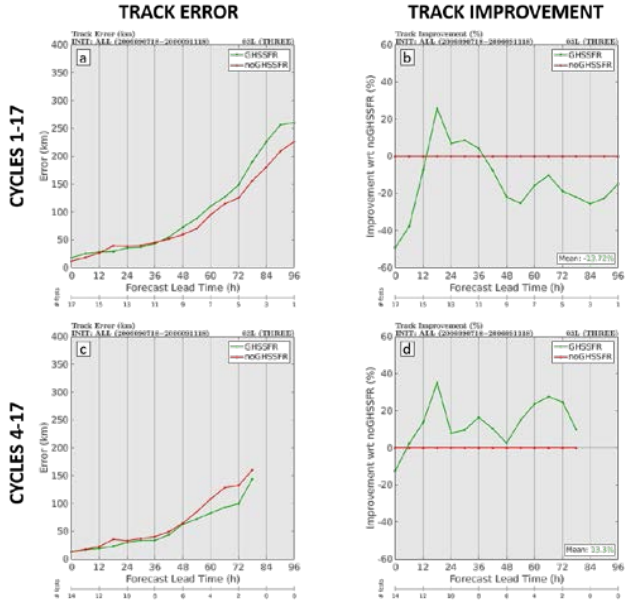

Figure 4-23. (a,c) Track errors (km) and (b,d) track improvement (%) for GHSSFR (green line) and noGHSSFR (red line) for (a,b) cycles 1-17 and (c,d) cycles 4-17. If present, squares (circles) indicate 95% (90%) significance as determined by a paired t-test w/ serial correlation.

DA Run OSSE

Overall track error in both GHSSDA and noGHSSDA is similar during the first 24 hours of the experiments. Afterwards, track error diverges, with GHSSDA having track errors up to 50 km larger than noGHSSDA (Fig. 4-24a). These track errors were found to be associated with the cycles two and three of the DA Run (Fig. 4-24b).

As in the Free Run, by decomposing track into along-track error (Fig. 4-24c,d) and across-track error (Fig. 4-24e,f), it was found that both the GHSSDA and the noGHSSDA were faster than and to the right of the BT, but their along-track and across-track components impacted the forecasts differently. Having GEO-HSS in the IBCs and directly assimilated into HWRF was found to improve along-track forecasts at nearly all lead times (Fig. 4-24c, d). On the other hand, the inclusion of GEO-HSS degraded the across-track forecast for lead times greater than 24 hours (Fig. 4-24e). As with the overall track error, these across-track errors were associated with cycles two and three of the experiments (Fig. 4-24f).

Fig. 4-25 depicts the track forecasts for all cycles of AL03. Consistent with Fig. 4-25f, GHSSDA cycles two and three (Fig. 4-25a) had track forecasts that were further east of both noGHSSDA (Fig. 4-25b) and the BT. Once again, the synoptic flow and AL03 structure were compared in order to understand why these track differences occurred. Results were qualitatively similar to those found in the Free Run: slightly different initialization locations of AL03 between GHSSDA and noGHSSDA combined with a similar synoptic setup led to a similar steering direction and a slightly more eastward-moving noGHSSDA due to trough proximity (not shown for brevity).

Therefore, as in the Free Run, track error and improvement were calculated excluding not just cycles 2 and 3 which had the large across-track errors but also the first cycle, for consistency. By doing so, GHSSDA was found to have negligible impact on track forecasts, with track error differences ranging from 0–27 km with an average difference of 8 km (4-23c, d). While there was minimal track degradation between 30–60, differences were small - around 12 km on average. Additionally, while track forecasts improved after 66 h by around 26 km on average (4-26c, d), the sample size was small.

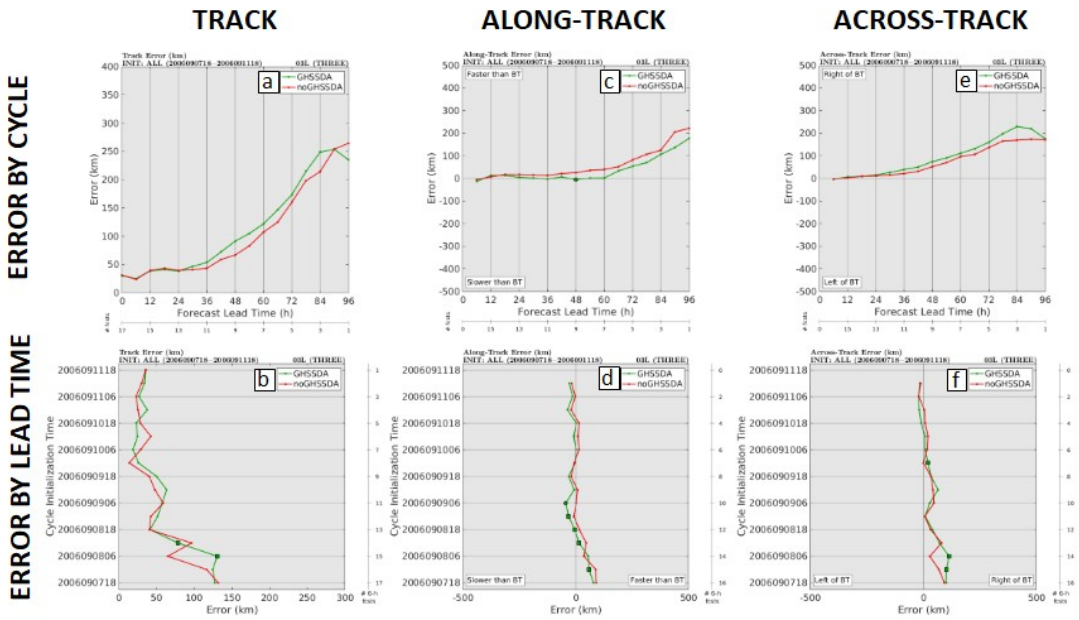

Figure 4-24. (a, b) Track errors, (c, d) along-track errors, and (e, f) across-track errors by (a, c, e) lead time and (b, d, f) cycle for GHSSDA (green line) and noGHSSDA (red line). If present, squares (circles) indicate 95% (90%) significance as determined by a paired t-test w/ serial correlation.

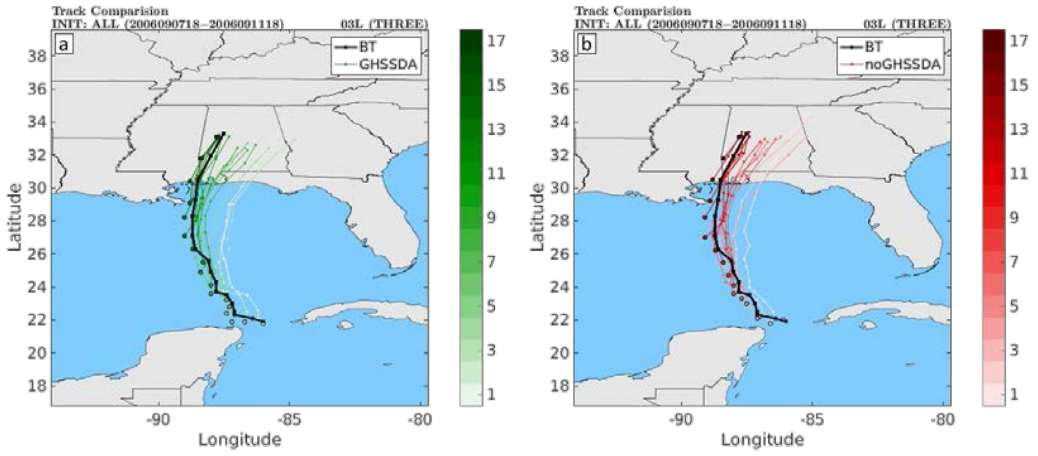

Figure 4-25. A comparison of track forecasts for (a) GHSSDA and (b) noGHSSDA to the best track (BT; black line) of AL03. The first cycle (2006090718) is shown in the lightest color while the last cycle (2006091118) is shown in the darkest color. Colored circles outlined in black indicate the location of AL03 at initialization time. Dots along each track occur every 6 h.

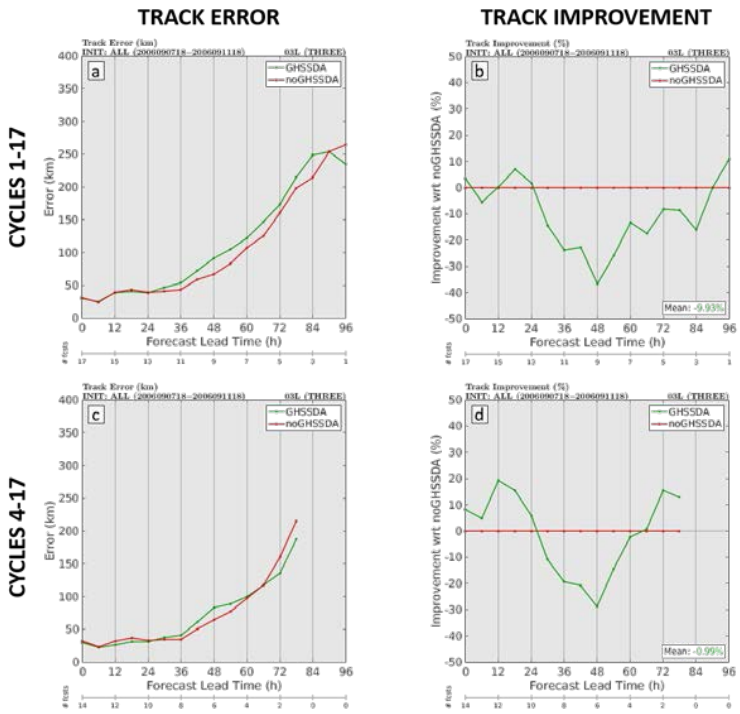

Figure 4-26. (a, c) Track errors (km) and (b, d) track improvement (%) for GHSSDA (green line) and noGHSSDA (red line) for (a, b) cycles 1-17 and (c, d) cycles 4-17. If present, squares (circles) indicate 95% (90%) significance as determined by a paired t-test w/ serial correlation.

Summary of the Hurricane OSSE

The impact of Geo-HSS on AL03 track forecast was found to differ between the two OSSEs. For the Free Run, the inclusion of Geo-HSS in the IBCs improved track forecasts at all lead times, particularly after 48 h. On the other hand, for the DA Run, the inclusion of Geo-HSS in the IBCs and as one of the data types assimilated directly into HWRF neither improved nor degraded the track forecasts. This difference could have occurred since data assimilation and relocation, both of which are turned off for the Free Run but turned on for the DA Run, act to adjust the initial vortex to match the G5NR vortex. Specifically, the assimilation of conventional and satellite data in the DA Run acts to modify the background synoptic flow and the near-AL03 environment while the relocation of AL03 modifies the vortex present in the IBCs to more closely match the storm location, intensity, and structure of AL03 in the G5NR. Since track forecast errors in the DA Run were smaller than in the Free Run to start, the removal of the first three cycles would further minimize the difference between the runs.

4.2 GMAO OSSE

The GMAO OSSEs are based on the Goddard Earth Observing System (GEOS) atmospheric data assimilation system (ADAS) used for both reanalysis and near-real-time forward processing. From fall 2019 to February 2020, GMAO worked to simulate five hyperspectral infrared instruments with spectral ranges similar to the Meteosat Third Generation (MTG) Infrared Sounder (IRS) in geostationary orbit where each acquired one full-disk measurement (4-km nadir spatial sampling). The orbital positions were placed at the longitudes occupied by GOES-East, GOES-West, Himawari, GIIRS/FY-4A, and s o o n MTG. An example of metrics produced is the Forecast Sensitivity Observation Impact (FSOI) shown in Figure 4-32. Based on this initial observation structure, GMAO has developed several other HSS scenarios for impact assessments: 1) the five-infrared hyperspectral sounders configuration in which the GOES-East and GOES-West positions exclude long wave spectral channels; 2) a three-infrared hyperspectral sounder configuration with positions including MTG, GOES-East, and GOES-West where all instrument have IRS-like spectral range; and
2) a three-infrared hyperspectral sounder configuration with positions including MTG, GOES-East, and GOES-West where the United States' infrared hyperspectral sounders exclude longwave spectral channels. In addition G M A O plan to investigate the impact of microwave observations from forecast error reduction projected into observation space. Results of these assessments are presented in 4.2.1-4.2.5 where the OSSE effort and results are detailed. Section 4.2.6 summarizes the results.

4.2.1 OSSE results for various Geo-ring and spectral configurations (GMAO)

The GMAO OSSE baseline system serves as the control for experimentation in these studies. The Nature Run used is a two-year integration of the GEOS model at approximately 7 km resolution with 72 vertical levels and 30 minute temporal output (Gelaro et al. 2015). The forecast model and data assimilation system used for forecasts are the GEOS version 5.17 and the hybrid 4D-ensemble variational GSI. The version of the GEOS model used to generate the Nature Run has higher horizontal resolution (7 km vs 25 km), an older model version, and different choices of model physics such as single versus two-moment cloud microphysics (Barahona et al. 2014) compared to the forecast model. These differences help to increase model error, resulting in a 'fraternal twin' setup. Full details of the GMAO OSSE framework are described in Errico et al. (2017).

The synthetic observations are based on the global observing network from July and August 2015, and largely mimic the count and distribution of real data from this period. The data types simulated include conventional data types such as aircraft, rawinsondes, and surface stations; also remote sensing data such as atmospheric motion vectors (AMVs), scatterometers, AMSU-A, MHS, GPS-RO, ATMS, AIRS, CrIS, IASI, HIRS4, and SSMIS. For s o m e conventional and radiance data types, the location and timing of simulated observations are based on the corresponding real data from 2015. However, other simulated observations are more sophisticated. For example, rawinsondes and dropsondes are advected by the Nature

Run wind fields, and AMVs are simulated based on the Nature Run fields of clouds and humidity (Errico et al. 2020). GPS-RO data are simulated using the ROPP - EXPLAIN THIS ACRONYM - (Culverwell et al. 2015) 2-dimensional operator to simulate the bending angle. Microwave and infrared radiances are calculated using the Community Radiative Transfer Model (CRTM, Han et al. 2006) with locations based on the swath footprint from real data, but with cloud effects from the Nature Run cloud field.

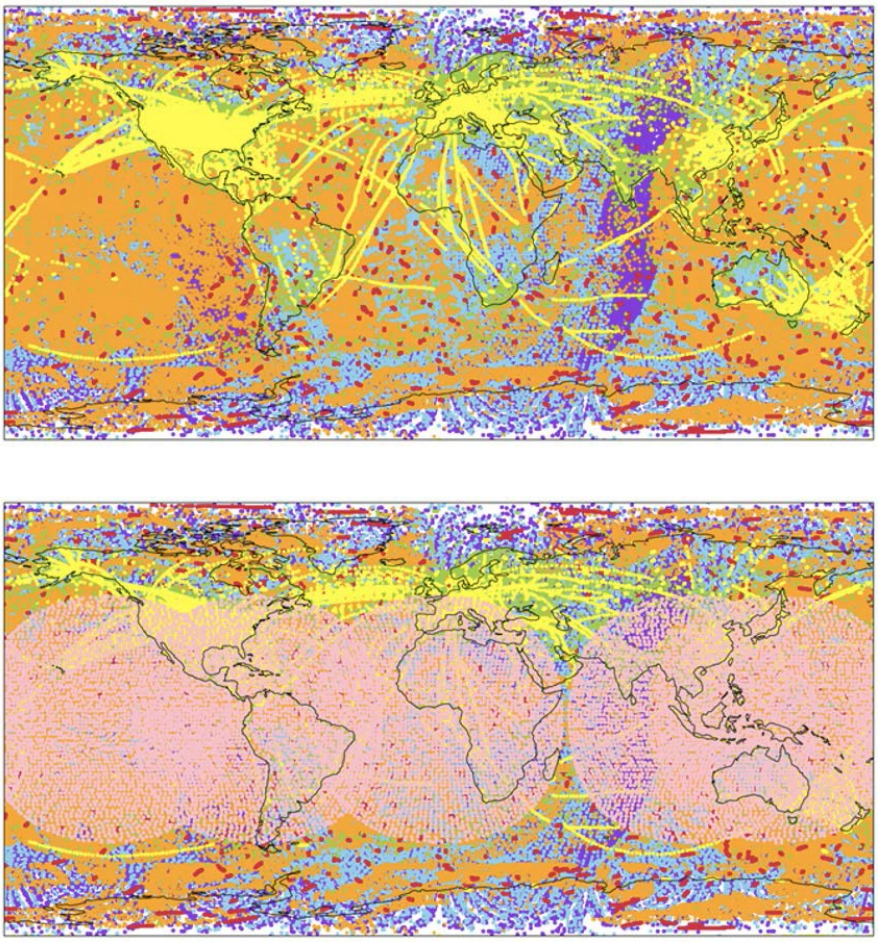

Figure 4-27. The GMAO OSSE baseline observations (top panel), consisting of passive microwave radiances (purple), passive infrared radiances (blue), conventional surface data (green), conventional upper-air and aircraft data (yellow), Global Navigation Satellite System radio occultation data (GNSS-RO, red), and satellite-derived winds (orange). The additional GEOIRS data are shown in addition to the baseline and are shown in pink (lower panel).

All synthetic observations in the OSSE baseline have added simulated errors that are calibrated to reproduce realistic statistics of ingested observation count and observation innovation by the data assimilation system. Uncorrelated random errors are added to all data types. Correlated random errors are added to select data types: vertically correlated errors are added to rawinsondes, AMV, and GPS-RO bending angles; horizontally correlated errors are added to AMSU-A, ATMS, HIRS-4, MHS, SSMIS, and AMV; and channel correlated errors

are added to AIRS, IASI, and CrIS observations. Results of the calibration and validation of the recent GMAO OSSE baseline are described in Privé and Errico (2019) and Privé et al. (2020).

Hereafter, the experimentation leveraging this baseline system will be referred to as CTL, and the experimentation is summarized in Table 4-2, and a sample six-hour observation distribution is shown in Figure 4-27 (top).

Table 4-2. Experimentation performed for this study

Experiment	Observing system	HSS Geostationary position				
		0°	-75° GOES -East	-135° GOES -West	141°	105°
CTL	Full conventional and satellite data circa 2017, described in Prive and Errico (2019) and Prive et al. (2020)	-	-	-	-	-
LWFULL	CTL + 5x GEO-IRS longwave	LW	LW	LW	LW	LW
LWSUB	CTL + 3x GEO-IRS longwave	LW	LW	LW	-	-
SWFULL	CTL + 2x GEO-IRS shortwave + 3x GEO-IRS longwave	LW	SW	SW	LW	LW

4.2.2 Hyperspectral Infrared Sounder Configuration

A standard Geostationary Infrared Sounder, referred to as GEOIRS in these results, was prototyped based on the MeteoSat Third Generation-Sounder (MTG-S) Infrared Sounder (IRS) instrument specifications. T his refers to the effective spectral sampling and response functions used in the generation of fast transmittance coefficients used in radiance simulation and assimilation via the CRTM. However, one key difference was assumed, specifically that the instrument had full spectral coverage from 650 to 2500 cm-1. While this is not necessarily expected for a future geostationary hyperspectral infrared sounder, it provided more up-front flexibility in terms of channel selection in these and future studies without the need to regenerate additional transmittance coefficients. A sample simulated IASI spectrum and a corresponding GEOIRS spectrum for the same profile is shown in Figure 4-28. It is noted that there were uncertainties relating to the forward line-by-line calculations in the highest wavenumbers – approximately larger than 2400 cm-1, which did not line up with the IASI spectrum. This discrepancy has since been fixed, though these channels are avoided in these results.

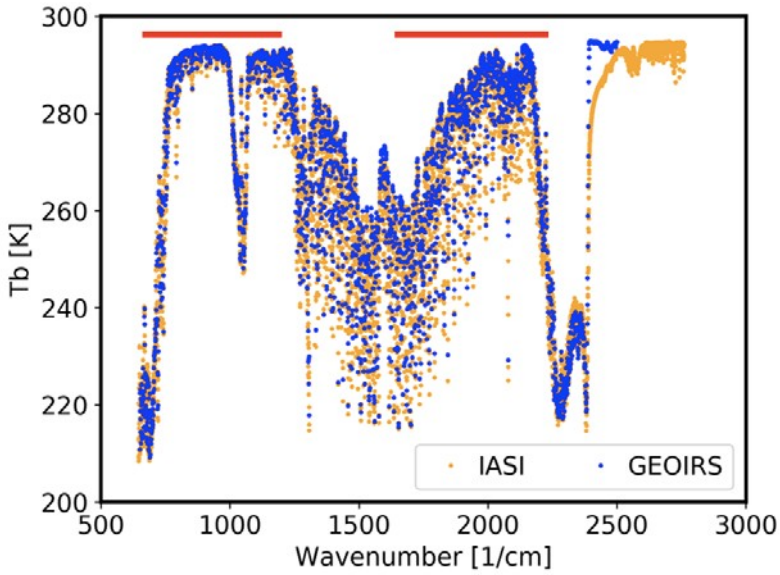

Figure 4-28. Simulated IASI (orange) and GEOIRS (blue) spectrum, generated from the same sample profile. The spectral coverage of the MTG-S IRS instrument is denoted by the red bars.

For each experiment, every GEOIRS instrument used these same specifications. No effort was made to fully simulate a separate coefficient file for the existing the Chinese Meteorological Agency (CMA) Geosynchronous Interferometric Infrared Sounder (GIIRS) or planned MTG-S IRS instrument, though their proper satellite sub-points were used.

4.2.3 Experiment – A Global Constellation of GEO Hyperspectral Infrared Sounders

The first experiment performed considered a full constellation of hyperspectral infrared sounders in geostationary orbit following the current or expected satellite subpoints occupied by the GOES-East, GOES-West, Japanese Meteorological Agency (JMA) Himawari, CMA GIIRS, and the European Organisation for the Exploitation of Meteorological Satellites (EUMETSAT) MTG-S satellites. In Figure 4-27 (bottom), the position of these data are shown in pink relative to the rest of the observations that make up the GMAO OSSE baseline system.

For this first experiment, 70 temperature and surface channels with wavenumbers ranging between 650 and 1000 cm^{-1} – or wavelengths between 10 and 15 μm – and 17 water vapor channels between 1200 and 1500 cm^{-1} – or wavelengths between 8.3 and 6.7 μm – were assimilated. These channels are shown in Figure 4-29 (yellow). This is consistent with the channel selection methodologies used for the currently assimilated infrared sounders. Furthermore, it relies on the spectral regions that have traditionally been used in infrared radiance assimilation for temperature and water vapor sounding.

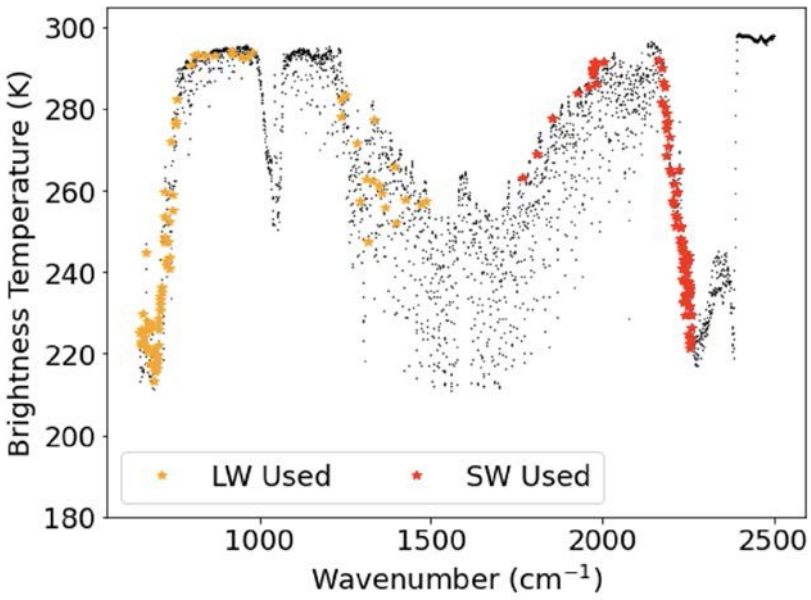

Figure 4-29. A sample GEOIRS spectrum and the corresponding longwave (orange) and shortwave (red) channel selections used in the experimentation.

A horizontal thinning mesh of 180 km is used, which is consistent with polar orbiting hyperspectral infrared sounders. Full disk observations are assimilated hourly, which is consistent with both projected MTG-S IRS operations and with the temporal binning within the GSI.

Hereafter, this experiment will be referred to as LWFULL, as summarized in Table 4-2.

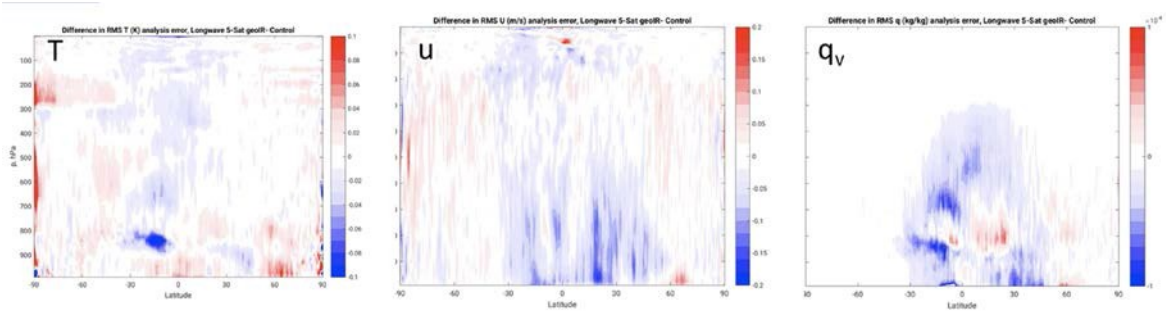

Figure 4-30. The difference in zonally-averaged analysis error between LWFULL and CTL for temperature (left), wind (center), and specific humidity (right). Blue (red) indicates a reduction (increase) in observation error by the addition of the GEOIRS instruments.

An advantage of an OSSE is the ability to directly assess how the new observations affect the underlying analysis error by comparing directly against the nature run, which serves as an absolute truth for experimentation. This differs from standard observing system experiments utilizing real data because in the real world, the underlying truth is unknown.

With the addition of the GEOIRS full constellation in the LWFULL experiment, the direct impact

on the analysis solution was generally positive globally, as shown in Figure 4-30 where blue contours indicate an improved analysis field. Temperature (Fig 4-30, left) showed mixed signals in terms of analysis improvement. The tropical column was generally positive above 900 hPa and became more consistent as you go up vertically. There were also degradations near the poles. Since these regions are outside of the core observing range of the geostationary sounders, this is indicative of an indirect impact of the observations that may require further investigation.

The LWFULL experiment had an apparent improvement on the analysis of the zonal wind (Fig. 4-30, center). This is a core result in that it is illustrative of the analysis system exploiting the temporal information of the GEOIRS constellation. The information content of radiances is related to the temperature and moisture of a scene. In a four-dimensional solution, the temporal movement of features encapsulated in these radiances imposes a wind response, which is known as the tracer effect (Peubey and McNally, 2009). The temporal information is directly translated to an improved wind analysis.

The observations showed a largely beneficial analysis for error reduction in specific humidity as compared to the control (Fig. 4-30, right). This improvement is two-fold. First, water vapor radiances are assimilated, so there should be a direct improvement in the analysis of specific humidity via the radiance inversion procedure. Second, the improvement in the zonal wind (Fig. 4-30, center) will improve the underlying moisture transport in the short-term forecasts used in the data assimilation procedure.

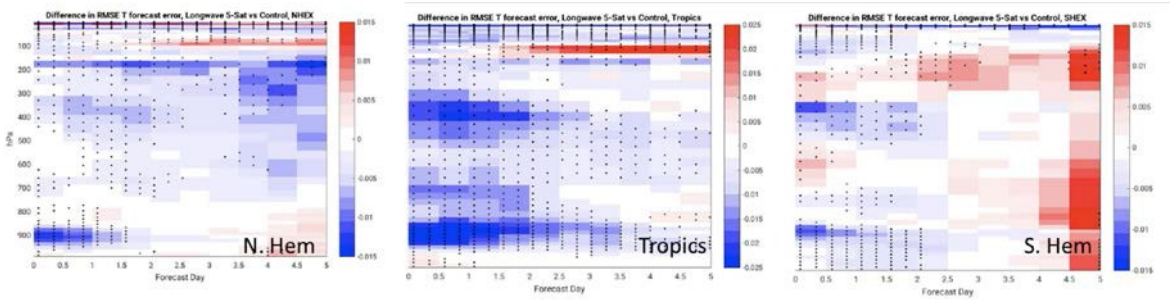

Figure 4-31. LWFULL Change in Temperature RMS error due to GEOIRS observations as a function of pressure height and forecast hour, as compared to CTL, for the Northern Hemisphere (left), tropics (center), and southern hemisphere (right). Stippling indicates statistical significance beyond 0.95.

The medium range forecast impacts were seen to be statistically neutral in terms of height anomaly correlation in both the southern and northern hemisphere. In terms of RMS forecast error of temperature, the northern hemisphere (Fig. 4-31, right) forecasts were seen to be statistically improved through the troposphere to day 2.5, though significant improvement was maintained to five days at 200 hPa. In the tropics (Fig. 4-31, center), improvement was seen largely through the tropospheric column and was maintained to two days. The improvement between 400 and 600 hPa and between 800 and 900 hPa was maintained further to days 4.5 and 5. In the southern hemisphere, the results were more mixed, with significant improvement seen between 300 and 400 hPa and 800 to 100 hPa and extending to day 2, but degradation was seen above 300 hPa and extended to day 3. Though not shown, wind and specific

humidity forecasts were seen to be similarly impacted with the largest forecast improvements being in the tropics, the northern hemispheric improvements were generally short range, and the southern hemisphere improvements were improved in the short range and degraded in the medium range.

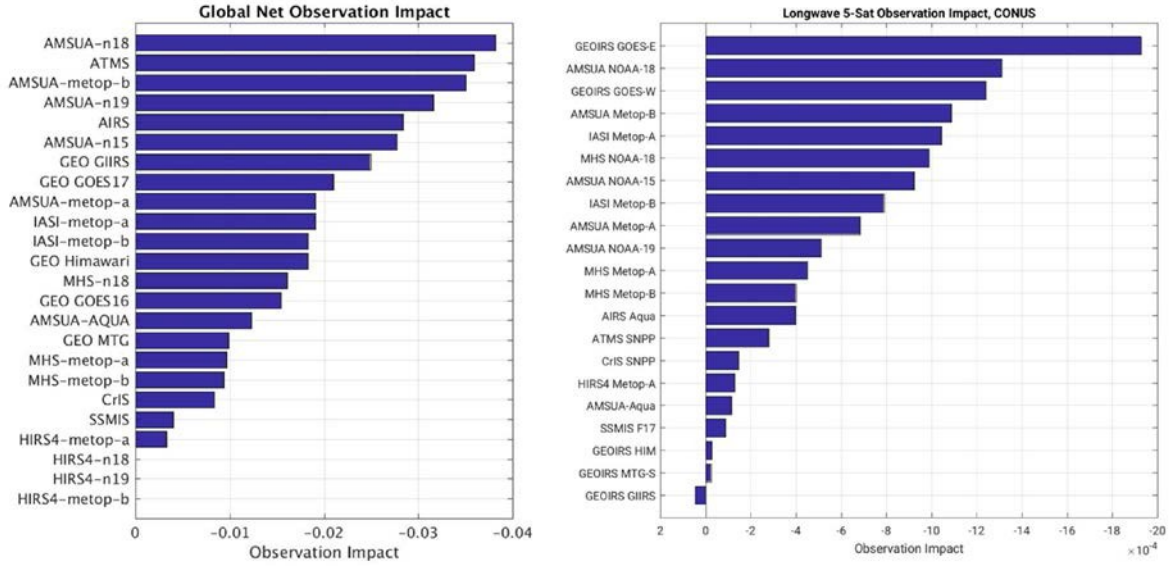

Figure 4-32. LWFULL Forecast Sensitivity Observation Impact (FSOI) for passive radiance satellite measurements for the Global domain (left) and CONUS (right), calculated for 00 UTC cycles.

The Forecast Sensitivity Observation Impact (FSOI, Langland and Baker 2004, Gelaro and Zhu 2009) metric for all satellite radiance types by instruments is shown in Figure 4-32. FSOI is a quantification on how each observation acts to reduce or increase the 24-hour forecast error of a selected norm, in this case the total wet energy norm (Holdaway et al. 2014).

For global forecast error, the largest impact is seen from the GEOIRS in the GIIRS and GOES-West locations. There are two reasonable interpretations to this. Cross-referencing with Figure 4-28, the GIIRS instrument corresponds with a lack of Atmospheric Motion Vectors (AMVs). Thus, the temporal information of the GIIRS-placed instrument may be carrying more unique wind information content. The GOES-West instrument has the largest water coverage, and it is expected that these observations would be better utilized over water versus land. Contrarily, this also can explain why the MTG instrument has the lowest FSOI, as it has the largest percentage of land coverage over its disk.

When focusing the metric to the CONUS 24-hour forecast error, it is seen that the GOES-East instrument has the largest impact of all radiance measurements. This is largely due to the direct coverage of the bounding domain by this instrument. The GOES-West ranks third, which is noteworthy in that many of the observations are outside of the bounding box, thus illustrating the impact of both direct and upstream measurements on the 24 hour forecast error. The Himawari, MTG, and GIIRS slots are shown to have limited impact on the CONUS by this metric.

4.2.4 Experiment – A Limited Constellation of GEO Hyperspectral Infrared Sounders

This experiment only considered a subset of the new instruments. The GOES-East, GOES-West, and MTG-S instruments are assimilated using the same methodology as LWFULL (this scenario excludes GIIRS-positioned and Himawari-positioned instruments). Hereafter, this experiment will be referred to as LWSUB as summarized in Table 4-2.

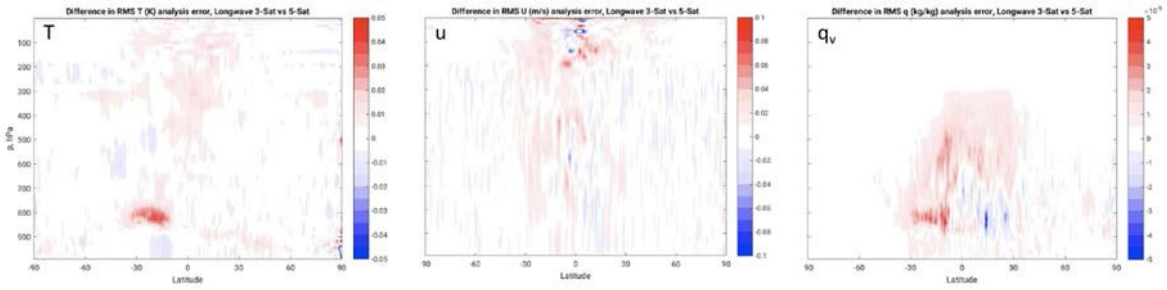

Figure 4-33. The difference in zonally-averaged analysis temperature error between LWSUB and LWFULL

In comparison to LWFULL, the LWSUB analysis error reductions were generally smaller in magnitude as the GEOIRS fleet went from five instruments to three. This is illustrated in Figure 4-33, where the pink indicates less improvement by LWSUB. It is noted that the magnitude of these differences is smaller compared to the absolute magnitudes seen relative to CTL in Figure 4-30.

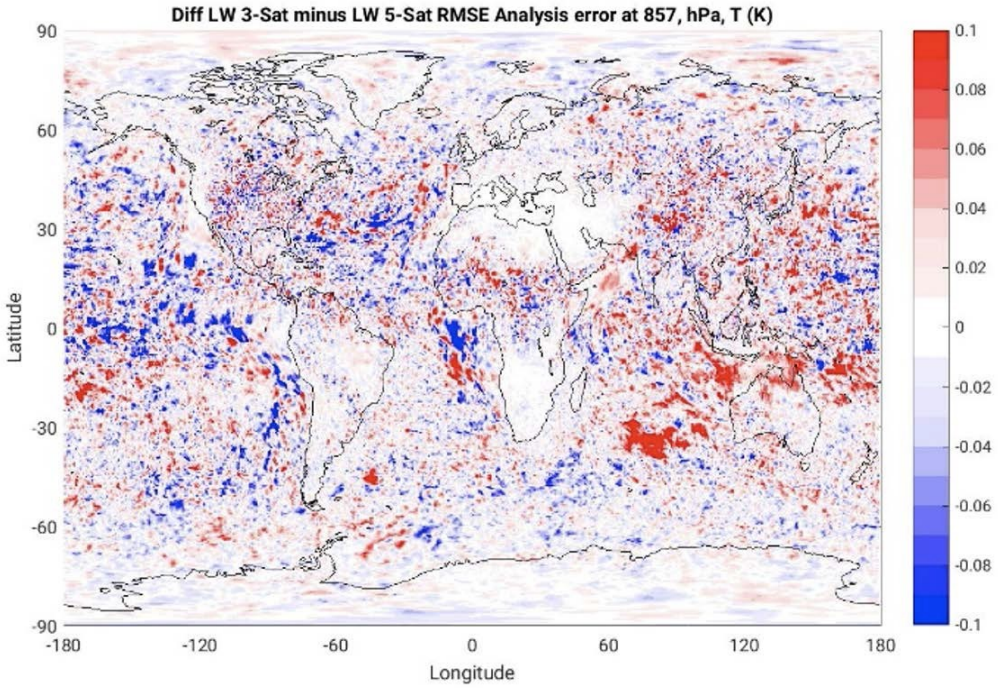

Figure 4-34. The difference in zonally-averaged analysis temperature error between LWSUB and LWFULL for the model eta level nominally corresponding to 857 hPa.

To better illustrate the reduction of impact, a spatial plot of the temperature error reduction difference between LWSUB and LWFULL is shown in Figure 4-34. Broad areas of reduced improvement are most apparent over the Indian Ocean and Western Pacific, illustrating that the analysis error impacts are occurring where the GIIRS and Himawari satellites are missing in LWSUB.

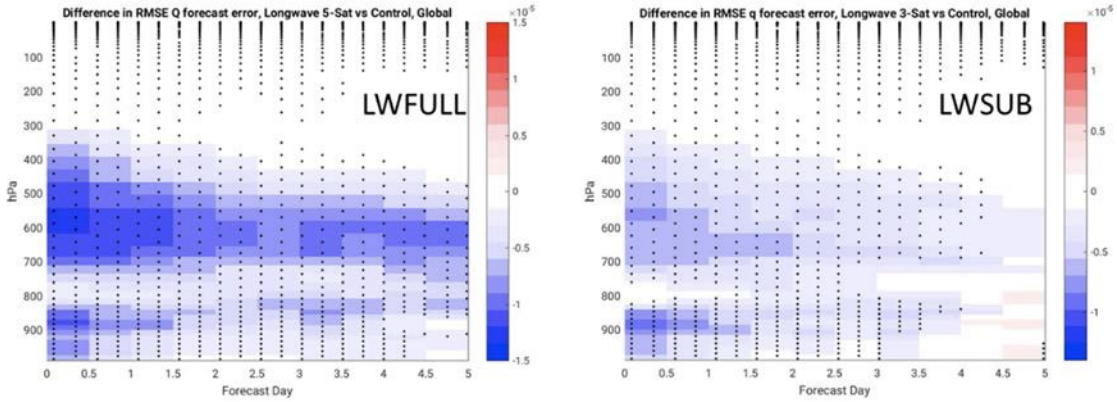

Figure 4-35. Global change in specific humidity RMS error due to GEOIRS observations as a function of pressure height and forecast hour, as compared to CTL, for LWFULL (left) and LWSUB (right). Stippling indicates statistical significance beyond 0.95.

In terms of forecast impact, the most apparent signal was seen in a general reduction of the forecast of specific humidity over both the short and medium range. This is illustrated globally in Figure 4-35, though the signal was most apparent in the Northern Hemisphere and Tropics.

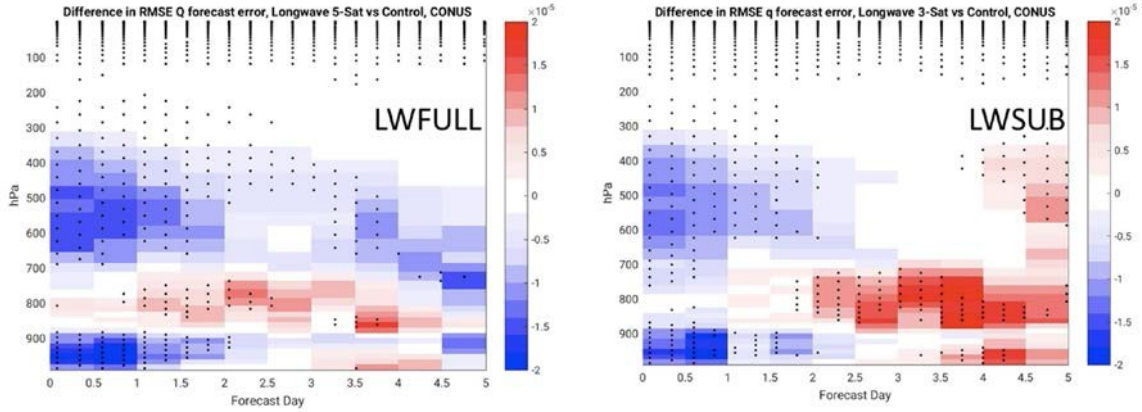

Figure 4-36. CONUS change in specific humidity RMS error due to GEOIRS observations as a function of pressure height and forecast hour, as compared to CTL, for LWFULL (left) and LWSUB (right). Stippling indicates statistical significance beyond 0.95.

These forecasts metrics were also considered over the CONUS, but fewer statistically significant differences were seen due to the limited spatial domain. However, there are noted changes in specific humidity (Fig. 4-36), particularly in a reduction of significant forecast

improvement duration between 400 and 600 hPa. For LWFULL, significance was maintained to day 3.5, while in LWSUB, significance was lost on day 2. Furthermore, in LWSUB, the forecasts were actually degraded at days 4 and 5 in this layer. This indicates that the forecast improvement in the medium range forecasts are affected by the upstream GIIRS and Himawari instruments.

A second experimental configuration consisted of a single sounder in the GOES-Central position (105 W), along with sounders over Europe and over the east Asia and west Pacific regions. The FSOI shown in Fig. 4-37 is estimated from the CONUS region only and averages results from the 00, 06, 12, and 18 UTC cycles. This shows that the sounder over the central U.S. provides the greatest impact over CONUS.

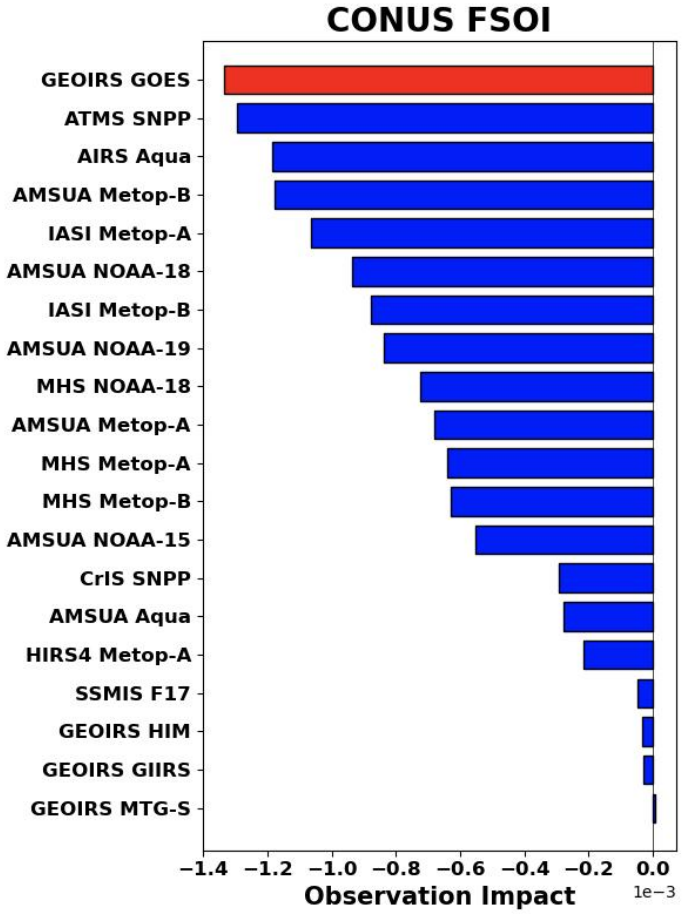

Figure 4-37. Forecast Sensitivity Observation Impact (FSOI) for passive radiance satellite measurements for the CONUS domain, calculated by averaging data from the 00, 06, 12, and 18 UTC cycles.

4.2.5 Experiment – Assessing the Potential Impact of Shortwave Temperature and Water Vapor Sounders

This experiment is similar to LWFULL, with the only difference being that the GOES-East and GOES-West instruments are now using a channel selection emphasizing the use of shortwave

thermal infrared radiances for temperature and water vapor radiance assimilation.

Specifically, 76 temperature channels were assimilated ranging from 2165 to 2260 cm-1, or 4.4 to 4.6 μm. Fifteen water vapor channels were assimilated ranging from 1780 to 2005 cm-1, or 4.9 to 5.6 μm. For the GIIRS, MTG-S, and Himawari instruments, the longwave channel selection of LWFULL was still used. Otherwise, the temporal and spatial sampling methodologies were the same.

An important caveat to the shortwave channel selection was the utilization of the longwave side of the 4.3 μm CO2 absorption line for temperature assimilation. While the shortwave side is a cleaner signal in that it is less sensitive to minor constituents, it was avoided due the aforementioned uncertainty in the transmittance model illustrated by the discrepancy compared to IASI near 2500 cm-1 in Figure 4-28. In addition, as is noted later, there remain issues with surface reflectance and non-local thermodynamic equilibrium that are assumed to be accounted for. Hereafter, this experiment will be referred to as SWFULL.

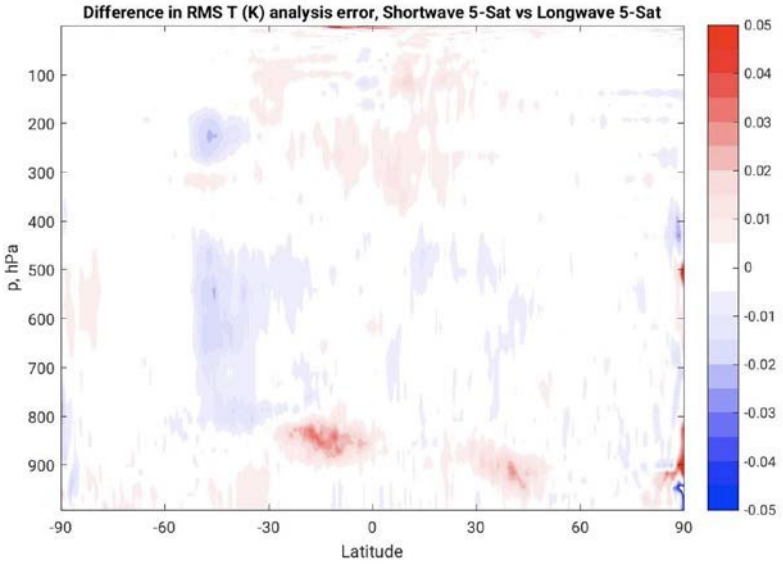

Figure 4-38. The difference in zonally-averaged analysis error between SWFULL and LWFULL for temperature

The SWFULL analyses were seen to have the most consistent differences with the LWFULL experiment in terms of temperature, and the zonally-averaged RMS difference of analysis error between the two experiments is shown in Figure 4-38. Temperature is less-accurately analyzed between 800 and 1000 hPa by using the SWFULL channel selection for the GOES satellites. Contrarily, there is an improvement between 400 and 800 hPa, most notable in the southern midlatitudes. This is perhaps illustrative of the cleaner mid-tropospheric temperature signal in the shortwave channels. In these experiments, though, the difference between LWFULL and SWFULL are much smaller than the differences between either experiment or CTL. Though not shown, there were differences, primarily in the tropics, in the analysis of specific humidity, and minimal coherent differences were seen in wind.

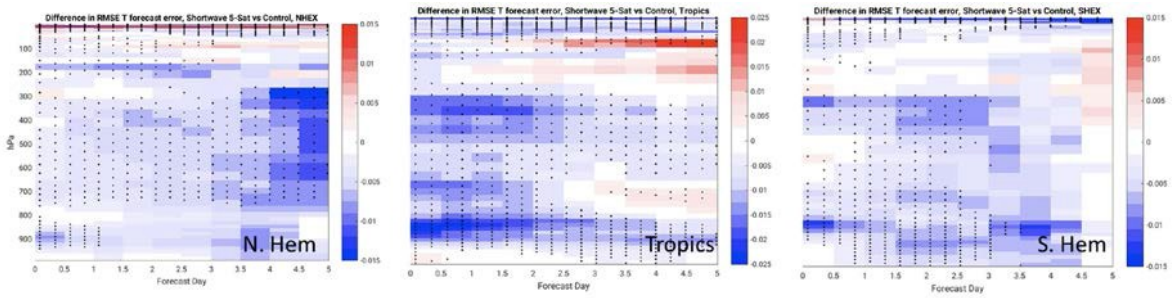

Figure 4-39. SWFULL Change in Temperature RMS error due to GEOIRS observations as a function of pressure height and forecast hour, as compared to CTL, for the Northern Hemisphere (left), tropics (center), and southern hemisphere (right). Dots indicate statistical significance beyond 0.95.

Forecast improvements for Temperature RMS between SWFULL and CTL are shown in Figure 4-39. Particularly compared to the LWFULL results (Figure 4-31), the improvements were seen to be more sustained through the forecast integration, particularly in the Northern Hemisphere and between 300 and 800 hPa. This is also seen in the Southern Hemisphere, with an additional 12 hours of statistically significant improvement between 300 and 400 hPa and an additional day of improvement between 800 and 1000 hPa. In the tropics, the forecast accuracy is more similar between SWFULL and LWFULL, though there are signs that the SWFULL is also improved, particularly at Day 5.

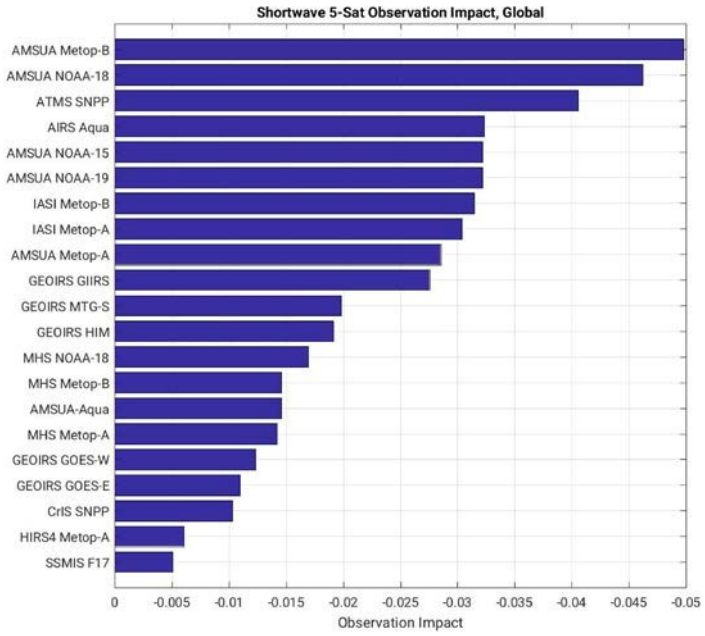

Figure 4-40. SWFULL Forecast Sensitivity Observation Impact (FSOI) for passive radiance satellite measurements for the Global domain, calculated for 00 UTC cycles.

However, when considering the short-term forecast error reduction via the Global FSOI metric, as shown in Figure 4-40, the shortwave channel selection is shown to be smaller than that of the longwave subset, as indicated by the noted drop in relative ranking of the GOES-East and West instruments. This is in some ways counter to the medium-range forecast improvements seen between SWFULL and LWFULL.

An important caveat to these results is that the heritage of infrared radiance assimilation in data assimilation is built upon the 15 μm CO2 absorption band. While there are heritage retrieval algorithms that have exploited the 4.3 μm CO2 band for temperature (Susskind et al. 2003), the full utilization of these observations in data assimilation is still in its infancy (Jones et al. 2020). Furthermore, core to these experiments is that no simulated errors are added to the GEOIRS measurements. Thus, while they may make a statement on information content, they do not fully characterize the difficulties that are particularly prevalent in these shortwave bands, including non-local thermodynamic equilibrium and solar reflective effects. A similar OSSE performed on the MISTiC Winds concept (McCarty et al. 2021) illustrated that while these shortwave observations maintained positive benefit when considered to be 'perfect', the application of an error model based on convolved IASI radiances dramatically decreased their benefit. Thus, while these shortwave channels may have the information content, further development of our assimilation systems to properly exploit these data is likely still required.

4.2.6 Summary

These results illustrate the potential impacts of a constellation of hyperspectral infrared sounders in geostationary orbit. The results are generally straightforward regarding the size

of the constellation as larger improvements in analysis error reduction, forecast skill, and FSOI are seen for a global constellation (LWFULL) as opposed to a reduced constellation (LWSUB). There are benefits to global coverage, as larger forecast impacts are seen both globally and over the CONUS with the inclusion of the two instruments covering the Indian Ocean and Western Pacific.

In comparing the longwave full constellation (LWFULL) with the full constellation containing shortwave instruments over the GOES positions (SWFULL), the results were more convoluted. The analysis error comparison between SWFULL and LWFULL showed that the LWFULL configuration acted to reduce the lower tropospheric analysis error more than the SWFULL. However, the SWFULL configuration retained a larger forecast impact through the medium range. Finally, the FSOI illustrated that there was a substantial drop-off in the metric of the two GOES satellites when used in a shortwave configuration as compared to longwave.

However, these results are all indicative of 'perfect' observations from these geostationary infrared sounders. Previous and ongoing efforts have long illustrated the difficulties in assimilating real (or realistic) shortwave infrared channels due to solar contributions, scene-dependent noise, and non-local thermodynamics equilibrium effects. These experiments only investigate the information content of the instrument characteristics that are predefined in terms of spectral resolution and coverage. The unrepresented and underrepresented sources of error stem from both instrument and representativeness errors. Instrument noise is often well-handled in data assimilation due to its normal and uncorrelated nature, but representativeness is often more difficult to interpret and model due to both the aforementioned misrepresentations of physical effects and discrepancies between the nature run and reality.

Contrarily, these experiments only performed a first-order attempt at optimizing the instrumentation – including channel weighting in the solution and channel selection. While there is an expectation that the results are overly perfect, there is also an expectation that the system could be further optimized.

Ultimately, there is heritage in the utilization of shortwave infrared bands near 4.3 μm in the retrieval community. Should data assimilation continue to utilize the lessons-learned from the retrieval community, then much of the information content of the shortwave should be recoverable. However, it should also be considered that the longwave bands are those that are operationally assimilated in numerical weather prediction, and thus the loss of these bands would be a fundamental loss of current operational capability.

4.3 University of Wisconsin / CIMSS Hybrid OSSE case studies

The CIMSS group has developed a hybrid OSSE where the majority of data in the simulation are real observations while the simulated instruments are generated by sampling global or regional reanalysis and forward models. The simulated HSS in this work has spectral coverage similar to Cross-track Infrared Sounder (CrIS) and has 14-km nadir spatial sampling.

This work investigated two severe storm case studies and assessed how geostationary-based infrared hyperspectral sounder observations improve storm prediction. Metrics provided by these studies include accuracy improvement of instability indices, temperature and water vapor profiles, and wind. Results of these assessments are presented in 4.3.1 which details the OSSE effort and details the results. Section 4.3.2 summarizes the results.

4.3.1 Hybrid OSSE results for Severe Storms (CIMSS)

Case 1

The 24-hour accumulated precipitation from CNTRL and EXP are compared with the observations (Figure 4-41). A rain belt from northwest to southeast covered from Colorado to Oklahoma. It is a strong and consistent rainfall belt. The rainfall belts in both CNTRL and EXP reflect the patterns from northwest to southeast. But the precipitation location from CNTRL is not as large as the observations. With the assimilation of GEO CrIS FSR data, the 24-hour accumulated precipitation is becoming a consistently large rain belt covered from Colorado to Oklahoma. The precipitation amount of EXP is also closer to the observations than the precipitation amount of CNTRL. The Equitable Threat Score (ETS) for the accumulated 18-hour precipitation and 24 –hour precipitation are plotted in Figure 4-42. The ETS scores at 0.1 mm reflect the rainfall greater than or equal to 0.1 mm. The ETS scores at 1200 UTC 24 June (Figure 4-42 left) represent the 18-hour accumulated precipitation from 1800 UTC 23 June to 1200 UTC 24 June. The ETS scores at 1800 UTC 24 June (Figure 4-41 right) represent the 24-hour accumulated precipitation from 1800 UTC 23 June to 1800 UTC 24 June 2018. For the whole 18-hour and 24-hour accumulated precipitation, the ETS scores of EXP are always higher than the ETS scores of CNTRL, especially for the 24-hour accumulated precipitation. The ETS scores indicate that with the assimilation of GEO CrIS FSR data, both the location and intensification of the LSS rainfall are improved for the whole period. For some of the higher precipitation bins, the ETS quality almost doubled.

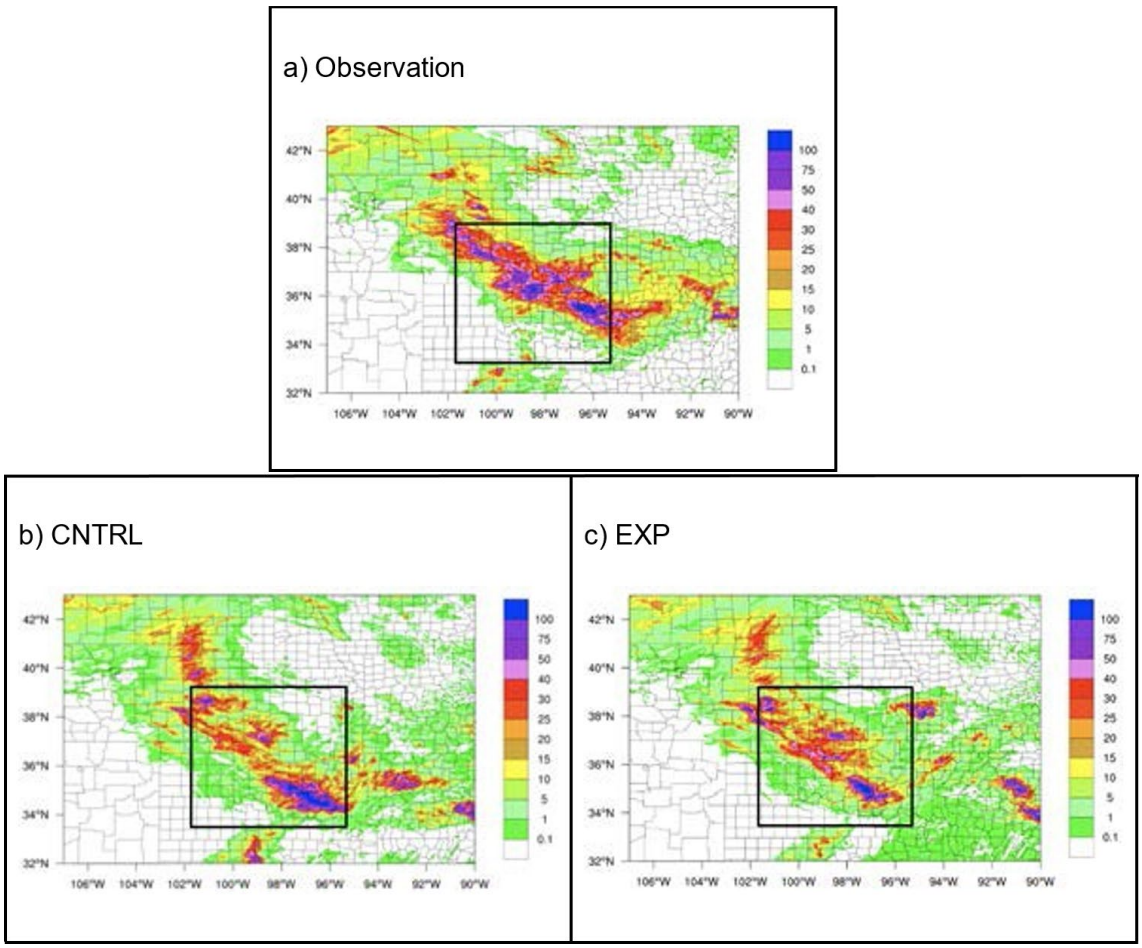

Figure 4-41. The 24-hour accumulated precipitation from 1800 UTC 23 June to 1800 UTC 24 June 2018 of (a) stage IV observations, (b) CNTRL and (c) EXP (unit: mm).

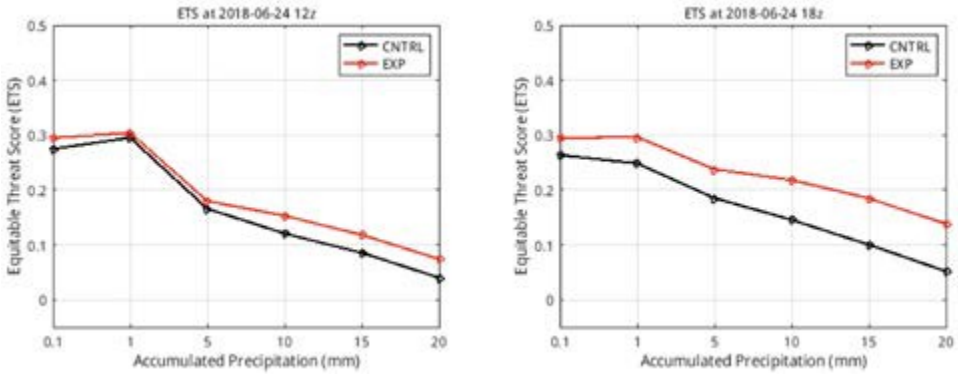

Figure 4-42. The ETS scores of CNTRL (black lines) and EXP (red lines) from 1800 UTC 23 June to 1200 UTC 24 June (left) and from 1800 UTC 23 June to 1800 UTC 24 June (right) 2018.

Case 2

The data coverage of GEO CrIS FSR data is much larger than that of CrIS FSR data. The data impact from the assimilation of GEO CrIS FSR data is also larger than that from the assimilation of CrIS FSR data at the analysis time. Since ERA5 data are used as the "truth" for the Hybrid OSSE, the GEO CrIS FSR data are simulated based on ERA5 data. Therefore, the atmospheric fields from the simulation forecasts can be compared with the atmospheric fields from ERA5 data. The differences between ERA5 and CNTRL (ERA5-CNTRL) and the differences between ERA5 and EXP (ERA5-EXP) at 850 hPa at 0600 UTC 27 May are shown in Figure 4-43. At the analysis time, the changes in the moisture fields are directly from the assimilation of the different datasets. The RMSE and STD of CNTRL are 2.8551 and 2.239, respectively. The RMSE and STD of EXP are 2.2794 and 2.0155, respectively. So the RMSE of EXP is improved around 20% and the STD of EXP is improved around 10% over CNTRL. The improvement is most evident over Texas. To further evaluate the data impact in the LSS region, a smaller domain is compared between the ERA5 and the forecast fields. The LSS domain is within the box from 32.5°N to 46°N, and 83°W to 108°W (black box region in Figure 4-43). The RMSE and STD of CNTRL over the LSS domain are 2.7481 and 2.1015, respectively, while the RMSE and STD of EXP over the LSS domain are 2.5713 and 2.0985, respectively. So over the LSS domain, the RMSE and STD of the moisture fields at the analysis time from EXP are improved around 6% and 0.14%, respectively, over CNTRL. For the temperature fields and wind fields, the results are similar to the moisture fields. Based on the comparison of analysis fields, assimilating the GEO CrIS FSR data can reduce analysis error in the boundary layer. The impacts at the analysis fields will continue to affect the other atmospheric fields in the following forecast.

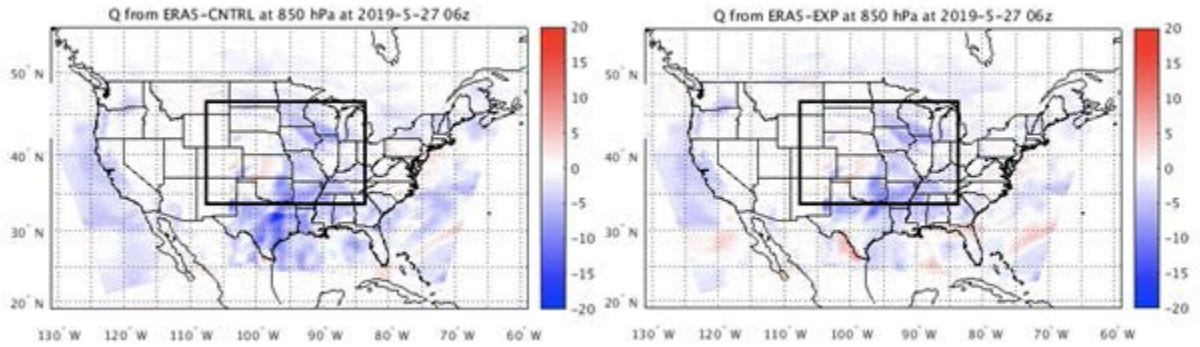

Figure 4-43. The specific humidity fields differences (unit: g/g) between ERA5 and CNTRL (left) and the differences between ERA5 and EXP (right) at 850 hPa at the analysis time.

The 6-hour accumulated precipitation from CNTRL and EXP are compared with the observations (Figure 4-44). The rainfall centers are mainly in Nebraska, South Dakota and Minnesota from the observations. From the CNTRL and EXP, the centers and the patterns of the rainfall are similar to the observations. But in CNTRL, there is a false storm center over northeastern Texas. Assimilating GEO CrIS FSR data removes the spurious storm from forming over northeastern Texas. The development of the spurious storm in CNTRL is further removed in EXP in the following forecast.

The ETS scores for all the experiments are shown in Figure 4-45. For each experiment, the value is the mean ETS scores of the accumulated 6-hour, 12-hour, 18-hour and 24-hour forecast precipitation. In the 8 groups of the experiments, the ETS scores varied between 0.3 and 0.7. In general, the ETS scores of EXP are higher or equal to the ETS of CNTRL. Only the experiments starting at 1800 UTC 26 May, the ETS scores of CNTRL are slightly higher than the ETS of EXP. Therefore, the assimilation of GEO CrIS FSR data can affect the atmospheric fields at the analysis time. The improved analysis fields can further improve or get the similar results for the LSS precipitation forecasts.

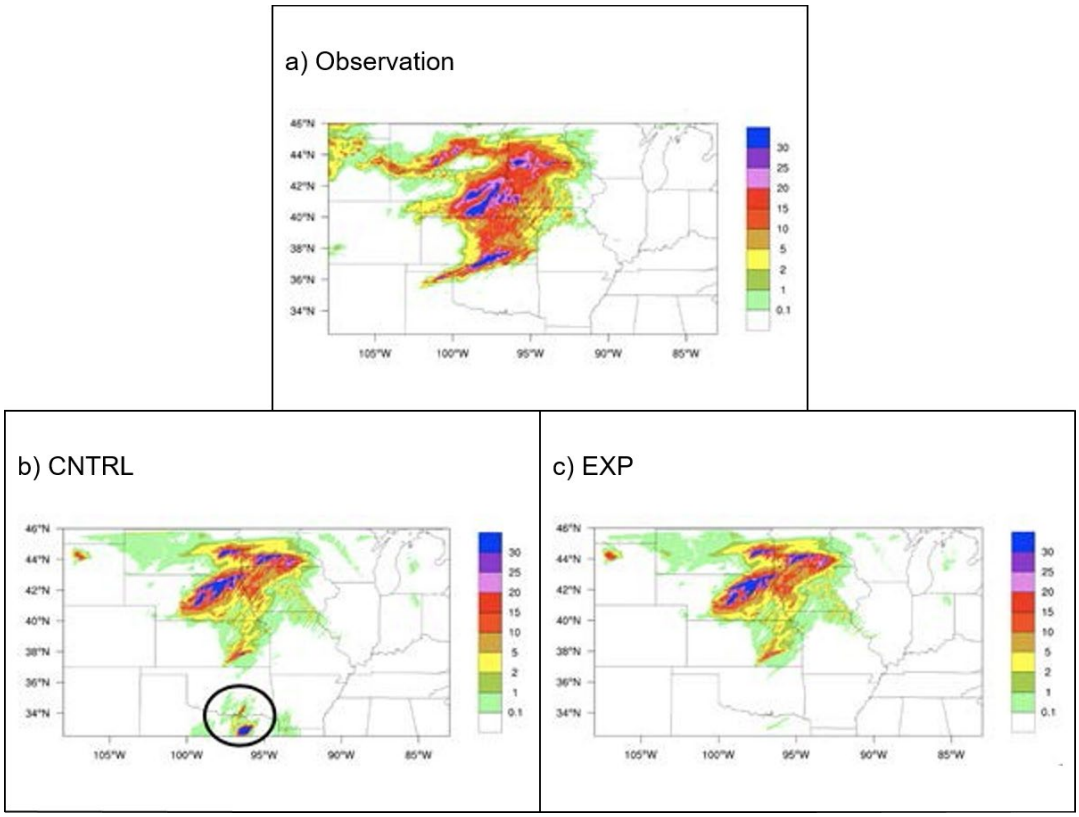

Figure 4-44. The 6-hour accumulated precipitation (unit: mm) from (a) Stage IV, (b) CNTRL and (c) EXP from 0600 UTC 27 May to 1200 UTC 27 May 2019.

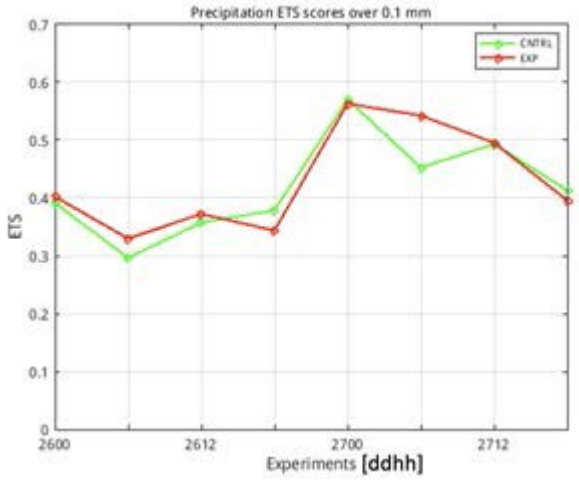

Figure 4-45. The statistical mean ETS scores of CNTRL (green) and EXP (red) from 0000 UTC 26 May to 1800 UTC 27 May 2019.

To access the impact of GEO CrIS FSR data on the atmospheric fields, such as the temperature, moisture, wind, and the precipitation forecast, the following overall evaluation strategy is carried out. The purpose is to use one single parameter to characterize the overall impact for the LSS simulations in the whole time period, which includes most of the important analysis/forecast parameters that are related to the local severe storms. For that purpose, the following parameters are selected: the temperature, relative humidity, and U/V

winds at four standard atmospheric levels (250 hPa, 500 hPa, 700 hPa and 850 hPa) to represent the atmospheric thermodynamic fields of the whole domain. In addition, the ETS scores, POD scores and FAR scores are used to reflect the precipitation forecast for LSS case. To be consistent with the RMSE for which lower values indicate better results, 1-ETS and 1-POD are used in the final RMSE calculation. The normalization process is carried out to remove the impact from the units for the variables. The final normalized RMSE (Li et al. 2018) is calculated using a weighted average: T, Q, U, and V for 40% along with (1-ETS), (1-POD), and FAR for 60%. The final RMSE scores are shown in Figure 4-46; CNTRL is 0.4763 and EXP is 0.4672 so assimilating GEO hyperspectral IR sounder radiances introduces a 2% reduction in RMSE. Overall, the GEO CrIS FSR data are adding value to the LSS simulation for both the analysis and forecast compared with CNTRL.

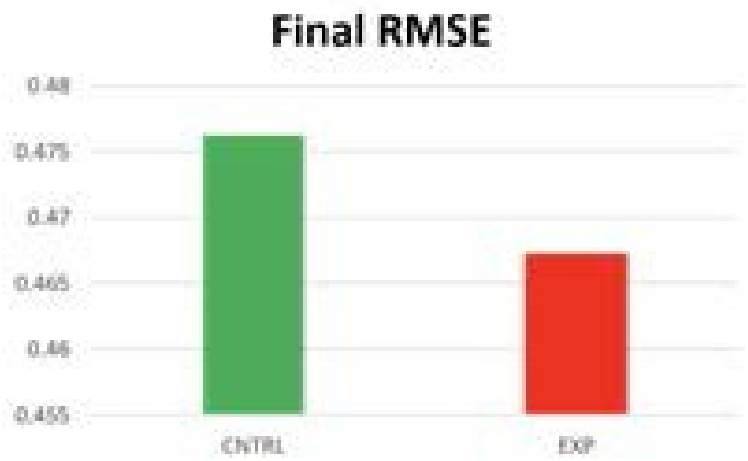

Figure 4-46. The final normalized RMSE for CNTRL (green) and EXP (red) for the second LSS case study.

4.3.2 Summary

In summary, the two cases in section 4.3.1 indicate that:

1) A “hybrid” OSSE allows for real observations for most of the observing system and simulated observations for the high-spectral IR sounder;

2) Compared to the current observing system data, adding GEO hyperspectral IR sounder data can further improve moisture and temperature profiles, winds and precipitation.

ERA5 data are used as the “True” Nature Run data for GEO hyperspectral IR simulation. The resolution of ERA5 data is still coarser than that of CrIS (14 km at nadir). Using imager data for assisting sounder assimilation was not considered in this study; it is noted that the collocated imager data can further amplify the positive impacts by improving sub-footprint hyperspectral IR sounder cloud detection for data assimilation (Li et al. 2004; Schmit et al. 2009; Wang et al. 2014) and by improving hyperspectral IR sounder data assimilation in partial cloud cover by removing the cloud effect using sub-footprint imager clear radiances (Li et al. 2005;

Wang et al. 2015, 2017). In addition, these "hybrid OSSE" results are consistent with Okamoto et al. (2020). Finally, it is important to explore how current assimilation systems and forecast models can take advantage of the high temporal and spatial resolution from GEO hyperspectral IR sounder. The estimates of the impact of a geo sounder may have been limited by the performance metrics of this system simulation including (1) ERA5 sampling is 7 km, not 4 km or finer; (2) the time resolution is hourly, not sub-hourly; (3) the assimilation was via 3D-var, not 4D-var; and (4) a subset of the spectral bands were used, not the full spectral range measured by the instrument.

5. Nowcasting Applications

While a LEO sounder provides global atmospheric profile data, one satellite only covers any given location of the Earth every 1-2 days. The location of storm initiation and development can coincide with the orbital gaps of a LEO satellite, causing a disruption in the continuity of the monitoring. As a result, existing LEO sounders are suitable for the coverage of large-scale weather systems, such as those falling within the synoptic scale. An advanced sounding mission from geostationary orbit would provide the needed high spectral (~0.5 cm^{-1}), high temporal (every 30 minutes) and finer horizontal (4 km) resolution observations that benefit timely forecasting of severe storms over the contiguous US (CONUS) as well as most of the Western Hemisphere. Nowcasting is currently defined by the WMO Working Group on Nowcasting Research as forecasting with local detail, by any method, over a period from the present to 6 hours ahead, including a detailed description of the present weather (WMO, 2017). Nowcasting and short-term forecasts include prediction of the weather within approximately a 6-h window (WMO, 2017: Guidelines for Nowcasting Techniques, Rept. No. 1198, 67 pp. 13) and the assimilation of observations into NWP forecast model that impacts 12-72 hour forecasts and beyond (Lu et al., 2017).

In a Nowcasting case study of the March 3, 2019 tornado outbreak in Alabama (see figure 5-1, left side), Smith (2019, personal communication) showed improved forecast skill of 6, 9, and 12 hour Significant Tornado Parameter (STP) forecasts using satellite sounding initialization compared to STP forecasts using only surface and radar observation initialization. High STP indicates high potential for tornadoes and is the sum of the CAPE, 0-1 km storm relative helicity (vorticity), 0-6 km bulk wind difference, and surface parcel Lifting Condensation Level height. The areal forecast improvement in the case studied is about 1/3 the size of Alabama and about 1/4 of South Carolina. Having real-time hyperspectral sounder data can lead to reducing the areal coverage for storm warnings.

Jones (2020) demonstrated that there is improvement in the updraft helicity prediction probabilities and locations relative to the subsequently observed storm center location by using 15 minute satellite profiles instead of hourly satellite profile or hourly conventional observations. (See Figure 5-1, middle.) GEO hyperspectral sounder has the potential to provide regional coverage with comparable cadence. Both reduced areal coverage and improved location accuracy of convective storms can lead to reduced shelter in place time, which has economic benefit (Sutter and Erickson, 2010). Additionally, both of these forecast improvements can potentially save lives. (See Figure 5-1, right.)

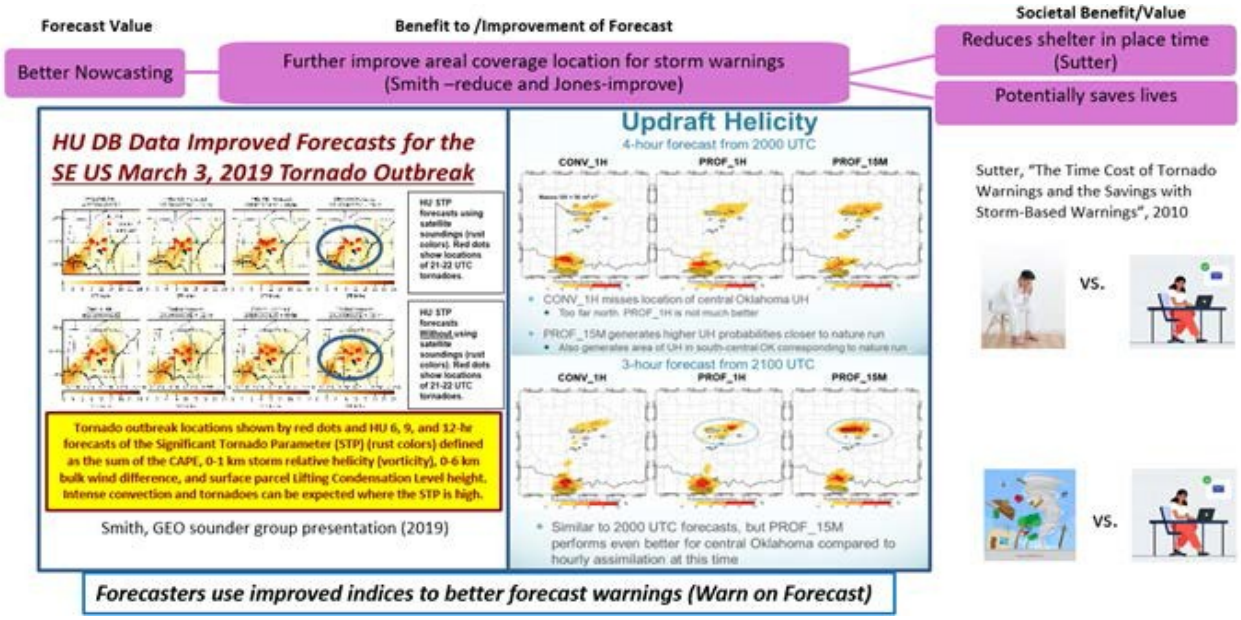

Figure 5-1. More accurate forecasts results can lead to improved area coverage for storms to reduce unnecessary shelter in place time. It can also potentially save lives.

6. Economic Benefits Analysis

6.1 Introduction

The purpose of this preliminary analysis is to estimate whether the benefits of adding a hyperspectral sounder (HSS) to the GeoXO satellite program is likely to exceed its cost and whether the strength of the evidence is sufficient to justify further consideration of this sensor. This analysis demonstrates an approach, identifies data needs, and provides preliminary information to the GeoXO program decision makers on whether or not to continue investing in developing a more robust economic or trade analysis of the HSS in phase A of the GeoXO program development.

In this preliminary study a break-even analysis is conducted to investigate the potential benefits of three high-value application areas for weather forecast improvements that could offset the cost of the HSS instrument over its operational lifespan of 2032-2051. The break-even analysis is supported by literature reviews, expert testimony, and the development of value-chain data analyses. It provides strong indication that the economic benefits associated with the GEO Hyperspectral Sounder (HSS) are substantial and sufficient to justify further economic study. However, this study alone should not be used to support the selection of the HSS on the GeoXO platform.

Given the time, staffing, and outreach constraints in this phase of the study, it is not possible to rigorously and comprehensively measure the benefits of HSS; instead, we evaluate the cost of the instrument to determine the magnitude of benefits that are needed to justify this cost (break-even analysis), developed scenarios under which benefits of this magnitude would be realized, and, to the extent possible, discussed scenarios with subject matter experts to assess their reasonableness.

It is important to note that this preliminary study evaluates whether positive benefits are likely to occur if a HSS is included on the GeoXO platform. It is possible that the societal benefits identified in this study which are realized through weather forecast improvements could be derived by other means. Further study of this instrument must consider alternative improvements to the forecast that reduce weather impacts to be certain that the HSS instrument is the most cost effective choice. Without this analysis we cannot confidently recommend the HSS instrument as the most cost-effective option to reduce weather-related damages and impacts. It is noted that a trade analysis approach has been proposed for GeoXO Phase A.

Additionally, many assumptions about the value of forecast improvements for end users were made in this initial analysis; these assumptions will need to determine ground-truth with subject matter experts. Finally, it will be important to establish a clear link between the data provided by the HSS instrument and the specific forecast improvements that lead to economic benefits, along with a quantitative measure of these improvements. Observing System Experiment (OSE) and Observing System Simulation Experiment (OSSE) studies are being conducted concurrently with this initial economic analysis that may begin establishing this connection.

Other important considerations not included in the analysis presented in this section include ground system costs, data assimilation issues, modeling improvement, and learning to use data over time. More time for iterative discussions with end users, meteorologists, modelers and other subject matter experts would be invaluable for the purpose of describing the particular benefits of weather forecast improvements and establishing clear linkages to the HSS instrument.

6.2 Economic Impacts Study Analysis

6.2.1 Identifying the Impact on NOAA Mission

The Technology, Planning, and Integration for Observation (TPIO) division within NESDIS maintains the NOAA Observing System Integrated Analysis (NOSIA) database that includes NOAA value chain information for all NOAA observational platforms, instruments, and products. TPIO analysts provided information about the relative importance of IR sounders and the products these instruments support. The IR sounders (NOAA and partner-maintained) included in the analysis are:

- Polar-orbiting Operational Environmental Satellite Series High Resolution Infrared Sounder (POES HIRS)

- Geostationary Operational Environmental Satellite 12-15 Sounder (GOES NOP Sounder)
- AQUA Atmospheric Infrared Sounder (AQUA AIRS)
- Metop-A and -B Infrared Atmospheric Sounding Interferometer (METOP IASI)
- Suomi National Polar-Orbiting Partnership Satellite Cross-track Infrared Sounder (S-NPP CrIS)
- Metop-A and -B High Resolution Infrared Sounder (METOP HIRS)

In terms of overall missions, the TPIO analysis reveals that the GOES Sounder is especially relevant to National Weather Service products focused on severe weather nowcasting and forecasting as well as climate analysis. Weather and climate along with ocean and coastal observations generally rely on all sounders. At the mission level, the following left graphic identifies which NOAA mission service areas, as defined by the NOSIA model, rely most heavily on IR sounders. Please note the scoring mechanism is used only to rank relative importance. TPIO's analysis reveals that Climate Predictions and Projections, Environmental Modeling and Prediction, Integrated Water and Prediction Information, the Fire Weather National Service Program, and Marine Weather and Coastal Events to be the most heavily reliant on IR sounder data from the previously listed satellite instruments. Reviewing outcomes and products on the right graphic, TPIO lists Satellite Derived Soundings and Profiles, the Extra-Tropical Storm Surge Model, New York Harbor Observing and Prediction System, Extratropical Surge and Tide Operational FOrecast System Model, and the ADvanced CIRCulation Model as the NOAA products most heavily reliant on IR sounder data.

MSA-wide Dependence on IR Sounders

	IR Sounders
Climate Prediction and Projections	0.1023
Environmental Modeling and Prediction	0.1000
Integrated Water and Prediction Information	0.0661
Fire Weather National Service Program	0.0613
Marine Weather and Coastal Events	0.0603
Weather Ready Nation Science, Services, and Stewardshi..	0.0591
Public Weather	0.0504
Tropical Cyclone	0.0452
Aviation Weather and Volcanic Ash National Service Progr..	0.0451
Winter Weather	0.0420
Climate Science and Improved Understanding	0.0319
Arctic Matrix Program	0.0295
Severe Weather National Service Program	0.0214
Assessments of Climate Changes and Its Impacts	0.0203
Ecosystems Monitoring, Assessment and Forecast	0.0183
Climate Mitigation and Adaptation Strategies	0.0141
Healthy Ocean Science, Services, and Stewardship Advanc..	0.0101
Coastal Water Quality	0.0052
Habitat Monitoring and Assessment	0.0044
Resilience to Coastal Hazards and Climate Change	0.0036
Protected Species Monitoring and Assessments	0.0024
Fisheries Monitoring, Assessment and Forecast	0.0020
Resilient Coasts Science, Services, and Stewardship Adva..	0.0016
Marine Transportation	0.0014
Planning and Management	0.0010

Surveyed Product Dependence on IR Sounders

	IR Sounders
Satellite Derived Soundings and Profiles	0.4726
Extra-Tropical Storm Surge Model	0.3446
New York Harbor Observing and Prediction System-proxy	0.3420
Extratropical Surge and Tide Operational Forecast System Model	0.3420
ADvanced CIRCulation model-proxy	0.3420
Arctic Cap Nowcast/Forecast System Model	0.3193
Pan-Arctic Ice Ocean Modeling and Assimilation System: Arctic Cap ..	0.3193
Coupled Arctic Region Modeling and Prediction Research	0.3066
Improved Understanding and Predictions of Hurricane Behavior: Se..	0.3025
Woods Hole Oceanographic Institution Heat/Moisture Flux Product..	0.2941
Objectively Analyzed Air-Sea Fluxes: Reanalysis-proxy	0.2941
North American Regional Reanalysis-proxy	0.2941
NCEP-Department of Energy Reanalysis 2-proxy	0.2941
National Centers for Environmental Prediction/National Center for ..	0.2941
Model Reanalysis: Reanalysis1, Reanalysis2, North American Regio..	0.2941
Climate Forecast System Reanalysis-proxy	0.2941
Atmospheric Reanalysis: International-proxy	0.2941
Atmospheric Model Intercomparison Project II Reanalysis-proxy	0.2941
Experimental Regional Ensemble Forecasting System	0.2918
Atmospheric Trace Gases and Aerosol Research: Retrieval Capabilit..	0.2791
Hybrid Single Particle Lagrangian Integrated Trajectory Model Disp..	0.2782
Global Circulation Models Research: Marine strato-cumulus Charac..	0.2781
Independent Climate Model Verification	0.2577
Flexible Particle Atmospheric Dispersion Model-proxy	0.2502
Coastal Flood Guidance: Ocean Prediction Center	0.2324
Quantitative Precipitation/Temperature Forecast Probabilities	0.2296
Ultraviolet Index Forecast	0.2211

Using TPIO results, the areas of potential benefit submitted by the GeoXO team were corroborated. However, other areas of potential benefit were also identified including climate, fire weather, aviation and volcanic ash advisories, marine and coastal weather, and marine

transportation. Additionally, while the GeoXO team identified hurricane track, intensity, and probability of detection as key areas to support hurricane and tropical storm modeling, it is understood that hurricane evacuations are highly dependent on storm surge models. The TPIO analysis identifies two storm surge models as highly sensitive to IR sounder data.

6.2.2 Economic Valuation and the Value Chain Approach

A microeconomic approach is used to establish a theoretical framework for the value of information, which is described in detail in many studies of the value of information. Examples in the weather, Earth observation, and satellite sensor domain include Williamson et al. (2002), Macauley (2005), Pearlman et al. (2016), Bernknopf et al. (2017), Abt Associates (2018), and Pearlman et al. (2019).

A value chain describes the process of turning data from the HSS instrument into actionable information. Outlining and describing this process is a key component of the analysis necessary for estimating the value of a product or process that is not directly used by an end user. For each of the case studies we examine in this report, it is important to trace how data from the HSS instrument is transformed into data that informs decision making. For each use case, the end users and the products they rely on may be different. However, the process that leads to the creation of the weather forecast products that rely on the HSS will be similar.

Similar to other sensors in the GEO orbit, information from the HSS sensor will not be used directly by decision makers to generate additional economic value. Instead the data generated by this sounder will be combined with other environmental data in a variety of models and analyzed to produce weather and water forecasts and other information products. These final outputs are what is ultimately shared to inform decision makers. Since the data produced by the HSS instrument is not directly used by decision makers it is important to trace the process of how data is transformed into actionable information using a value-chain framework. The existence of data alone does not necessarily generate additional economic value; the value of additional data will depend on the ability to assimilate new data into the existing forecast production process. This tracing process is also required because improvements to weather forecasts could come from a variety of different inputs. Establishing the value chain linkages ensures that we measure improvements that are associated with data from the new instrument. Understanding the different mechanisms that can lead to weather forecast improvements and reduce damage is an important part of analyzing the trade-offs and opportunity costs associated with the instrument being considered. This will be important if the HSS is selected for further consideration.

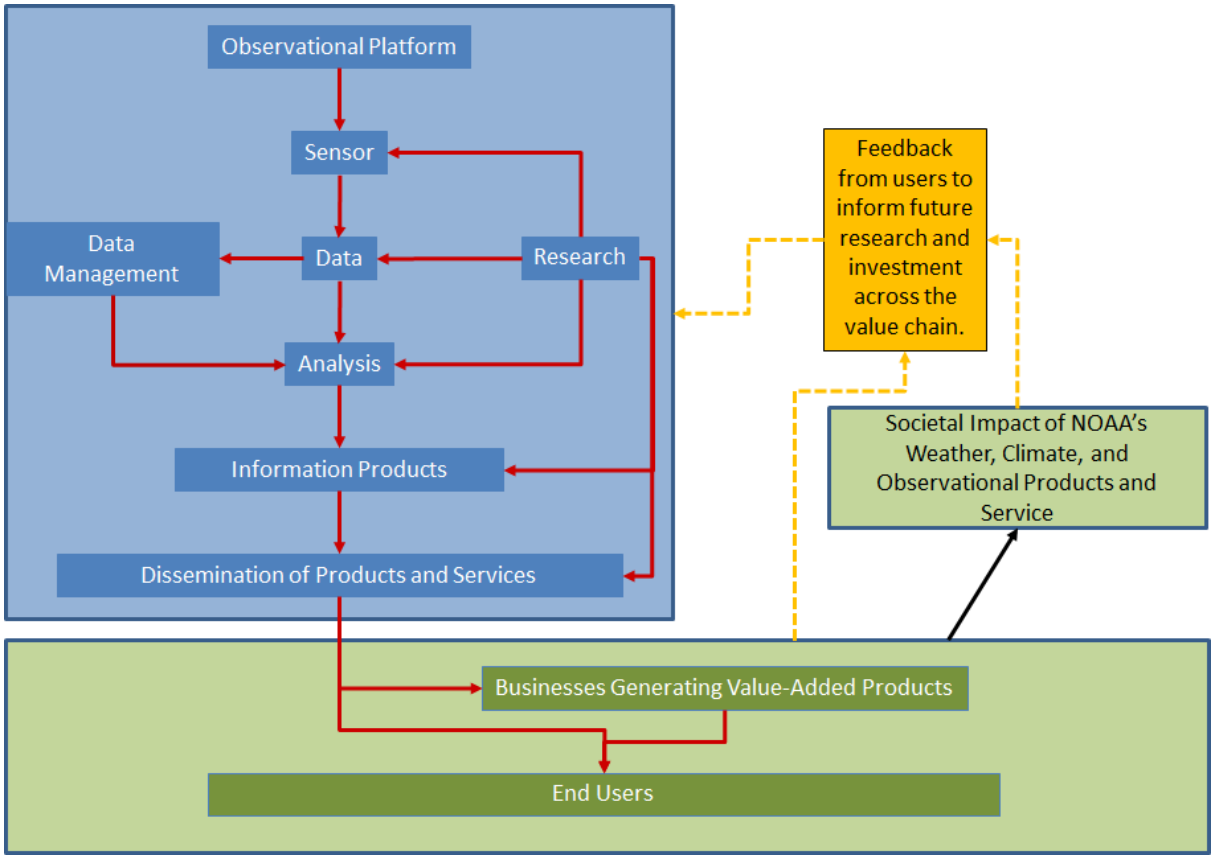

Figure 6-1. NOAA Value Chain Depiction

Adding a HSS to future GeoXO satellites is expected to provide better information about the state of the atmosphere. This information has the potential to improve the information products and forecasts distributed by the National Weather Service (NWS) and other modelers. Information has value when it can inform decisions that result in better outcomes (Williamson et al 2002). Assessing the value of information requires understanding this decision-making process: Who makes decisions, what information informs the decision making process and what results from that process? The value of new information is determined by comparing the outcomes that result from decisions that are made with and without the new information. In this case the new information is the improved forecast products that result from the use of data generated by a HSS on future GeoXO satellites. A formal depiction of this can be seen in Figure 6-1.

The needs of end users should be the primary factor in determining future investments in observing systems. It may be possible to address these needs at one or more points in the value chain. End users may find that different components of the forecast or other products are more important in some applications than others. They may also have thresholds where small improvements in a particular dimension of the forecast or other output can lead to significant advances in decision making and the resulting outcomes. In other cases, large improvements to the forecast may have minimal influence on the outcomes. Important questions about the decisions made by key end users are described in the following section.

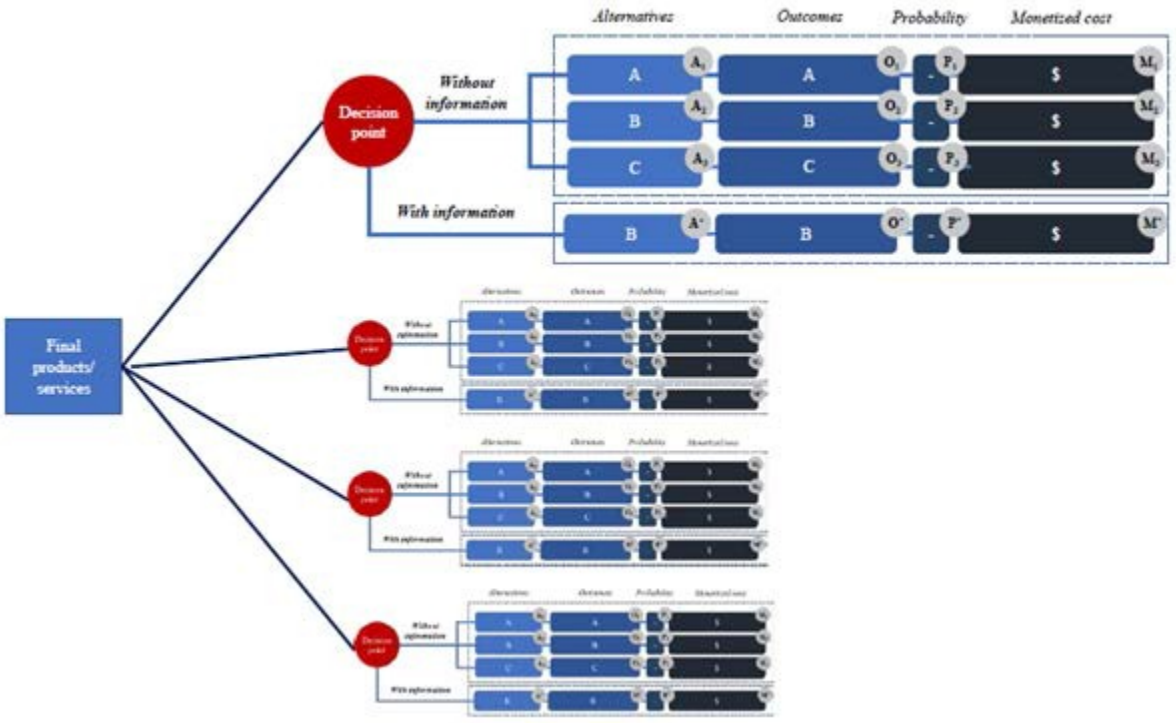

Figure 6-2. From Pearlman et al (2019) depicts the process for estimating value of information for a specific decision, and how that links back to the product or service that connects to the value chain.

6.2.3 Information Collection through Expert Elicitation

In addition to understanding how data from a new instrument is used to create actionable information, it is necessary to understand the decision-making context for end users. For this study we engaged in outreach to experts in the areas identified by the team as likely to be impacted by data from the HSS instrument. The people we talked to represent a convenience sample of connections within the GeoXO valuation working group. There are currently efforts underway as part of the larger GeoXO planning process to engage in a formal, systematic, and more comprehensive outreach to experts in the weather information user community. Follow-on studies should seek to leverage these efforts. More information can be provided by contacting the authors.

Several common themes emerged in conversations with subject matter experts. Most experts, including NOAA service providers and external users, could not provide clear linkages between the potential benefits of the hyperspectral sounder and their subject area. When the improvements were elaborated upon, the experts displayed optimism but also explained that model improvements from enhanced infrared sounder data would take time to be implemented. The experts also expressed current challenges in data assimilation and limitations in making complete use of existing data. These challenges and limitations are likely to also affect the utility of HSS data. Furthermore, the subject matter experts, especially in

discussions related to precipitation and storm track intensity explained that many of the OSSE-provided results from surveys of the existing literature did not align with how weather forecasts and emergency planning decisions were made, as other data inputs such as radar are leveraged, and decisions are made prior to the 18-hour lead time listed in one of the published OSSEs was provided to NOAA economists. It is not possible to quantitatively measure the value of information that does not contribute to user decisions. Qualitatively, several meteorologists suggested that accurate forecasts contribute to trust and improved working relationships even in cases when the forecasts were made too late to influence decisions.

6.2.4 Break-Even Analysis Scenario Selection

The purpose of this preliminary analysis is to determine whether the benefits of adding a HSS to future GeoXO satellites are likely to exceed its cost and whether the strength of the evidence is sufficient to justify further consideration of this sensor.

To establish a complete and robust analysis, the full life-cycle costs should be analyzed to determine the average annual cost of adding a HSS to the GeoXO satellites. However, the cost of ground systems, operations, maintenance, and spacecraft accommodation was not known throughout this valuation study and are not included in the analysis. Only the cost of the instrument is used. Estimated costs were tabulated on an annual basis and discounted to determine the present value of those costs. Expressing these costs in terms of present value allowed the economic consideration of the 'time value of money,' or the fact that a dollar received today has a higher value than a dollar received next year or in the remote future. This is an important consideration because the cost of investments tend to be concentrated near the present whereas benefits are spread more evenly across the project life.

During the course of this study, a number of benefit areas were explored for assessing the potential benefits of the HSS. A comprehensive assessment of benefits would consider both the contribution of the HSS to weather forecasting capabilities and other product outputs and the economic consequences (benefits) of the resulting improvements to these products and services. The rigor with which each component of a comprehensive assessment can be addressed varies across scenarios and is limited by the availability of data needed to conduct the analysis.

Three benefit categories that include an assessment of the contribution of HSS to weather forecasting capabilities were identified:

- Improvements to Severe Weather Forecasts
- Improvements to Weather Forecast Skill
- Improving Predicted Hurricane Track and Intensity Accuracy.

However, the benefit categories described above are broad in scope and are likely to generate a broader range of societal benefits, many of which could not be quantified in this study. In order to estimate the value of these improvements we focused on a subset of decision scenarios that are influenced by improvements to this information:

- Scenario 1: Reductions in weather-related airline delay costs resulting from improvements to severe weather forecasts
- Scenario 2: Reductions in electric power generation and acquisition costs resulting from improvements to weather forecasting skill
- Scenario 3: Reductions in hurricane evacuation costs resulting from improved predicted hurricane track and intensity

The selection was based on a review of previous studies of similar instruments, the availability of existing data, and the expert judgment of the valuation working group. These scenarios were assessed to determine the nature and magnitude of benefits that would be required for each scenario to independently justify the addition of the HSS. Each scenario describes the nature of forecast improvements, the mechanisms by which forecast improvements advance societal outcomes, and the specific HSS data that lead to those forecast improvements.

In all three cases, benefits resulted from avoided costs. To allow the subjective assessment of the reasonableness of these cost-reductions, they were expressed in both absolute terms and in terms of percent of total costs; the latter reflects the assumption that a 1 percent reduction in weather-related costs is more achievable than a 50 percent, 75 percent, or 90 percent reduction in costs. To the extent possible within time constraints, analysts discussed these scenarios and the associated benefit estimates with subject matter experts to subjectively assess their reasonableness.

6.2.5 HSS Cost Analysis

This analysis reflects the estimated cost of HSS instruments needed for GeoXO satellites, with an operational life spanning the years 2032 to 2051. The preliminary estimated cost of $854 million does not reflect ground costs, operations, maintenance, and spacecraft accommodation; these costs were not available at the time the economic analysis was initiated. Annual costs will vary significantly over the years 2023 to 2040.

Thus, the cost of the HSS instrument is incurred over the years 2023 to 2040 while the benefits accrue over the years 2032 to 2051.

The Office of Management and Budget's (OMB) preferred method of handling temporal differences in benefit and cost streams is to discount them at the rate consumers and savers would normally use in discounting future consumption benefits.[2] Two different discount rates are commonly used, one showing the effects of government spending on the allocation of capital and the other showing the effects on private consumption. A 7 percent discount rate reflects the average before-tax rate of return to private capital in the U.S. economy and is used to approximate the cost of displacing or altering the use of capital in the private sector. A 3 percent discount rate is used to approximate the effect of government spending on private consumption; because people prefer to consume sooner rather than later, a 'social rate of time

[2] For more details, see pp. 33-34 of OMB Circular A-4 dated September 17, 2003, located at https://www.whitehouse.gov/sites/whitehouse.gov/files/omb/circulars/A4/a-4.pdf.

preference' is used, calculated as the real rate of return (net of inflation) on 10-year US Treasury notes.

Because the nature of the impact of government spending is unknown in this case, results are calculated using both the 7 percent and 3 percent discount rates. These discount rates were applied to the costs incurred in each year between 2023 and 2040 to compute discounted, or "present value" costs. The present value of the HSS instruments is $693 million at a 3 percent discount rate and $456 million at a 7 percent discount rate. In order for this investment to be economically justified, the discounted benefits must be equal to or greater than these figures.

The present value costs are used in the break-even analysis below, determining the magnitude of benefits that are needed to offset costs. It is suggested as of September 2020 that the features required to operate the HSS (ground costs, operations, maintenance, and spacecraft accommodation) will add another 20 to 60 percent to the costs analyzed here; this differential is addressed in the text of the three scenarios below.

6.3 Economic Analysis Scenarios

6.3.1 Scenario 1 - Reductions in Weather-Related Airline Delay Costs (Benefits for Aviation)

Statistics produced by the Federal Aviation Administration (Federal Aviation Administration 2019) show that in 2018 delays of all types cost the airline industry and passengers $28.2 billion, 67 percent of which ($18.9 billion) were weather-related. These totals, which have been generally increasing since 2012, include the following categories of costs:

- Airlines (cost of delay to airlines): Increased expenses for crew, fuel, maintenance, etc. (23 percent of total delay costs)
- Passengers (cost of delay to passengers): Time lost due to schedule buffer, delayed flights, flight cancellations, and missed connections (57 percent of total delay costs)
- Lost demand (cost of passenger decisions to avoid future air travel): Estimated welfare loss incurred by passengers who avoid future air travel as the result of delays (7 percent of total delay costs)
- Indirect (indirect cost of delay): Other business sectors depend on air travel for transportation. Air travel delays impact these sectors by increasing costs in terms of dollars and time (13 percent of total delay costs).

Relevant data obtained from the Federal Aviation Administration (FAA) report are summarized in Table 6-1 below.

Table 6-1. Summary of Information on Flight Delays

Number of Flight Delays	260,325
Percent Weather-Related	67%
Number of Weather-Related Delays	174,157
Cost of all Delays (billions)	$28.2
Cost per Delayed Flight	$ 108,326
Cost of Weather-Related Delays	$ 18,865,800,000

Source: Federal Aviation Administration, 2019.

6.3.1.1 Assumptions Regarding HSS that will Affect Airline Operations

Two satellites with HSS capabilities are needed to reduce weather-related airline delays nationwide. The cost estimates shown above reflect the HSS becoming operational by 2032, generating benefits from 2032 to 2051. However, only one GeoXO satellite will be in operation in 2031, providing only half the coverage needed to support nationwide benefits to the airline industry. A second GeoXO satellite will be operational during the next year, providing nationwide coverage through 2048. During the last three years in the period of analysis (2049 to 2051), only one satellite with HSS capabilities will be in operation; during these years, only half of the nation would benefit from the HSS. Although there is no reason to expect the phase-out of the use of HSS after 2048, the assumption that only one satellite with HSS capabilities will be in use from 2049 to 2051 is necessary to estimate the benefits that correspond to the costs that are used in this analysis; continued investment in HSS capabilities would be required to ensure nationwide coverage beyond 2048.

6.3.1.2 Estimating Benefits

As noted above, the goal of this economic assessment is to estimate the magnitude of benefits that are needed to justify the cost of the HSS, describe the outcomes that would be needed to generate benefits of that magnitude, and, with the assistance of experts, assess the reasonableness of achieving those outcomes.

To estimate the magnitude of benefits to the airline industry that would justify the cost of the HSS, we started with the discounted costs described above and determined the stream of benefits whose present value is equal to the present value of costs. Based on the assumptions stated above on the years during which the HSS would cover half versus all of the nation, the annual benefits accruing during 2032 and 2049-2051 were estimated to be one-half of the benefits accruing during the years 2033 to 2048. These benefits were discounted at 3 percent and 7 percent to allow comparison with discounted costs so a breakeven value of benefits could be determined.

At a 3 percent discount rate, total discounted benefits and costs (the present value of benefits

and costs) are equal with the following benefit stream:

2032: $32.7 million annually
2033 - 2048: $65.4 million annually
2049 - 2051: $32.7 million annually

At a 7 percent discount rate, total discounted benefits and costs (the present value of benefits and costs) are equal with the following benefit stream:

2032: $49.4 million annually
2033 - 2048: $98.9 million annually
2049 - 2051: $49.4 million annually

6.3.1.3 Description of Benefit Scenarios

As stated above, the airline industry incurred $18.9 billion of weather-related delay costs in 2018, a figure that has been trending upward since 2012. To assess the reasonableness of the cost-savings, we express the savings as a percentage of the total cost of weather-related delays to the airline industry. The required annual cost-savings are greater when a 7 percent discount rate is used; for that reason, the discussion below focuses on the required savings associated with the use of a discount rate of 7 percent.

Estimates of benefits align with the GeoXO operations (one vs. two satellites) that are reflected in the cost estimates. The benefits associated with a reduction of weather-related delays will exceed the cost of the HSS instruments if the resulting reductions in weather-related delays equal:

- 0.3 percent in 2032 (one satellite with HSS will provide only partial coverage of the U.S.)
- 0.5 percent between 2033 and 2048 (years when full national coverage of HSS data will be available) and
- 0.3 percent between 2049 and 2051 (one satellite with HSS will provide only partial coverage of the U.S.)

These figures show that investments in HSS instruments are worthwhile if this leads to improvements in NWS products and services that reduce weather-related airline delays costs by about one-half of one percent. Any larger reduction in weather-related costs to the airline industry will yield positive net benefits. In this case, a one percent reduction in weather-related delay costs would, for example, provide almost $2 of benefits for every dollar spent on HSS.[3,4]

---

[3] Using a 3 percent discount rate, delay-reductions ranging from 0.17 to 0.35 percent would be required to achieve a present value benefit:cost ratio of 1.0; a one-percent reduction in weather- related delay costs would achieve a benefit:cost ratio of almost 3:1.

[4] For computations, see the Breakeven tab in this Google Sheet.

Experts in airline industry operations from MIT Lincoln Laboratory (MIT LL) were consulted to assess the reasonableness of achieving benefits of the magnitude needed to offset the costs of the HSSs (0.17 percent to 0.52 percent); they characterized cost-reductions of this magnitude as “conservative” in comparison to findings in similar studies.

MIT LL experts note that cascading delays are a significant issue, where queuing delays compound as delays on runways lead to delays at gates, resulting in non-linear increases in delay costs. Even small time savings can generate large benefits by avoiding cascading delays.

Even if ground systems, operations, maintenance, and spacecraft accommodation double the costs used in this analysis, reductions in weather-related airline delay costs of just over 1 percent will offset the entire cost of an operational HSS on future GeoXO satellites (note that the inclusion of these costs is expected to increase total costs by no more than 60 percent).

Future studies should explore the extent to which weather-related airline delays are avoidable. Some delays are related to forecast error and can be avoided as forecast accuracy is improved; however, other delays are related to actual hazardous conditions and cannot be avoided.

6.3.1.4 Linkage to HSS Instrument

Airline industry experts at the MIT LL suggest that airline benefits will predominantly come from improvements in numerical weather prediction (NWP) models and severe storm prediction, with fewer benefits coming from hurricane prediction because of the long lead time associated with the latter. Thus, forecast improvements will have the greatest impact during the convective storm season. Forecast improvements that provide the greatest benefit to the airline industry include:

- Predictability, better skill better trust
- Precipitation
- Needs to inform binary decisions
- Turbulence
- Icing and winter weather
- Wind shifts at the surface
- Compression issues aloft

HSS data will support other forecast improvements that can reduce weather-related delays to the airline industry, include a 40% increase in the probability of detection of precipitation from severe storms at 6 hours, better prediction of precipitation and precipitable water, winds, and stability indices for forecasts, (> 4% wind forecast error reduction ~ 400 hPa) and improved prediction of elevated Convective Available Potential Energy (CAPE) for storms detection.

6.3.2 Scenario 2 - Electric Load Forecasting

6.3.2.1 Weather-related costs related to electric power production

Weather predictions play an important role in electricity load forecasting models used by power companies to plan their electricity production. This is one of the benefit areas identified

by a 2002 study of the value of GOES data (NOAA NESDIS 2002). Electric power producers use short term load forecasting models, which rely heavily on 3-24 hour forecasts of temperature, wind, and humidity (Hong and Kim 2015) to plan electricity production. One example of a load forecast model, used by PJM Interconnection[5], identifies several weather-related variables including wind-adjusted temperature, temperature humidity index, heating degree days (HDD), and cooling degree days (CDD) (PJM 2016). Overproduction of electricity leads to costs because companies may be unable to sell the excess power or forced to sell at a loss; underproduction requires the use of more expensive generating technologies or the purchase of additional electricity on the spot market. In rare cases it may even lead to brownouts or blackouts.

[5] From their website: "PJM Interconnection coordinates the movement of electricity through all or parts of Delaware, Illinois, Indiana, Kentucky, Maryland, Michigan, New Jersey, North Carolina, Ohio, Pennsylvania, Tennessee, Virginia, West Virginia and the District of Columbia."

6.3.2.2 Description of Benefit Calculations

This analysis builds on the assumption from a 2002 study of the value of GOES data for the electric power industry (NOAA NESDIS 2002). We assume that the average load forecasting error is 1.79% for the industry. This assumption is based on a 2017 presentation made public by PJM, a regional transmission organization that coordinates the movement of wholesale electricity (Anastasio 2017).

Data about the price of wholesale electricity, and the amount of electricity produced was acquired from the US Energy Information Administration (EIA 2020). For the initial analysis we used the average wholesale price over the period of Jan 2014-March 2020 which was $38.74/MW (The price for individual transactions over this period ranged from $14.30-$498.68/MW, the range of yearly averages was $29.74-$53.34 for 2014-2019).

Similar to the 2002 study we assume that the load forecasting error is equally probable to over or underestimate the true energy demand and that the consequences of an error in either direction are equally costly. In practice, overestimates and underestimates will lead to different types of costs (NOAA NESDIS 2002).

We multiplied the average load forecast error by the total number of kilowatt hours of electricity sold to consumers and multiplied the result by the average wholesale price of electricity to estimate the cost of the load forecast errors for electricity suppliers.

The discounted cost of the HSS instrument assuming a 3% discount rate is $639.3M. To achieve the break-even level of benefits which would cover the cost of the HSS instrument, the total load forecast error needs to be reduced by 2.5% (i.e., reducing load forecast error from 1.79 percent to 1.74 percent). The use of a 7% discount rate implies the need to reduce the total load forecast error by 3.9% (i.e., reduction load forecast error from 1.79 percent to 1.72 percent).

There are many variables that affect the load forecast error rate, only a portion can be attributed to weather forecast errors (PJM 2016). The 2002 CBA study assumed that 40% of the load forecast error could be attributed to weather forecasting errors (NOAA NESDIS 2002). This was determined based on informal personal communication and has likely changed in the ensuing years. More recent literature about short term load forecasting (Hong & Kim 2015, Hong 2014) suggests that weather information remains a crucial explanatory variable in these models, but we were unable to determine what portion of the load forecasting error can be explained by weather data inputs. Following the 2002 CBA study (NOAA NESDIS 2002) we can divide the needed improvement in the load forecast (2.56% for the 3% discount rate case, 3.88% for the 7% discount rate case) by the 40% of the load forecast error that can be attributed to weather variables. The resulting 6.4% to 9.7% (for 3% and 7% discount rates respectively) is the accuracy improvement necessary for the temperature, wind, and humidity

forecasts needed to justify the cost of this instrument. We will need to see the results of the OSSE/OSE studies to see if these kinds of improvements are realistic.

There are issues with this approach that would need to be addressed in future work. While temperature is included as a variable in almost every load forecasting model, many models also include additional variables such as wind and humidity. Additionally, many load forecasting models include interaction terms, splines, or other non-linear terms, which imply a nonlinear relationship between weather forecast improvements and electricity load forecast improvements. Different forecast models are used by different companies, so we are likely to see heterogeneous benefits across the industry. Additionally, it is not clear where weather information for load forecast models comes from. A survey of the literature suggests that many load forecast models rely on in-situ weather station data (Hong et al 2015) rather than satellite data. There is no guarantee that the improved weather information would be incorporated optimally into load forecasting models. It may be necessary to account for a lag in the use of improved information. Future studies will need to provide a more thorough exploration of these issues. All of these caveats imply that this analysis provides a rough estimate of the forecast improvements that would need to result in order for load forecasting improvements to justify the cost of this new instrument.

6.3.2.3 Sensitivity analysis

Many of the variables used in this analysis could change over the ensuing 30 years. In addition to the discount rate discussed above, there could be other factors that influence the outcome of this analysis. We assumed that the load forecast error was 1.79% but this is based on information supplied by one regional power supplier. Other companies or regions may have different error rates, and this rate will change as modeling improves. It is also possible that there are significant changes in the price of electricity, which could be driven by a number of factors. The yearly average wholesale price fluctuated between $29.74/MW and $53.34/MW over the period analyzed. The weather portion of the forecast error which we assume is 40% of the total error based on previous studies, may also change. This number is based on very weak evidence and the study it comes from is almost 20 years old already; it will be 50 years old at the end of the period being analyzed. Advances in modeling ability, or changes in the technology used to produce energy could substantially affect the portion of the load forecasting error that can be attributed to weather. Small changes in these parameters could result in large changes to the results reported in this analysis. Readers of this report should recognize that there are large error bounds on the numbers reported in this section. A simple sensitivity analysis was conducted using the minimum and maximum yearly average prices over the period examined. We also varied the weather portion of the load forecast error and the magnitude of the total load forecast error by 20%. In this sensitivity analysis the improvement to temperature, wind, and humidity forecast accuracy necessary to justify the cost of the HSS ranged from 2.8% to 30.1%

6.3.2.4 Linkage to HSS instrument

Electric load modeling requires quality measurement/prediction of surface conditions for accuracy. In-situ observations are likely to continue to be important in this application area, but NWP which rely on satellite data input are likely to also play a key role. Further study of

the process used by electric power producers to ingest weather information will be important for future studies in order to establish a clear link between the HSS instrument and the benefits to this industry. At the time of this writing there is no clear evidence that the HSS instrument will improve surface predictions of temperature, wind and humidity by 6-10%. Although, literature OSSE results indicate that HSS will improve temperature, moisture, and wind predictions higher in the atmosphere by at least these.

6.3.3 Scenario 3 - Hurricane Evacuation

A third area of potential benefit identified by both the GeoXO working group and the analysis submitted by NESDIS/TPIO includes improved decision support in administering hurricane evacuations. As outlined in the Table 6-2 below, the XORWG-provided OSSE results expect the HSS to provide improved vertical profiles of atmospheric parameters in temperature, moisture, and vectored winds at a higher temporal frequency. For hurricanes, this could potentially lead to refinement in landfall location, hurricane intensity tracking through eye surface pressure and winds, an improvement in the probability of tropical storm and hurricane detection, and more frequent temporal samples in temperature, moisture, and wind profiles to improve numerical weather models. Unless otherwise stated these improvements are found at an 18-hour lead time prior to hurricane landfall from a status quo value not provided in the OSSE table.

Table 6-2. GeoXO Provided OSSE Summary Results (summarized from previous section results)

Refined landfall locations	33 km
Refined hurricane intensity (eye surface pressure and winds)	4 hPa
Improved probability of detection	0.35 in POD at 6 hours out; 0.1 in POD at 18 hours
More frequent temporal samples, with more vertical samples and more horizontal samples of T, q, u, and v for finer sampling of the atmospheric state	5 min Meso profiles and 60 min SFD vs 60 min legacy vert profiles from ABI and ~ 4 hour profiles for polar; ~2x smaller in each of two directions compared to polar; 1 K rms error vs 2 K rms error compared to ABI; 8 vert DOF layers vs 3 vert DOF with legacy vert profiles.

6.3.3.1 Assumptions Regarding the Hyperspectral Sounder

As previously stated, adding the HSS to the GeoXO platform is expected to cost $853 million over the period of 2023 to 2040. Assuming a discount rate of 3 percent, the 2020 present value is $639.3 million. Given most tropical storms are focused on the Atlantic and Gulf coasts of the United States, satellite coverage and constellation configurations play a significant role in how the HSS can improve hurricane evacuation decisions. The benefits derived from this case study apply primarily to GeoXO platforms observing the Atlantic Ocean and its respective US coastal areas. This analysis also focuses solely on the improvements offered by a geosynchronous hyperspectral sounder on the next-generation GOES platform. Improvements and alternatives from computational modeling, decision support, data assimilation, and other instruments or platforms are not considered.

6.3.3.2 The Cost of a Hurricane

Hurricanes, or tropical cyclones formed in the Atlantic Ocean, pose a regular threat to the Southern and Mid-Atlantic coasts of the United States. According to the NOAA National Hurricane Center (Blake and Gibney, 2011), about 5.4 tropical storms become hurricanes per year with 1.91 evolving into major hurricanes (S-S Category 3, 4, or 5). From the same dataset, the U.S. incurs on average 1.78 land-falling hurricanes per year. While total damage estimates of hurricanes do not include damage a storm causes once it moves inland or the cost to an individual of an evacuation, the median cost, using NCEI's methodology (Website, Billion Dollar Weather and Climate Disasters), of a land-falling hurricane is $1.8 billion with an average value of $9 billion (Accuweather 2011). The skew of average value is due to high- impact storms such as Hurricane Katrina, which was valued to cost $145 billion (2011 adjusted) and not including hurricanes and other tropical storms that do not reach this disaster threshold.

6.3.3.3 The Cost of Hurricane Evacuations

A study of the cost of hurricane evacuation (Whitehead et al. 2003) estimated that the cost of an evacuation of a North Carolina coastal zone, or county, is $1 million to $50 million (2000 USD) [$1.49 mi to $74.45 mil in 2020], with variation accounted for by storm intensity and socioeconomic indicators. The evacuation costs per capita extrapolated from Whitehead's North Carolina predicted evacuation costs range from $211 [$322 USD, 2020] to $292 [$446 USD, 2020].

Table 6-3. Predicted Evacuations Costs by Order and S-S Scale for North Carolina

Predicted Evacuation Costs (2000, USD) by Order and S-S Scale for North Carolina							
		Watch		Voluntary Evacuation Order		Mandatory Evacuation Order	
S-S Scale	PerCapita Cost	Evacuees	Total Costs	Evacuees	Total Costs	Evacuees	Total Costs
1	$211.51	4,942	$1,045,272	5,775	$1,221,429	69,402	$14,679,118
2	$232.69	7,290	$1,696,258	8,430	$1,961,627	81,799	$19,033,256
3	$273.27	18,703	$5,110,912	21,031	$5,747,169	116,564	$31,853,788
4	$256.10	3,2618	$8,353,550	35,983	$9,215,274	138,582	$35,490,907
5	$292.31	88,148	$25,766,37	93,139	$27,225,118	172,462	$50,411,975
Whitehead, "One Million Dollars a Mile? The Opportunity Costs of Hurricane Evacuation,"							

While evacuations are unavoidable, not all are necessary. Regnier (2008) outlines the emergency manager decision process and highlights the cost of false positives or false alarms in evacuating coastal populations. Regnier estimates that for large cities,

evacuations begin at 60-72 hours prior to the hurricane striking with small cities taking 24-36 hours. Discussing these estimates with the National Hurricane Center (NHC), the evacuation decisions for major cities are made four days or 96-hours in advance of landfall with internal agreement among emergency managers usually the day before. Special circumstances can create the need for even longer lead times; for example, the 2020 hurricane season compounded by impacts from COVID-19, the NHC noted that South Carolina will make hurricane advisories and evacuation decisions five days in advance of landfall.

6.3.3.4 Connecting Observations to Decisions

Hurricanes cannot be controlled but their effects can be mitigated through preparedness and proper disaster management. To identify the benefits of the GeoXO HSS, the improvements to hurricane prediction must be realized by decision-makers such as public officials, federal, state, and local emergency managers or the public. As presented in the value chain above, the GeoXO HSS data must be processed through NOAA and delivered through weather models and decision support tools. NOAA's National Weather Service (NWS) develops the following TPIO-identified key products to be used directly or to be included in value-added commercial products:

- Hurricane Local Statements
- Tropical Cyclone Forecasts and Analyses
- Tropical Cyclone Vitals
- Tropical Cyclone Wind Position and Intensity Tracking
- Tropical Weather Outlooks.

While these weather products are helpful to inform evacuation decisions, one of the most critical decision support tools for hurricane evacuations comes from the NOAA NWS Sea, Lake, and Overland Surges from Hurricanes (SLOSH) model (Website, National Hurricane Center). The inputs for this model come through National Hurricane Center advisories along with observations from aircraft, ships, buoys, radar, and satellites either directly or through intermediate products such as numerical weather prediction. The model is then overlaid to a specific area's shoreline to identify areas most prone to storm surge. The outputs are the Maximum Envelopes of Water (MEOWs; Fig. 6.3), which are detailed at a county level, and Maximum of MEOWs (MOMs, Fig. 6.4), which provide a coastal or state-level view. As stated by National Hurricane Center Staff, decisions are made as early as four to five days prior to landfall especially in critical or heavily-populated areas. Regnier (2006) identifies evacuation decisions to be made 60-72 hours prior to landfall.

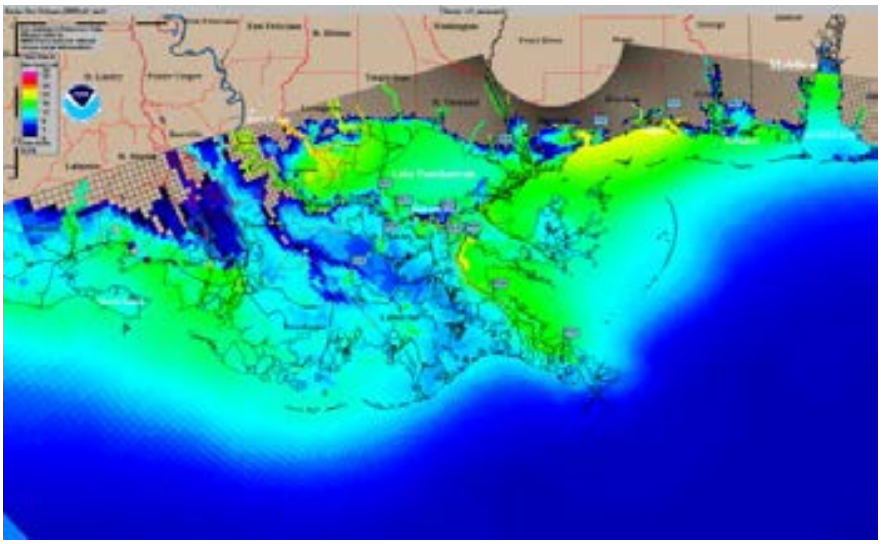

Figure 6.3. Maximum Envelopes of Water (MEOW)

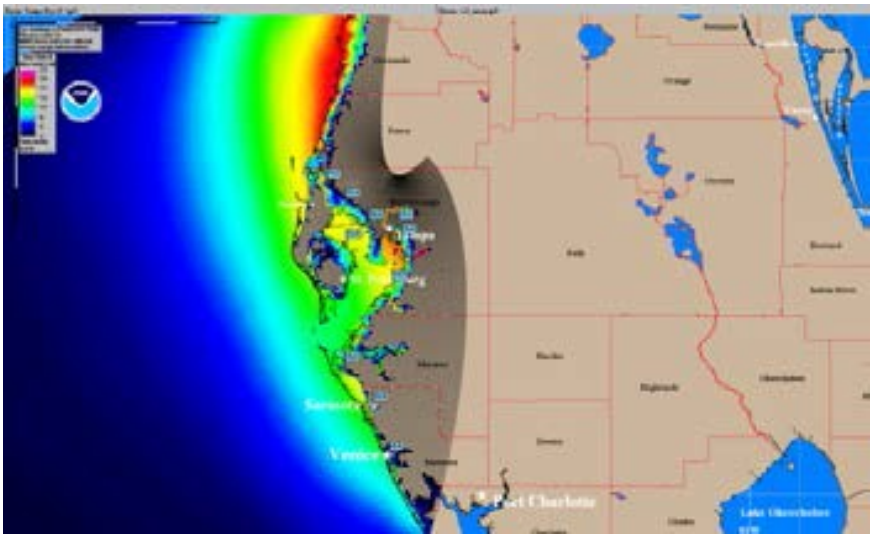

Figure 6.4. Maximum of MEOWs (MOM) Output

To properly understand the benefit of the HSS instrument, a comparison must be made between the status quo decisions of the end-user using the above, or derived, hurricane products and any improvements to decisions realized by including HSS data in the models. As stated in Glahn et al (2009) a NOAA compilation of hurricane evacuation studies, Florida's Division of Emergency Management's evacuation studies and corroborated by staff at NOAA's National Hurricane Center, the SLOSH model a key NWS decision support tool evacuation managers use to decide which hurricane evacuation zones.

Reviewing the proposed improvements provided in the table, the benefits identified (at the 18-hour mark) do not directly support hurricane evacuation decisions, especially at the lead time required. It is also identified by NHC that an improvement of 33km (or 20.5 miles) currently falls within the noise threshold of

hurricane track prediction. Furthermore, storm surges do not necessarily align with hurricane landfalls.

6.3.3.5 A Method to Estimate the Benefits of Improved Hurricane Evacuations

While further analysis is required to properly identify how the GEO- XO HSS instrument could potentially improve hurricane emergency management decisions, the following method is proposed as a prototypical benefit transfer model on how to derive benefits from improvements to hurricane and storm surge models. This valuation approach attempts to generalize available information from completed studies and other resources measured in different contexts while clarifying the assumptions made in specificity (generalizing North Carolina value assessment to the Atlantic coast) and imperfect parametric analogs (using hurricane landfall versus storm surge modeling).

Table 6-4. Whitehead Predicted Evacuation Costs by S-S Category

Whitehead Predicted Evacuation Costs by S-S Category	
S-S Cat	2020 USD
1	$4,562,724.89
2	$6,373,911.51
3	$13,703,776.05
4	$18,804,687.62
5	$45,058,686.63

Whitehead's (2003) case study for the 1998 Category 3 Hurricane Bonnie where 70% of North Carolina fell under Watch, 14% under Voluntary Evacuation, and 16% under Mandatory Evacuation, he estimated the total opportunity cost incurred to evacuees to be $9.4mil (USD, 2000 dollars). In 2020, this amounts to $14.5mil USD. While historical datasets are still being developed for SLOSH and storm surge modeling, the NHC does report the "typical size of a hurricane" to be around 300 miles. As North Carolina has 322 miles of ocean shoreline, we generalize Whitehead's evacuation costs to be the total cost of evacuation per hurricane by Saffir-Sampson (S-S) hurricane wind scale (see table).

The NHC reports that 1.78 Atlantic hurricanes (Cat. 1 or greater) make landfall per year. Multiplying the Whitehead predicted evacuation cost of a Category 1 hurricane by 1.78 for each year and 20 for the lifecycle of the GeoXO platform, the associated costs are $8.1mil and
$162.4mil respectively. Reviewing North Carolina's ocean shoreline mileage by evacuation zone/county, we roughly estimate each evacuation zone to be 20 miles in length, which coincides with the GeoXO team's proposed landfall refinement improvement of 33km (20.5mi). Assuming a uniform population distribution in the

hurricane landfall location, removing one county or evacuation zone from the hurricane watch, voluntary, or mandatory order could reduce the evacuation costs by 1/15 as calculated by dividing the estimated 20 mile county into a typically-sized 300 mile-wide hurricane (Website, National Hurricane Center). Per hurricane, this cost savings is around $300k. Assuming 1.78 hurricanes a year over 20 years, the rough baseline savings could be $10.8m, as this assumes only Category 1 hurricanes over the period. While this represents significant potential savings, these benefits alone, given the current frequency of hurricanes and expected improvements, do not offset the cost of the new instrument. Cost savings associated with hurricane evacuation costs will need to be considered in conjunction with other benefits derived from the HSS.

The above benefit assessment provides a cursory understanding of the magnitude of cost- savings associated with one of the proposed improvements of the hyperspectral sounder provided by previous OSSE results (section 3.3). As established above, the proposed improvements to refinement in landfall location, hurricane intensity tracking through eye surface pressure and winds, improvement in the probability of tropical storm and hurricane detection, and more frequent temporal samples in temperature, moisture, and wind profiles to improve numerical weather models at the 18-hour lead time do not directly support the hurricane evacuation manager's decision process. Identifying how the instrument supports storm surge modeling at lead times beyond 72 hours is necessary. To further refine the benefit assessment, hurricane landfall probabilities could be replaced by coastal storm surge prediction with population count per evacuation zones as the data become available. NHC staff reported storm surge modeling and data collection is still fairly new. Once available, this information can be used in conjunction with Whitehead's (2003) per capita evacuation cost by S-S category. Combining these elements and comparing them against any further improvements identified by the hyperspectral sounder team will provide a valid measure of benefits relating to hurricane evacuation costs.

NHC National Storm Surge Hazard Map

Figure 6.5. National Hurricane Center Storm Surge Hazard Map

6.4 Recommendations to Improve Economic Valuation in Remote Observation Systems Planning

This work examines a few large categories of weather-related losses and HSS-linked improvements in weather forecasts with the potential to reduce those losses. We show that relatively minor improvements in forecast quality have the potential to reduce weather-related damages sufficient to offset the cost of HSS. Experts in relevant fields (including aviation and weather forecasting) agree that such loss reductions are likely consequences of the deployment of HSS in future GeoXO satellites. Additional studies are required to produce a more accurate and complete estimate of the potential benefits of HSS. Several important lessons from the current effort should be incorporated into future studies:

1. The use of a systems approach will help to account for the addition of an instrument to a complex, dynamic system and to optimize NOAA's investments in that system. The weather enterprise is a complex system that depends on the interactions of many different instruments, data processing choices, models, human analysis, communication, and relationships. There are at least three reasons why new instruments should be considered in the context of the system within which they will operate. First, the effects of adding a new instrument could ripple across the entire system or could be constrained by limitations in other parts of the system. Second, the system within which a new instrument will be used is continuously changing. Other instruments will be added to other new satellites and models are in a state of continuous refinement, as are central and local data transmission and management capabilities. Changes to the system could eliminate the need for data from the new instrument or amplify its beneficial effects. Third, even when the addition of a new instrument can be shown to generate benefits in excess of costs, it is possible that other, less costly changes could produce similar benefits; it is also possible that other improvements to the system could produce greater net benefits (benefits in excess of costs).

   One model developed by NASA and MIT provides a framework for optimizing satellite constellations to meet predetermined scientific requirements (Le Moigne, Jacqueline, et al 2017). NOAA/NESDIS/OSAAP has performed assessments of architecture performance to meet user needs through the NSOSA study (St. Germain, et al , 2018). The ASPEN model is currently being developed as a system wide model for the GEO-XO planning process to consider the trade-offs between different architectures. NOAA should focus their effort on developing and improving these models to optimize its investments in future satellite constellations.

2. OSSEs should be designed from the start to focus on scenarios with strong implications for decision-making and societal benefit. For example, OSSE experiments that focus on 18-hour hurricane forecasts are irrelevant when analyzing cost-reductions associated with hurricane evacuations, since these decisions are normally made at least 48 hours prior to predicted landfall. User needs are the foundation of economic

valuation and should be the foundation for observing system planning. Understanding users and their decisions helps identify which forecast improvements are the most valuable. OSSEs should to the maximum extent possible, be framed to anticipate the NWP modeling infrastructure to be available at the time of deployment (e.g., 2030-2050, rather than the more-limited capacity at the time of the OSSE (e.g., 2020). This framing will help ensure that OSSE/OSE studies, which are required by Section 107 of the Weather Act, will be aligned with improvements that create measurable value and facilitate more effective valuation studies.

Improving the connection between OSSE experiments and the needs of decision makers would help provide meaningful input for economic analysis and valuation studies, and improve NOAA's ability to effectively evaluate a new instrument's contribution to societal value.

3. The numbers in this report do not reflect the true value of the HSS instrument. Instead, they are an estimate of the magnitude of benefits that would be needed to offset the cost of the HSS instrument, with a judgement about whether improvements of that magnitude are reasonable. Further study and a longer time horizon would allow NOAA to generate more complete and accurate estimates of the true benefits that are likely to arise due to forecast improvements made possible by HSS. This will require a better understanding of the decisions that are influenced by weather information, and additional ground-truthing with industry experts to assess the reasonableness of assumptions and magnitude of benefits. It may also require designing OSSE/OSE experiments around end user decisions to generate useful counterfactual scenarios.

4. Future studies should investigate and account for the period of time required to realize the full benefits of HSS. One important assumption that underlies this analysis is that benefits will begin as soon as the instrument is deployed, and that benefits will be equally distributed over the time period. This assumes that there will be no period of learning to use, assimilate, and interpret the data from the HSS. If the HSS instrument does not immediately result in improvements to the forecast, this lag will reduce the benefits of HSS.

5. Further exploration of the benefits of HSS will require the consideration of both the capabilities of the instrument and the potential to improve societal outcomes. These two criteria can be used to identify cases where the use of HSS is likely to generate significant benefits. These are areas, as identified through the TPIO analysis, literature review, and discussions with subject experts, suggest other applications where HSS data could lead to societal benefits:
    a. Volcanic Ash
    b. Climate
    c. Fire Weather
    d. Winter Weather
    e. NWP Data Points
    f. Tornado Shelter in Place Orders
    g. Public Confidence and the False Alarm Rate
    h. Air Quality Monitoring

6.5 Economic Evaluation Conclusion

The cases presented in this report are not a comprehensive accounting of all of the potential benefits associated with improvements in our weather forecasting ability, but they do demonstrate that improvements to weather forecasts are likely to continue to result in substantial benefits to society. While there may be some applications for which the forecast is already adequate, even small improvements are likely to result in large benefits for at least some application areas.

The HSS instrument has been identified as one means to achieve additional improvements to our forecasting ability. However, there are many other alternative investments that have the potential to create similar improvements. This is one of the primary weaknesses of studying observing instruments individually instead of considering new and existing instruments as part of a system. It is likely that high value improvement to the weather forecast could be created in more than one way and NOAA should seek to optimize its investments in satellite technology to maximize benefits to society while minimizing costs.

This preliminary study shows that the improvements to weather forecasts that are likely to result from the HSS instrument has the potential to generate societal benefits that exceed the cost of the instrument. However, further study of this instrument is needed to produce a more complete and accurate estimate of its benefits and to assess its cost effectiveness in comparison to alternative means for improving weather forecast information.

7. Summary and Conclusions

The societal economic benefits of an operational GEO hyperspectral IR sounder were examined through recent research. Forecast benefits, resultant societal benefits, and derived societal economic benefits were explored in the areas of severe weather nowcasting and short-range forecasting, Numerical Weather Prediction (NWP) skill enhancements, hurricane and tropical storms, and other applications areas, including aviation. Recent research included literature on Observing System Experiments (OSEs) and Observing System Simulation Experiments (OSSEs), as well as existing analyses. More focused OSEs/OSSEs for severe storms and for a potential international GEO ring of sounders were developed for this study to examine NWP skill improvements. NWS users were also consulted on benefits, data usage, and forecast dissemination to decision makers. Additional benefits to NOAA Mission Service areas were identified by TPIO. Benefit can only be derived if NWS users and their forecasts employ observations operationally, and disseminate trusted forecasts to decision makers. Initial economic benefit was examined by the NOAA Office of the Chief Economist.

OSEs and OSSEs were developed to examine forecast skill improvement from a h yperspectral IR sounder. With the addition of the GEO-IRS full constellation in the complete GEO-ring of IR sounders (2 US, 1 European, 1 Chinese and I Japanese) (LWFULL) experiment, it was seen that the direct impact on the analysis solution was generally positive

globally. (Recall that the Chinese are already flying their hyperspectral sounder, and EUMETSAT will launch their sounder in ~2023).

An experiment including a ring of international GEO sounders had an apparent improvement on the analysis of the east-west winds and is illustrative of the analysis system exploiting the temporal information of the GEO hyperspectral sounder constellation. The temporal information is directly translated to an improved wind analysis. A reduced subset of the GEO ring of sounders (2 US and 1 European) has reduced benefits. These experiments produced the following findings:

- The observations showed a largely beneficial analysis for error reduction in specific humidity.

- In terms of RMS forecast error of temperature, the northern hemisphere temperature forecasts from the experiment start through 2.5 days later were statistically improved through the troposphere, though significant improvement was maintained higher in the atmosphere from the experiment start out to 5 day forecasts.

- In the tropics, forecast improvement was seen from the experiment start through 2 days later, largely through the troposphere; the forecast improvement was maintained further to 4.5 and 5 days in some regions of the mid and lower atmosphere.

- In the southern hemisphere, the results were more mixed, with significant forecast improvement through 2 days later seen in the mid- and lower atmosphere, but forecast degradation from start to 3 days later was seen above the mid-atmosphere.

- Wind and specific humidity forecasts were similarly impacted, with the largest forecast improvements in the tropics. The northern hemispheric forecast improvements were generally short range in time, and the southern hemisphere improvements were improved in the short range and degraded in the medium range.

- A GOES-East Hyperspectral Sounder simulation in a simulated GEO ring of sounders was shown to provide the largest Forecast Sensitivity Observation Impact (FSOI) over CONUS for all passive IR measurements, compared to existing systems, with today's state of the art models and computer processing capabilities. Recall that FSOI is a quantification on how each observation acts to reduce or increase the 24-hour forecast error of a selected norm, in this case the total wet energy norm.

Europeans are planning the MTG IRS sounder for ~2023 launch and have optimized their concepts of operations to best utilize the 3D temperature, moisture, and horizontal wind information these instruments will provide, including skill improvement of their (e.g., ECMWF) NWP model forecasts. The Japanese and Korean Meteorological Agencies (JMA and KMA) are moving forward with plans for inclusion of IR hyperspectral sounders in GEO in the 2028-2029 timeframe, to align with the WIGOS 2040 GEO ring vision.

Estimating vertical atmospheric temperature, moisture, and horizontal wind profiles from radiance observations is only one of the many applications with potential benefit from high-

spectral resolution infrared measurements. The list includes, but is not limited to: atmospheric composition, atmospheric circulation, planetary boundary layer structure and temporal evolution, cloud information, surface parameters, and volcanic plumes.

Initial cost estimates exploring the areas of severe weather short-range forecasting and n owcasting, NWP skill enhancement, hurricane and tropical storm, and other applications including aviation applications, were performed against the cost of the flight-side hardware, development, testing, spacecraft, and launch, and subsequently will include the ground processing cost estimate. Based on an initial break-even economic analysis by NOAA economists of societal economic benefit from US GEO hyperspectral IR sounders, even small levels of forecast improvements in the areas studied were found to provide positive economic benefits to society that exceed the flight hardware costs. There are likely more additional economic benefits to the public that need to be studied further to extract the cases where the better observations produce better forecasts and produce better decisions with significant resulting economic benefit. However, the several hundred billion U.S. weather forecasts accessed by the U.S. public through various media (i.e. internet, television, NWS webpages) are valued by the U.S. public at $31.5 B each year (in 2009 dollars), as determined through surveying the annual price that households would be willing to pay for forecasts (Lazo, 2009). Although only a portion of any forecast improvement is tied to the IR sounder, only about 4% of this annual value for forecasts in a single year would be comparable to the lifetime cost of the flight plus the ground costs estimated in this report. Additionally, a study performed in 2007 showed that when looking at only five impact areas and assuming a 7% discount rate, the estimate benefit from a geo high-spectral resolution sounder was estimated to be over $2B (Centrec, 2007).

Further studies of instrument details, analysis of alternatives, and of economic benefit will be performed in the next phase of study efforts to confirm the best method to achieve the high temporal cadence and fine spatial resolution achievable from a GEO IR hyperspectral sounder as well as its economic value.

The key findings of the aforementioned studies are:

1. Providing low latency, rapid refresh, and high-fidelity HSS data to the NWS weather enterprise would be key to severe weather prediction in providing positive forecast value for nearly every weather forecast process. The NWS weather enterprise has stated that IR hyperspectral data will be used at nearly every step of the weather forecast process by providing real-time deep tropospheric data at a much higher frequency than legacy methods. These data would be included in rapid refresh modeling systems that are the backbone of the 3-6 hour forecast and a key timeframe for providing core partners with decision support services in advance of severe weather. They would also be used in advanced modeling systems, such as NOAA/OAR/NSSLs Warn on Forecast (WoF), which are designed to allow forecasters to give severe weather and flash flood warnings with greater lead times than a r e currently available. Modeling, forecasters would get additional high-frequency datasets to help with near-storm environment assessment, the key to effectively anticipating severe convection, flash flooding, and extreme fire weather.

2. Geostationary hyperspectral IR instruments will provide measurement performance advantages of spatial persistence, spatial resolution, vertical resolution, temporal availability/refresh (rapid cadence), weather event focus, and low data latency compared to LEO IR hyperspectral sounders. They would provide the greatest benefit to forecast processes, including NWP and forecaster's storm situational awareness.

3. Analytic results of the OSSE/OSE record and mature state-of-the-science OSSE/OSE results show potential for improved skill to both regional and global forecasts over periods of hours to many days, providing better lead times for higher confidence predictions.

    a. Historical regional OSSE/OSE analysis, with one hyperspectral IR instrument data stream, shows improvements of temperature from 7-40%, water vapor (q) improvements from 7-33%, and winds (u, v) of 2.5-15%.

    b. Current Global OSSEs and ECMWF OSEs show a statistically significant improvement of T, q, u, and v and provide value measurement metrics for a 24- hour forecast that show a US manifested HSS would be the 4th most impactful contributor to the global forecast and the top contributor over a CONUS forecast region.

    c. Forecast Sensitivity Observation Impact (FSOI)) improvements were observed to 2.5 days forecasts in most regions, with some vertical regions retaining value out to 5-day forecasts.

    d. Current analytic results of regional OSSE/OSE analyses indicate HSS data could potentially improve local severe storm (LSS) temperature measurements up to 7%, water vapor up to 5%, winds improvement from 7% and up to 20% over the LSS mesoscale region.

    e. Recent OSSE analysis of a single hurricane track prediction shows that the addition of simulated HSS data produced either insignificant impact or even slight degradation. Further investigation identified causes of the cases of degradation and the effort continues to investigate how to better initialize this type of experiment. A significant benefit of this experiment is that it confirms the amount of preparatory work required to properly assimilate data from a new instrument – work that needs to be done in parallel with instrument development prior to launch.

    f. NOTE: Errors of actual and simulated systems could degrade these potential benefits. Current limitations on the nature run spatial and temporal resolutions, data assimilation, model maturity, and processing capabilities potentially limit the fidelity of these outcomes and might under-represent the full value of the measurements. Most of the benefits shown in the report are from single case studies and do not represent a statistically significant analysis of the potential benefit, Data assimilation science and high performance computing are likely to mature and improve between now and the 2030s, when the HSS would first fly.

    g. Recent OSE using observed GIIRS information have shown improved monitoring of several core atmospheric variables, plus improved forecast skill including the track and

intensity for a typhoon (Ma et al., 2021; Ying et al., 2020; Ying et al., 2021).

4. HSS data with higher-fidelity IR radiances, smaller spatial footprint, higher observing cadence, and lower data latency provide potentially high value to severe storm leading indicators (such as Lifted Index (LI), Convective Available Potential Energy (CAPE), Convective Inhibition (CIN), Significant Tornado Parameter(STP), and Updraft Helicity (UH)) improving forecast skill.

5. Model winds (u, v) were shown to significantly benefit from improved HSS like data with current global forecast OSSE winds results improved by 1-5% with current LEO IR sounder measurements.

6. Current nowcasting methodologies (NSSL Warn on Forecast (WoF)) were demonstrated to show improved forecast skill with IR data assimilation experiments outperforming almost all radar-only experiments for all observation types. Current atmospheric composition OSSE analysis indicates that IR HSS like data could also potentially augment composition and air quality measurements.

7. Geostationary-based HSS measurements would provide overall improved information to benefit a variety of important weather-sensitive fields: aviation weather, operational emergency management, air quality, climate, fire weather, volcanic ash advisories, marine and coastal weather, marine transportation, and fundamental research.

8. Manifesting a geostationary HSS on a US system would provide consistency with international organization recommendations for a “GEO ring” of hyperspectral (WIGOS 2025 and 2040 vision statements) and correlate with the recommendations from both Earth Science and Applications from Space (ESAS) Decadal Surveys.

9. Full exploitation of HSS data may require optimization of ground data processing as well as improved NWS data processing and NWS infrastructure including the 4D-Var data assimilations and NWP models to prepare users to realize the benefit from the added information content resulting from higher spectral, spatial, and temporal resolutions of the likely instrument performance.

10. Economic/societal benefit from a HSS instrument on the GeoXO platform will be realized from any personal/NGO/Government or commercial decision making that is derived from weather forecast. Current analysis by the NOAA Office of the Chief Economist shows that cost benefit studies in a limited number of different applications areas indicate benefit will realize and exceed the incremental cost of developing the HSS instrument system. The return on investment for manifesting a HSS likely significantly exceeds the cost of adding the instrument to the GEO XO system.

Through the careful consideration of data gleaned from the review of the IR hyperspectral sounding research record, the results from the extension of the OSSE record with matured models, and initial socio-economic benefit analysis, the team found that the measurements from an IR HSS have potential to provide both technical benefit to weather forecasting skill

and a potentially large return on investment if manifested in a geostationary orbit with performance commensurate with the specifications of the GOES-R Hyperspectral Environmental Suite (HES) or European Meteosat Third Generation Infrared Sounder (MTG-IRS).

The conclusion of the assessment team is that this type of observation should have thoughtful consideration for inclusion on the next generation geostationary weather data system development implemented by the GeoXO Program.

8. References

Abt Associates Inc. and Corona Environmental Consulting (2018). NOAA Fleet Societal Benefit Study, Final Report. NOAA Office of Marine & Aviation Operations

Accuweather (2011) How much does a hurricane cost? Retrieved May 18, 2020 from https://www.accuweather.com/en/weather-news/how-much-does-a-hurricane-cost/253437

Anastasio, Elizabeth. (2017) Load Forecasting at PJM [Slides] retrieved 4/30/2020 from:https://www.pjm.com/~/media/committees-groups/committees/oc/20170110/20170110-item-06-load-forecasting-at-pjm.ashx

Barahona, D., A. Molod, J. Bacmeister, A. Nenes, A. Gettelman, H. Morrison, V. Phillips, and A. Eichmann, 2014: Development of two-moment cloud microphysics for liquid and ice within the NASA Goddard Earth Observing model GEOS-5.Geoscience Model Development,7, 1733-1766, doi: 10.5194/gmd-7-1733-2014.

Barnet, C.D., M. Goldberg, L. McMillin, and M.T. Chahine (2004), Remote sounding of trace gases with the EOS/AIRS instrument, in Atmospheric and Environmental Remote Sensing Data Processing and Utilization: an End-to-End System Perspective, H.-L. Huang and H.J. Bloom (Eds.), 5548, 300–310, Society of Photo-Optical Instrumentation Engineers, Bellingham, WA, USA.

Bernknopf, R. L., et al. (2017). "The Value of Remotely Sensed Information: The Case of a GRACE-Enhanced Drought Severity Index." Weather, Climate, and Society.

Blake, Eric and Gibney, Ethan (2011). The deadliest, costliest, and most intense United States tropical cyclones from 1851 to 2010 (and other frequently requested hurricane facts)., NOAA Technical Memorandum NWS NHC-6 https://www.nhc.noaa.gov/pdf/nws-nhc-6.pdf

Bormann, N., H. Lawrence, and J. Farnan, 2019: Global observing system experiments in the ECMWF assimilation system, ECMWF Technical Memorandum 839.

Boukabara, S.-A., and Coauthors, 2016a: Community Global Observing System Simulation Experiment (OSSE) Package (CGOP): Description and usage. J. Atmos. Oceanic Technol., 33, 1759–1777, https://doi.org/10.1175/JTECH-D-16-0012.1

Boukabara, S.-A., K. Garrett, and V. K. Kumar, 2016b, “Potential gaps in the satellite

observing system coverage: assessment of impact on NOAA's numerical weather prediction overall skills," Mon. Weather Rev. 144(7), 2547–2563.

Boukabara, S., and Coauthors, 2018: Community Global Observing System Simulation Experiment (OSSE) Package (CGOP): PeCentrerfect Observations Simulation Validation. J. Atmos. Oceanic Technol., 35, 207–226, https://doi.org/10.1175/JTECH-D-17-0077.1.

Centrec Consulting Group LLC, 2007: An Investigation of the Economic and Social Value of Selected NOAA Data and Products for Geostationary Operational Environmental Satellites (GOES). A Report to NOAA's National Climate Data Center.

Chahine, M. T., et al., 2006: AIRS: improving weather forecasting and providing new data on greenhouse gases, B. Am. Meteorol. Soc., 87, 911–926, https://doi.org/10.1175/BAMS-87-7-911.

Chen, Y., F. Weng, Y. Han, and Q. Liu, 2008: Validation of the Community Radiative Transfer Model by using CloudSat data. J. Geophys. Res., 113, D00A03, https://doi.org/10.1029/2007JD009561

Culverwell, I., H. Lewis, D. Offiler, C. Marquardt, and C. Burrows, 2015: The radio occultation processing package, ROPP. Atmos. Meas. Tech.,8, 1887–1899, doi: 10.5194/amt-8-1887-2015.

DeSouza-Machado, S., L. L. Strow, S. E. Hannon, B. Imbiriba, K. McCann, R. Hoff, J. V. Martins, O. Torres, D. Tanre, F. Ducos, F. Deuze, 2010: "Dust studies using AIRS Infrared data : A comparison of infrared dust column optical depth and height retrievals from AIRS against PARASOL, MODIS, OMI and CALIPSO retrievals," Journal of Geophysical Research, 115, D15201, doi: 10.1029/2009JD012842

Errico, R., and Coauthors, 2017: Description of the GMAO OSSE for Weather Analysis software package: Version 3. Tech. Rep. 48, National Aeronautics and Space Administration, 156 pp NASA/TM-2017-104696.

Errico, R., D. Carvalho, N. Privé, and M. Sienkiewicz, 2020: Simulation of atmospheric motion vectors for an observing system simulation experiment. J. Atmos. Ocean Tech.,37, doi: 10.1175/JTECH-D-19-0079.1.

Federal Aviation Administration. 2019. Air Traffic by the Numbers 2019. Downloaded from https://www.faa.gov/air_traffic/by_the_numbers/media/Air_Traffic_by_the_Numbers_2019.pdf. Verified on July 21, 2020

Feng, J., Huang, Y., and Qu, Z.: A simulation-experiment-based assessment of retrievals of above-cloud temperature and water vapor using a hyperspectral infrared sounder, Atmos. Meas. Tech., 14, 5717–5734, https://doi.org/10.5194/amt-14-5717-2021, 2021.

Franco, B., Clarisse, L., Stavrakou, T., Müller, J.-F., Van Damme, M., Whitburn, S., et al. (2018). A general framework for global retrievals of trace gases from IASI: Application to

methanol, formic acid, and PAN. Journal of Geophysical Research: Atmospheres, 123, 13, 963–13, 984. https://doi.org/10.1029/2018JD029633

Gelaro, R., and Y. Zhu, 2009: Examination of observation impacts derived from observing system experiments (OSEs) and adjoint models. Tellus A, 61, 179-193.

Gelaro, R., and Coauthors, 2015: Evaluation of the 7-km GEOS-5 nature run. NASA/TM2014-14606. Tech. rep., NASA.

Glahn, B., A. Taylor, N. Kurkowski, and W. A. Shaffer, 2009:The Role of the SLOSH Model in National Weather Service Storm Surge Forecasting. National Weather Digest, Volume 33, Number 1, 3-14.

Han, Y., P. van Delst, Q. Liu, F. Weng, B. Yan, R. Treadon, and J. Derber, 2006: JCSDA Community Radiative Transfer Model (CRTM) - Version 1. NOAA Tech. Rep., NESDIS 122, 40 pp.

Holdaway, D., R. Errico, R. Gelaro, and J. G. Kim, 2014: Inclusion of Linearized Moist Physics in NASA's Goddard Earth Observing System Data Assimilation Tools. Monthly Weather Review, 142, 414-433.

Hong, J. and Kim, W.S. (2015), Weather impacts on electric power load: partial phase synchronization analysis. Met. Apps, 22: 811-816. doi:10.1002/met.1535

Hong, T. (2014). Energy forecasting: past, present and future. Foresight: The International Journal of Applied Forecasting, (32), 43-48.

Iturbide-Sanchez, F., S. R. S. da Silva, Q. Liu, K. L. Pryor, M. E. Pettey and N. R. Nalli, "Toward the Operational Weather Forecasting Application of Atmospheric Stability Products Derived From NUCAPS CrIS/ATMS Soundings," IEEE Transactions on Geoscience and Remote Sensing, vol. 56, no. 8, pp. 4522-4545, Aug. 2018, doi: 10.1109/TGRS.2018.2824829

Jones, E., C. D. Barnet, Y. Ma, K. Garrett, K. Ide, and S.-A. Boukabara, 2020: Efforts to Evaluate Shortwave Observations from the CrIS Hyperspectral Infrared Instrument in the NOAA Global Data Assimilation System. 24th Conference on Integrated Observing and Assimilation Systems for the Atmosphere, Oceans, and Land Surface (IOAS-AOLS), Boston, Amer. Met. Soc.

Jones, T. A., Skinner, P., Yussouf, N., Knopfmeier, K., Reinhart, A., Wang, X., Bedka, K., Smith, W., Jr., & Palikonda, R. (2020). Assimilation of GOES-16 Radiances and Retrievals into the Warn-on-Forecast System, Monthly Weather Review, 148(5), 1829-1859

Joo, S., J.Eyre, and R.Marriott, 2013: The impact of MetOp and other satellite data within the Met Office global NWP system using an adjoint-based sensitivity method. Mon. Wea. Rev., 141, 3331–3342, https://doi.org/10.1175/MWR-D-12-00232.1.

Langland, R. H., and N. L. Baker, 2004: Estimation of observation impact using the NRL atmospheric variational data assimilation adjoint system. Tellus A: Dynamic Meteorology and Oceanography, 56, 189-201.

Lazo, J. K., Morss, R. E., & Demuth, J. L. (2009). 300 Billion Served, Bulletin of the American Meteorological Society, 90(6), 785-798.

Lee, S. J., M.-H. Ahn, and S.-R. Chung, Atmospheric profile retrieval algorithm for next generation geostationary satellite of Korea and its application to the Advanced Himawari Imager, Remote Sensing 9, 1294, http://dx.doi.org/10.3390/rs9121294, 2017.

Lee, Yong-Keun, Jun Li, Zhenglong Li, and Tim Schmit, 2017: Atmospheric temporal variations in the pre-landfall environment of Typhoon Nangka (2015) observed by the Himawari-8 AHI, Asia-Pacific Journal of Atmospheric Sciences. DOI:10.1007/s13143-017-0046-z.

Le Moigne, Jacqueline, et al. "Tradespace analysis tool for designing constellations (TAT-C)." 2017 IEEE International Geoscience and Remote Sensing Symposium (IGARSS). IEEE, 2017.

Li, J., W. P. Menzel, F. Sun, T. J. Schmit, and J. Gurka, 2004: AIRS subpixel cloud characterization using MODIS cloud products. J. Appl. Meteorol., 43, 1083 - 1094. Missing Li et al. 2005

Li, J., C. Y. Liu, H.-L. Huang, T. J. Schmit, W. P. Menzel, and J. Gurka, 2005: Optimal cloud-clearing for AIRS radiances using MODIS. IEEE Trans. On Geoscience and Remote Sensing, 43, 1266 - 1278.

Li, Zhenglong, Jun Li, Pei Wang, Agnes Lim, Jinlong Li, Timothy J. Schmit, Robert Atlas, Sid-Ahmed Boukabara, and Ross N. Hoffman, 2018: Value-added Impact of Geostationary Hyperspectral Infrared Sounders on Local Severe Storm Forecasts—via a Quick Regional OSSE, Advances in Atmospheric Sciences, 35(10): 1217-1230.

Li, Jun et al., 2016: Value-added Impact from FengYun-4 hyperspectral IR sounder observations on regional NWP, 6th Workshop on the Impact of Various Observing Systems on NWP, Shanghai, China (10-13 May 2016).

Lin, H., S.S. Weygandt, S.G. Benjamin, and M. Hu, 2017: Satellite Radiance Data Assimilation within the Hourly Updated Rapid Refresh. Wea. Forecasting, 32, 1273–1287, https://doi.org/10.1175/WAF-D-16-0215.1

Liu, H., and J. Li, 2010: An improved in forecasting rapid intensification of Typhoon Sinlaku (2008) using clear-sky full spatial resolution advanced IR soundings, J. Appl. Meteorol. and Cli., 49, 821 – 827.

Lu, Q., *et al.*, 2017: Brief introduction of the hyper-spectral infrared sounder from FY-4A and FY-3D

Ma, Z., Li, J., Han, W., Li, Z., Zeng, Q., Menzel, W. P., et al. (2021). Four-dimensional wind fields from geostationary hyperspectral infrared sounder radiance measurements with high temporal resolution. Geophysical Research Letters, 48, e2021GL093794. https://doi.org/10.1029/2021GL093794.

Macauley, Molly K. The value of information: a background paper on measuring the contribution of space-derived earth science data to national resource management. No. 1318-2016-103485. 2005.

McCarty, W., N. Privé, and I. Moradi, 2021: Observing System Simulation Experiments Investigating a Constellation of 4-5 μm Infrared Sounders. J. Ocean and Atmos. Tech. https://journals.ametsoc.org/view/journals/atot/38/2/JTECH-D-20-0109.1.xml.

McNally, A. P., 2020, Impact of HSIR on NWP, Presented to Coordination Group for Meteorological Satellites - CGMS-48 Plenary, Session: HSIR observations, Agenda item 4.1. August 2020

Menzel, W. P., F. C. Holt, T. J. Schmit, R. M. Aune, A. J. Schreiner, G. S. Wade, G. P. Ellrod, and D. G. Gray, 1998. Application of the GOES-8/9 soundings to weather forecasting and nowcasting. Bull. Amer. Meteor. Soc., 79, 2059-2077.

Menzel, W.P., T.J. Schmit, P. Zhang, and J. Li, 2018: Satellite-Based Atmospheric Infrared Sounder Development and Applications. Bull. Amer. Meteor. Soc., 99, 583–603, https://doi.org/10.1175/BAMS-D-16-0293.1

National Oceanic and Atmospheric Administration (NOAA) National Environmental Satellite, Data, and Information Service (NESDIS) Office of Systems Development (2002) Geostationary Operational Environmental Satellite System (GOES) GOES -R Sounder and Imager Cost/Benefit Analysis (CBA), Prepared for the Department of Commerce.

National Oceanic and Atmospheric Administration (NOAA) National Environmental Satellite, Data, and Information Service (NESDIS) National Centers for Environmental Information (NCEI)., Billion-dollar weather and climate disasters. Retrieve July 12, 2020 from https://www.ncdc.noaa.gov/billions/summary-stats

National Oceanic and Atmospheric Administration (NOAA) National Weather Service (NWS) National Hurricane Center and Central Pacific Hurricane Center (NHC/CPHC)., Sea, Lake, and Overland Surges from Hurricanes (SLOSH). Retrieved July 14, 2020 from https://www.nhc.noaa.gov/surge/slosh.php/

Okamoto et al. 2020: Assessment of the potential impact of a hyperspectral infrared sounder on the Himawari follow-on geostationary satellite, Scientific Online Letters on the Atmosphere (https://doi.org/10.2151/sola.2020-028).

Pearlman, Francoise, Pearlman, Jay, Bernknopf, Richard, Coote, Andrew, Craglia, Massimo, Friedl, Lawrence, Gallo, Jason, Hertzfeld, Henry, Jolly, Claire, Macauley, Molly, Shapiro, Carl, and Smart, Alan, 2016, Assessing the socioeconomic impact and value of

open geospatial information: U.S. Geological Survey Open-File Report 2016–1036, 36 p., http://dx.doi.org/10.3133/ofr20161036.

Pearlman, F., Lawrence, C.B., Pindilli, E.J., Geppi, D., Shapiro, C.D., Grasso, M., Pearlman, J., Adkins, J., Sawyer, G., and Tassa, A., 2019, Demonstrating the value of Earth observations—Methods, practical applications, and solutions—Group on Earth Observations side event proceedings: U.S. Geological Survey Open-File Report 2019–1033, 33 p., https://doi.org/10.3133/ofr20191033.

Peubey, C., and A. P. McNally, 2009: Characterization of the impact of geostationary clear-sky radiances on wind analyses in a 4D-Var context. Quarterly Journal of the Royal Meteorological Society, 135, 1863-1876.

PJM Interconnection Resource Adequacy Planning Department (2016) Load Forecasting Model Whitepaper. Retrieved from: https://www.pjm.com/~/media/library/reports-notices/load-forecast/2016-load-forecast-whitepaper.ashx 4/30/2020

Privé, N., and R. Errico, 2019. Uncertainty of observation impact estimation in an adjoint model investigated with an Observing System Simulation Experiment. Mon. Weather Rev., 147, 3191-3204. doi: 10.1175/MWR-D-19-0097.1.

Privé, N. C., R.M. Errico, R. Todling, and A. El Akkraoui, 2020. Evaluation of adjoint-based observation impacts. Q. J. Roy. Meteor. Soc. Submitted.

Putman, W. M., and S.-J. Lin, 2007: Finite-volume transport on various cubed-sphere grids. J. Comput. Phys., 227, 55–78, https://doi.org/10.1016/j.jcp.2007.07.022

Regnier, Eva, 2008, Public evacuation decisions and hurricane track uncertainty: Management Science 54:1 p. 16-28 https://doi.org/10.1287/mnsc.1070.0764

Schmit, T.J., J. Li, S.A. Ackerman, and J.J. Gurka, 2009: High-Spectral- and High-Temporal-Resolution Infrared Measurements from Geostationary Orbit. J. Atmos. Oceanic Technol., 26, 2273–2292, https://doi.org/10.1175/2009JTECHA1248.1

Schmit, T. J., Griffith, P., Gunshor, M. M., Daniels, J. M., Goodman, S. J., & Lebair, W. J. (2017). A Closer Look at the ABI on the GOES-R Series, Bulletin of the American Meteorological Society, 98(4), 681-698.

Schmit, T. J., S. S. Lindstrom, J. J. Gerth, M. M. Gunshor, 2018: Applications of the 16 spectral bands on the Advanced Baseline Imager (ABI). J. Operational Meteor., 6 (4), 33-46, doi: https://doi.org/10.15191/nwajom.2018.0604

Sieglaff, Justin M.; Schmit, Timothy J.; Menzel, W. Paul and Ackerman, Steven A. Inferring convective weather characteristics with geostationary high spectral resolution IR window measurements: A look into the future. Journal of Atmospheric and Oceanic Technology, Volume 26, Issue 8, 2009, pp.1527-1541.

Smith, W. L., and Coauthors, 1990: GHIS—The GOES high-resolution interferometer sounder. J. Appl. Meteor., 29, 1189–1204. https://doi.org/10.1175/1520-0450(1990)029<1189:GGHRIS>2.0.CO;2

St Germain, K., Gallagher, F. W., Maier, M.W., Coakley, M.M., Adams, E., Zuffada, C., and Piepmeier, J. R., 2018: The NOAA Satellite Observing System Architecture (NSOSA) Study Results, presented at AMS Annual Meeting January 10, 2018. https://ams.confex.com/ams/98Annual/webprogram/Paper333325.html, NOAA Satellite Observing System Architecture (NSOSA) Study: SPRG Report, https://www.nesdis.noaa.gov/sites/default/files/SPRWG_Final_Report_20180325_Posted.pdf

Susskind, J., C. D. Barnet, and J. M. Blaisdell, 2003. "Retrieval of Atmospheric and Surface Parameters from Airs/Amsu/Hsb Data in the Presence of Clouds." *IEEE Transactions on Geoscience and Remote Sensing* 41, no. 2 (2003): 390-409

Sutter, D., & Erickson, S., 2010: The Time Cost of Tornado Warnings and the Savings with Storm-Based Warnings, *Weather, Climate, and Society*, *2*(2), 103-112.

US Energy Information Administration (2020) Retail sales of electricity United States monthly Retrieved from:https://www.eia.gov/electricity/data/browser/#/topic/5?agg=0

Velden, C. S., and Coauthors, 2005: Recent innovations in deriving tropospheric winds from meteorological satellites. Bull. Amer. Meteor. Soc., 86, 205–223. Link, Google Scholar

Van Damme, M., Clarisse, L., Whitburn, S., Hadji-Lazaro, J., Hurtmans, D., Clerbaux, C., and Coheur, P.-F.: Industrial and agricultural ammonia point sources exposed, Nature, 564, 99–103, https://doi.org/10.1038/s41586-018-0747-1, 2018.

Wang, P., Jun Li, M. Goldberg, T. J. Schmit, et al., 2015: Assimilation of thermodynamic information from advanced IR sounders under partially cloudy skies for regional NWP, Journal of Geophysical Research – Atmosphere, 120, doi:10.1002/ 2014JD022976.

Wang P., Jun Li, Z. Li, A. H. N. Lim, Jinlong Li, T. J. Schmit, and M. D. Goldberg, 2017: The Impact of Cross-track Infrared Sounder (CrIS) Cloud-Cleared Radiances on Hurricane Joaquin (2015) and Matthew (2016) Forecasts, Journal of Geophysical Research – Atmospheres, 122, DOI: 10.1002/2017JD027515.

Wang, Pei; Li, Jun and Schmit, Timothy J, 2020. The impact of low latency satellite sounder observations on local severe storm forecasts in regional NWP. Sensors, Volume 20, Issue 3.

Wang, X., and T. Lei, 2014: GSI-based four-dimensional ensemble–variational (4DEnsVar) data assimilation: Formulation and single-resolution experiments with real data for the NCEP Global Forecast System. Mon. Wea. Rev., 142, 3303–3325, https://doi.org/10.1175/MWR-D-13-00303.1

Weaver, Gail, Smith, N., Berndt, E. B., White, K. D.,Dostalek, John. F., & Zavodsky, B. T., 2019: Addressing the Cold Air Aloft Aviation Challenge with Satellite Sounding

Observations. Journal of Operational Meteorology, 138–152. https://doi.org/10.15191/nwajom.2019.0710

Weisz, E.; Smith, N.; Smith, W.L.; Strabala, K.; Huang, H.L. Assessing Hyperspectral Retrieval Algorithms and Their Products for Use in Direct Broadcast Applications. In Proceedings of the 20th International TOVS Study Conference (ITSC-20) Proceedings, Lake Geneva, WI, USA, 28 October–3 November 2015.

Williamson, Ray A., Henry R. Hertzfeld, and Joseph Cordes. "The socio-economic value of improved weather and climate information." Space Policy Institute, The George Washington University, Washington, DC 20052 (2002).

Whitehead, John C. "One million dollars per mile? The opportunity costs of hurricane evacuation." Ocean & coastal management 46, no. 11-12 (2003): 1069-1083.

WMO, 2013 https://www.cgms-info.org/Agendas/WP/CGMS-30-WMO-WP-07

WMO, 2017: Guidelines for Nowcasting Techniques, Rept. No. 1198, 67 pp. 13 https://library.wmo.int/doc_num.php?explnum_id=3795

Yin, R., Han, W., Gao, Z., & Li, J. (2021). Impact of high temporal resolution FY-4A Geostationary Interferometric Infrared Sounder (GIIRS) radiance measurements on Typhoon forecasts: Maria (2018) case with GRAPES global 4D-Var assimilation system. Geophysical Research Letters, 48, e2021GL093672. https://doi.org/10.1029/2021GL093672

Yin, Ruoying, Wei Han, Zhiqiu Gao, and Di Di. “The evaluation of FY4A’s Geostationary Interferometric Infrared Sounder (GIIRS) long-wave temperature sounding channels using the GRAPES global 4D-Var.” Quarterly Journal of the Royal Meteorological Society 146, no. 728 (2020): 1459-1476. https://doi.org/10.1002/qj.3746

Zhou, D. K., and Coauthors, 2002: Thermodynamic product retrieval methodology for NAST-I and validation. Appl. Opt., 41, 6957–6967. https://doi.org/10.1364/AO.41.006957

Zhou, Y., N. Shahroudi, S. Boukabara, K. Ide, T. Zhu, R. Hoffman, S. Casey, and F. Iturbide-Sanchez, 2019: "Assessment of the CubeSat Infrared Atmospheric Sounder impact on global numerical weather prediction using observational system simulation experiments," J. Appl. Rem. Sens. 13(3), 032508. https://doi.org/10.1117/1.JRS.13.032508

9. Acronyms

Acronym	Definition
4DEnsVar	Four-Dimensional Ensemble–Variational
ABI	Advanced Baseline Imager
ABS	Advanced Baseline Sounder
AC-VC	Atmospheric Composition – Virtual Constellation
ADAS	Atmospheric Data Assimilation System
AERI	Atmospheric Emitted Radiance Interferometer
AIRS	Atmospheric Infra Red Sounder
AMDAR	Aircraft Meteorological Data Relay
AMV	Atmospheric Motion Vector
AoA	Analysis of Alternatives
AOML	Atlantic Oceanographic and Meteorological Laboratory
ASAP	Automated Shipboard Aerological Programme
ASHOE	Airborne Southern Hemisphere Experiment
ATBD	Algorithm Theoretical Basis Documents

ATMS	**Advanced Technology Microwave Sounder**
BT	**Brightness Temperature**
CDC	**Concept Design Center**
CEOS	**Committee on Earth Observing Satellites**
CICAS	**Cooperative Institute for Climate and Satellites**
CIMAS	**Cooperative Institute for Marine and Atmospheric Studies**
CIMSS	**Cooperative Institute for Meteorological Satellite Studies**
CIRA	**Cooperative Institute for Research in the Atmosphere**
CIRES	**Cooperative Institute for Research In Environmental Sciences**
CGOP	**Community Global OSSE Package**
CMA	**China Meteorological Administration**
COCOA	**Coastal Ocean Carbon Observations and Applications (GEO orbit)**
COSMIC2	**Constellation Observing System for Meteorology, Ionosphere, and Climate-2**
COURL	**Consolidated Observing User Requirements List**
CrIS	**Cross-track Infrared Sounder**

CRTM	**Community Radiative Transfer Model**
CWP	**CloudWater Path**
D&G	**Data Collection & GEOSAR**
DA	**Data Assimilation**
DBNet	**Direct Broadcast Network**
DRDA	**Dual Regression De-Aliased**
DSCOVR	**Deep Space Climate Observatory**
ECMWF	**European Centre for Medium-Range Weather Forecasts.**
EFSOI	**Ensemble Forecast Sensitivity to Observations Impact**
ESA	**European Space Agency**
ESEI	**Extended Special Events Imager (for Coastal Waters)**
ESTO	**Earth Science Technology Office**
ETS	**Equitable Threat Score**
EVI	**Earth Venture Instruments**
FAR	**False Alarm Ratio**
FCI	**Flexible Combined Imager**
FFRDC	**Federally Funded Research & Development Centers**

FOR	**Field of Regard**
FPCCR	**Formulation Phase Concept and Cost Review**
FSOI	**Forecast Sensitivity - Observation Impact**
FV3GFS	**Finite- Volume Cubed-FV3 Global Forecast System**
FY-4	**Feng-Yun- 4A satellite**
G5NR	**GEOS-5 Nature Run**
GCM	**Global Climate Model**
GCOM/DFS	**Global Change Observation Mission / Dual Frequency Scatterometer**
GEO Cape	**GEOstationary Coastal and Air Pollution Events**
GEOS-5	**Goddard Earth Observing System, Version 5**
GFS	**Global Forecast System**
GHI	**Global Horizontal Irradiation**
GHIS	**Geostationary Hyperspectral IR Sounder**
GIFTS	**Geostationary Imaging Fourier Transform Spectrometer**
GIIRS	**Geostationary Interferometric InfraRed Sounder**
GMAO	**Global Modeling and Assimilation Office**

GOES	**Geostationary Operational Environmental Satellite**
GSI	**Global Statistical Interpolator**
GSI	**Gridpoint Statistical Interpolation**
HAB	**Harmful Algal Blooms**
HES	**Hyperspectral Environmental Suite**
HICO	**Hyperspectral Imager for the Coastal Oceans (LEO orbit)**
HLOS	**Horizontal Line of Sight**
HREF	**High Resolution Ensemble Forecast**
HiResW	**High Resolution Window**
HIIS	**Hyperspectral Imaging IR Sounder**
HIS	**High-resolution Interferometer Sounder**
HRRR	**High Resolution Rapid Refresh**
Hy-IR	**Hybrid InfraRed**
IASI	**Infrared Atmospheric Sounding Interferometer**
IR	**Infra Red**
IRS	**IR Sounders**
JMA	**Japan Meteorological Agency**

JPL	**Jet Propulsion Laboratory**
JPSS	**Joint Polar Satellite System**
KDP	**Key Decision Point**
KPP	**Key Performance Parameters**
L0	**Level 0**
L1	**Level 1**
LACs	**Local Area Zones**
LI	**Lightning Imager**
LEO	**Low Earth Orbit**
LSS	**Local Severe Storm**
LW	**Long Wave**
LWIR	**Long Wave Infra Red**
M/SW	**Medium/Short wave**
MISTiC™ Winds	**Midwave Infrared Sounder for Temperature and humidity in a Constellation for Winds**
ML	**Machine Learning**
MPAS	**Model for Prediction Across Scales**

MTG	**METEOSAT Third Generation**
MTG-I	**METEOSAT Third Generation- Imager**
MTG-S	**METEOSAT Third Generation- Sounder**
MTG-IRS	**METEOSAT Third Generation- Infra Red Sounder**
MW	**Mid Wave**
MWIR	**Mid Wave Infra Red**
NAM	**North American Mesoscale**
NCAR	**National Center for Atmospheric Research,**
NCEP	**National Centers for Environmental Prediction**
NESDIS	**National Environmental Satellite, Data, and Information Service**
NLTE	**Non-Local Thermodynamic Equilibrium**
NGGPS	**Next Generation Global Prediction System**
NOSC	**NOAA Observing Systems Council**
NRT	**Near Real Time**
NSOSA	**NOAA Satellite Observing System Architecture**
NSSL	**National Severe Storms Laboratory (Norman OK)**

NWP	**Numerical Weather Prediction**
NWS	**National Weather Service**
OPPA	**Office of Projects, Planning and Analysis**
OSAAP	**Office System Architecture and Advance Planning**
OSCAR	**Observing Systems Capability Analysis and Review tool**
OSE	**Observing System Experiments**
OSSE	**Observing System Simulation Experiment**
p	**Cloud Top Height**
PanFTS	**Panchromatic imaging Fourier Transform Spectrometer**
PHS	**Polar Hyper Spectral**
POD	**Probability of Detection**
q	**Water Vapor (moisture)**
QC	**Quality Control**
R2O	**Research To Operations**
RAOB	**Radiosonde Observation**
RAP	**Rapid Refresh**
RARS	**Regional ATOVS Retransmission Service (RARS)**

RASS	**Radio Acoustic Sounding System**
RCSC	**Reduced Capability Sounder Concept**
RH	**Relative Humidity**
rOSSE	**regional Observing System Simulation Experiment**
RRFS	**Rapid Refresh Forecast System**
RRTMG	**Rapid Radiative Transfer Model-Global climate model**
SAM	**Summary Assessment Metric**
SIPS	**Science Investigator-led Processing System**
SME	**Subject Matter Expert**
S-NPP	**Suomi NPOESS Preparatory Project**
SPIE	**International Society for Optics and Photonics**
STAR	**Center for Satellite Applications and Research**
SW	**Short Wave**
SWIPE	**Storm Warning In Pre-convection Environment**
SWIR	**Short Wave Infra Red**
SW/MWIR	**Short Wave / Mid Wave Infra Red**
T	**Temperature**

Td	**Dewpoint**
TIR	**Thermal Infra Red**
TMP	**Technology Maturation Program**
u	**Wind**
V	**Precipitation**